Gravitational clustering and detection of cosmological neutrinos

Anders Misfeldt

Department of Physics and Astronomy
University of Aarhus

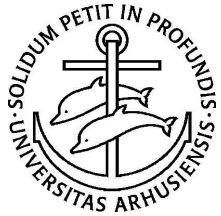

July, 2005

Preface

This thesis has been submitted to the Department of Physics and Astronomy at the University of Aarhus in order to obtain a master's degree in physics. The date of submission was the 1st of July 2005.

Acknowledgment

First of all, I would like to thank my supervisor Jes Madsen for introducing me to the subject and theories on which this thesis is built. He's also thanked for always being willing to help out with whatever problem I might have had with the thesis.

Also, I would like to thank Andreas Ringwald and Yvonne Y. Y. Wong from "Deutsche Elektronen-Synchrotron" (DESY) for supplying me with their data for a comparison.

I also want to thank Henrik Robenhagen Jensen for our discussions on LaTeX and for always having a pot of hot coffee. Also Morten Stejner Sand Pedersen should be thanked for our discussions on miscellaneous integrals and physical argumentations.

I need to thank my aunt for proof reading my thesis for typos and linguistic errors.

Last but not least, I would like to thank my beloved girlfriend for her patience with me the last month when things were a bit hectic.

To the people not mentioned in the acknowledgment: Don't worry, you're not forgotten!

Contents

Chapter 1

Introduction

Ever since the prediction of the neutrino in the Standard Model the quest has been on for detecting them. So far a lot of successful experiments have been carried out and various neutrinos have been detected. The Super-Kamiokande proved, by detection of Cherenkov radiation, that neutrinos carry mass. The mass of the different neutrinos are still to be measured, only a bound on the masses can be established.

One type of neutrinos has still to be detected, the relic neutrinos, a remnant from Big Bang. They could perhaps provide us with information conserning their masses by the way they cluster in gravitational potentials such as galaxies.

In this thesis I'll look at relic neutrino clustering and look at what implications this has for our possibilities of detecting them using present day techniques.

I'll start out by introducing the issues of netrinos and how come I ended up writing my master's thesis about this perticular subject. Also I'll briefly describe the program that I wrote and used for my numerical calculations. I'll end with an outline of this thesis.

1.1 Conserning neutrinos

According to the Big Bang theory, relic neutrinos are predicted to be the second most abundant particles in the Universe. In fact, as many as 10^{87} neutrinos per flavour is predicted. This high number of particles is only surpassed by the cosmic microwave background photons. Interacting only weakly the neutrinos decoupled only a second after Big Bang. Ever since, they've been an important part of our Universe.

The Standard Model predicts the neutrinos to be massless. However, when we extend the Standard Model to include neutrino masses, we find that massive neutrinos can change type whereas massless neutrinos can't. This phenomenon, known as neutrino oscillation, was observed in atmospheric neutrinos using the Super-Kamiokande (Fukuda *et al.*, 1998). Located 1 km underground, it consists of 50000 tons of water surrounded by about 11000 photomultiplier tubes. The water tank, which is 40 m tall and 40 m across, is a large detector which detects Cherenkov radiation. The discovery of neutrino oscillations was clear evidence of the fact that neutrinos carries a non-zero mass.

The cosmological (relic) neutrinos, however, have still to be detected. These neutrinos still carries a signature of their nature from the time of the decoupling, when the Universe was merely one second old. Predictions are that the relic neutrinos are now non-relativistic and therefore sensitive to gravitational clustering on existing cold dark matter structures.

In order to detect relic neutrinos, it's therefore crucial to understand how the clustering behaves and how their number density differs from the average present value of $\overline{n}_\nu = \overline{n}_{\overline{\nu}} \simeq 56\,\mathrm{cm}^{-3}$. This study will therefore mainly be conserned about relic neutrino clustering in cold dark matter halos called NFW halos.

1.2 Motivation

When the time came and I had to write my master's thesis, I asked Jes Madsen about a subject and he came up with the study of relic neutrinos in gravitational potentials. The subject immidiately had my interest since it involves both the field of physics and the field of astronomy.

This study is a based on the relic neutrino clustering research done by (Ringwald and Wong, 2004) (RW). First task is to try and "reproduce" their data using a different approach in the numerical calculations. By "reproduce" I don't mean to exactly copy their procedures, but to come close to their results in a more straight forward way. This way might even be better than the method used by RW.

Instead of doing a time-evolving simulation I only look at the present day where the redshift $z = 0$, where RW uses a initial redshift of $z = 3$ and then do re-

simulations until $z = 0$. Also, RW don't concern about whether the neutrinos form bound or unbound states with the halos, where I, on the other hand, distinguish between bound and unbound neutrinos and do different numerical calculations depedent on the state of the neutrinos. All the time, I'm working with a finite reservoir of relic neutrinos where RW uses an almost infinite reservoir for light halos and a relatively small one for the heaviest halo. I'm then extending my study by also doing phase-space considerations and energy considerations for bound and unbound neutrinos respectively. Also, I'll be looking at relic neutrino clustering in our Solar System and around massive black holes. Finally, I'll try to use a super-massive black hole in the center of galactic halos and see what this would mean for the number densities. I'll examine what these considerations implicate in the quest for the relic neutrinos.

I thus want to study the relic neutrino clustering in galactic halos and point mass potentials in a different way than RW. By distinguishing between bound and unbound neutrinos I expect to see differences between my data and the data produced by RW. Furthermore, the enhancements, I'm making, will cause an even larger difference between my data and the data from RW. How this will effect the possibilities of detecting relic neutrinos will be discussed in detail as well, where my results will be compared with those from RW.

1.3 Programming

The results in my thesis are all based on numerical calculations made by a computer program I wrote. The program is written in the C language and uses of a standard scientific library of mathematical routines called GSL (Gnu Scientific Library)[1].

The program is build up in a way that it requires five input parameters. The parameters are

- M - The large mass in the system (eg. virial halo mass, point mass) in $M_\odot$.
- M_{BH} - The mass of the central black hole in the NFW + Black Hole potential in $M_\odot$. In other potentials this needs to be specified as well, but can be set equal to 0.
- m - Mass of the particle (eg. neutrino) in eV.

[1] http://www.gnu.org/gsl

- Φ - The gravitational potential. Enter as a number corresponding to

$$\Phi = \begin{cases} 1 - \text{NFW potential} \\ 2 - \text{Point Mass potential} \\ 3 - \text{NFW + Black Hole potential} \end{cases}$$

- R - Units in which distance are calculated. Enter as a number corresponding to

$$R = \begin{cases} 1 - \text{Mpc}/h \\ 2 - \text{kpc} \\ 3 - \text{pc} \\ 4 - \text{AU} \\ 5 - R_{\oplus} \end{cases}$$

The program is then run as the following example

```
main 1e13 3.2e9 0.3 3 1
```

This example has a $M_{\text{vir}} = 10^{13}\, M_{\odot}$ NFW halo with a central $M_{\text{BH}} = 3.2 \cdot 10^{9}\, M_{\odot}$ super massive black hole. We're using $m_{\nu} = 0.3\,\text{eV}$. We're telling that we're using the "NFW + Black Hole" potential (3) and measure distances in Mpc/h.

During a run the program generates a total of 12 files (three for number density, four for neutrino numbers and five for neutrino masses used). These are located in a subdirectory called "Data". The filenames tells you which run they corresponds to, eg.

"*density_tot_M*1*e* + 13*Mbh*3.2*e* + 09*m*0.3_*NFW* + *Point_Mpc.dat*"

which holds the data for the total number density of the above mentioned run.

The source code consists of two files "*constants.h*" and "*neutrino.c*". The first of the two holds the constants that the program makes use of and the last file contains the program itself. Also included in the package is a "*makefile*". Thus, the source code can be compiled using the command "**make**", the executable is then called "*main*". Note, however, that in order to compile the source code or to run the executable one needs to have GSL installed. This program was build on Mandrake 10.1 with GSL installed using the RPM package system. On other systems and installations one might need to alter the "*makefile*" in order to make the program compile and run.

Currently the program only runs at the present day $z = 0$, but can of course be extended to include redshift. This is left out of this program due to time limitations.

Two versions of the program can be downloaded from my homepage[2], namely the original NFW and a phase-space modified version.

All software used is Open Source software.

1.4 Outline

This thesis is build up by eight chapters. The first chapter is a small introduction to the thesis. Chapters 2, 3 and 4 are dedicated to neutrino clustering in galactic cold dark matter halos. Each chapter extends the ideas of the previous and conclude with a discussion of the results. In chapter 5, I then turn to look at point masses like massive black holes and how neutrinos cluster in these potentials. Continued from chapter 5, I substitute the massive black hole with Solar and Earth point masses and examines the clustering effects in chapter 7. In chapter 6 I combine the gravitational potentials from chapters 2 and 5 and see how a super-massive central black hole can influence galactic cold dark matter halos. I then turn to possible ways of detecting relic neutrinos in chapter 8, based on the results from previous chapters. The last chapter is a conclusion of the thesis.

For each configuration of masses in each chapter a plot is produced. In each chapter only a few of the plots are shown. The remaining plots are placed in the end of this thesis in appendix A.

[2] http://www.misfeldt.dk/Neutrino/

Chapter 2

Galactic NFW halos

In this chapter I'll look at neutrino number densities in cold dark matter halos using a gravitational potential calculated from the so-called NFW density profile. I'll be doing numerical calculations of the neutrino number densities for various neutrino masses and galactic masses. Starting out by defining the NFW density profile, I move on to the gravitational potential calculations and conclude with my numerical calculations of the neutrino number densities. Furthermore, I'll examine how much mass the neutrinos will occupy in the halos.

2.1 The NFW density profile

When computing neutrino number densities in galactic halos we need to have a good density profile of the halo. In 1996 Navarro, Frenk and White (NFW) found that the density profiles of cold dark matter halos adjust to a universal shape, independent of the halo mass, the cosmological parameters and the initial conditions (Navarro *et al.*, 1996). This density profile ρ_{halo} takes the form of

$$\rho_{\text{halo}} = \frac{\rho_s}{\left(\frac{r}{r_s}\right)\left(1+\frac{r}{r_s}\right)^2} \tag{2.1}$$

The parameters ρ_s and r_s are determined by the virial mass M_{vir} of the halo and a dimensionless concentration parameter c[1], which is defined as

$$c \equiv \frac{r_{\text{vir}}}{r_s} \tag{2.2}$$

where r_{vir} is the virial radius within which M_{vir} is located. The virial mass is defined by the average density Δ_{vir} of the matter times the mean matter density $\overline{\rho}_m$ at a given redshift (Ringwald and Wong, 2004), thus

$$\begin{aligned} M_{\text{vir}} &\equiv \frac{4\pi}{3}\Delta_{\text{vir}}\overline{\rho}_m a^3 r_{\text{vir}}^3 = \frac{4\pi}{3}\Delta_{\text{vir}}\overline{\rho}_{m,0} r_{\text{vir}}^3 \\ &= 4\pi\rho_s a^3 r_s^3\left[\ln(1+c) - \frac{c}{1+c}\right] \end{aligned} \tag{2.3}$$

where a is the scale factor

$$a = \frac{1}{1+z}$$

hence,

$$\begin{aligned} \rho_s &= \frac{\Delta_{\text{vir}}}{3}\overline{\rho}_{m,0} c^3 (1+z)^3 \frac{1}{\left[\ln(1+c) - \frac{c}{1+c}\right]} \\ &= \frac{\Delta_{\text{vir}}}{3}\overline{\rho}_{m,0} \frac{c\,(z=0)^3}{\left[\ln(1+c) - \frac{c}{1+c}\right]} \end{aligned} \tag{2.4}$$

where $\overline{\rho}_{m,0}$ is the mean matter density at present day, determined by the critical density ρ_{crit} times the present matter density parameter $\Omega_{m,0}$, thus

$$\overline{\rho}_{m,0} = \Omega_{m,0}\frac{3H^2}{8\pi G} \tag{2.5}$$

[1]This is not to be mistaken with the speed of light which is also denoted by c. However, the context should revial which of the two parameters being used.

since the critical density is given as

$$\rho_{\text{crit}} = \frac{3H^2}{8\pi G} \tag{2.6}$$

with H being Hubble's constant and G the universal gravitational constant. From the definition of the virial mass we can find an expression for r_s. By inserting equation (2.4) in (2.3) we find

$$\begin{aligned} M_{\text{vir}} &= \frac{4\pi}{3}\Delta_{\text{vir}}\overline{\rho}_{m,0}\left(\frac{c(z=0)}{1+z}\right)^3 r_s^3 \\ &= \frac{4\pi}{3}\Delta_{\text{vir}}\overline{\rho}_{m,0}c(z)^3 r_s^3 \end{aligned}$$

where equation (2.11) for the concentration parameter has been used. Hence r_s can be expressed as

$$r_s = \frac{1}{c(z)}\left(\frac{3}{4\pi\Delta_{\text{vir}}}\frac{M_{\text{vir}}}{\overline{\rho}_{m,0}}\right)^{1/3} \tag{2.7}$$

Instead of the virial mass we could also find interest in the physical mass of a sphere with radius r inside a NFW halo. The halo mass is simply given as

$$M_{\text{halo}}(r) = 4\pi a^3 \rho_s r_s^3 g(x)\,, \qquad x \equiv \frac{r}{r_s} \tag{2.8}$$

where the dimensionless function $g(x)$ is defined as

$$g(x) \equiv \ln(1+x) - \frac{x}{1+x} \tag{2.9}$$

The concentration parameter has been found in the analysis of around 5000 halos in the mass range $10^{11} \rightarrow 10^{14}\, M_\odot$ of (Bullock *et al.*, 2001) to be described as (at $z = 0$)

$$c\,(z=0) = 9\left(\frac{M_{\text{vir}}}{1.5\cdot 10^{13} M_\odot/h}\right)^{-0.13} \tag{2.10}$$

with h being the Hubble parameter, which for any given redshift yields

$$c(z) = \frac{c\,(z=0)}{1+z} \tag{2.11}$$

2.2 The NFW potential

It was needed to calculate the gravitational potential from the NFW density profile since the numerical calculations require the escape velocity.

From classical mechanics, we know that the escape velocity from a potential $\Phi(r)$ is given by

$$v_{\text{esc}}(r) = \sqrt{2|\Phi(r)|} \tag{2.12}$$

From the potential theory (Binney and Tremaine, 1987), we have

$$\begin{aligned}\Phi(r) &= -4\pi G\left\{\frac{1}{r}\int_0^r \rho_{\text{halo}} r^2\,\mathrm{d}r + \int_r^\infty \rho_{\text{halo}} r\,\mathrm{d}r\right\} \\ &= -4\pi G\rho_s\left\{\frac{1}{r}\int_0^r \frac{r^2}{\frac{r}{r_s}\left(1+\frac{r}{r_s}\right)^2}\,\mathrm{d}r + \int_r^\infty \frac{r}{\frac{r}{r_s}\left(1+\frac{r}{r_s}\right)^2}\,\mathrm{d}r\right\}\end{aligned} \tag{2.13}$$

hence the potential takes the form

$$\Phi(r) = -4\pi G\rho_s \frac{r_s^3}{r}\left(\ln\left(1+\frac{r}{r_s}\right)\right) \tag{2.14}$$

We can verify that this is the correct potential by solving the Poisson equation

$$\begin{aligned}\nabla^2\Phi(r) &= 4\pi G\rho_{\text{halo}} \\ &= \frac{1}{r^2}\frac{\partial}{\partial r}\left(r^2\frac{\partial\Phi(r)}{\partial r}\right)\end{aligned} \tag{2.15}$$

which the gravitational potential must obey in order to be valid. When inserting our newly calculated NFW potential (2.14) into the Poisson equation we end up with the NFW density profile (2.1).

2.3 Numerical calculations

The neutrino distribution is taken to be an isotropic Fermi-Dirac distribution

$$f(p) = \frac{1}{\mathrm{e}^{\frac{E-\mu}{kT}} + 1} \tag{2.16}$$

where μ is the chemical potential of the neutrinos and k is Boltzmann's constant. The current value for the neutrino chemical potential is $\frac{\mu}{kT_{\nu,0}} \leq 0.3$ (Dolgov *et al.*, 2002). A value of that size won't cause a large alteration of my calculations, hence

the neutrino chemical potential is ignored. When the neutrinos decoupled from the plasma that made up our Universe in the first seconds after Big Bang the temperature was around $T_{\text{decouple}} \sim 10^{10}\,\text{K} \sim 1\text{MeV}$ (Kolb and Turner, 1994). Hence the neutrinos were ultra relativistic and had a relativistic Fermi-Dirac distribution given by

$$f(p(z)) = \frac{1}{\mathrm{e}^{\frac{p(z)c}{kT(z)}} + 1} \tag{2.17}$$

with $p(z)$ denoting the magnitude of the neutrino momentum at a given redshift z, $T(z)$ the temperature at a given redshift and c the speed of light. When the Universe cooled down, the neutrinos became non-relativistic, but due to Liouville's theorem[2] the microscopic phase-space distribution (the Fermi-Dirac distribution given by equation (2.17)) is conserved during the expansion of the Universe. In a homogeneous Universe the momentum p of the neutrino scales as a^{-1}. Thus, in order to satisfy Liouville's theorem, the temperature T also needs to scale as a^{-1}, that is

$$\begin{aligned} p(z) &= p\,(1+z) \\ T(z) &= T_{\nu,0}\,(1+z) \end{aligned}$$

The Fermi-Dirac distribution for the present day neutrinos can be written in the same form as (2.17) with a substitution for the present day momentum and temperature $T_{\nu,0}$, hence

$$f(p) = \frac{1}{\mathrm{e}^{\frac{pc}{kT}} + 1} \tag{2.18}$$

The number density for the neutrinos will therefore be

$$\begin{aligned} n_\nu &= \frac{\gamma}{h_p^3} \int f(p)\,\mathrm{d}^3 p \\ &= \frac{4\pi\gamma}{h_p^3} \int \frac{p^2}{\mathrm{e}^{\frac{pc}{kT_{\nu,0}}} + 1}\,\mathrm{d}p \end{aligned} \tag{2.19}$$

where h_p is Planck's constant, and γ is the internal degrees of freedom (helicity states) of the particle for which the distribution is calculated, eg. electrons have $\gamma = 2$ (spin $= \frac{1}{2} \Rightarrow m_S = \pm\frac{1}{2}$). Neutrinos always have left helicity (spin oriented opposite of it's velocity). If neutrinos have $\gamma = 1$ they are Majorana particles and

[2] Liouville's theorem states that an entire, bounded function is constant. In other words, a function that is analytic everywhere and not constant increases without bound

if they are Dirac particles, they have γ close to 1. In the following γ will be set to 1. We further assume that the number of antineutrinos and neutrinos are the same, thus the effective γ is $\gamma_{\text{eff}} = 2\gamma$.

The present day neutrino temperature is $kT_{\nu,0} = 1.676 \cdot 10^{-4}\,\text{eV}$, which corresponds to the cosmic neutrino background (CνB) temperature of $\sim 1.945\,\text{K}$. This is an analogue to the 2.725 K cosmic microwave background (CMB), with a connection written as

$$\frac{T_\nu}{T_\gamma} = \left(\frac{4}{11}\right)^{1/3}$$

All calculations are made for the present day, thus $z = 0$. The average density is taken to be $\Delta_{\text{vir}} = 200$. Calculations are made for neutrinos with masses $m_\nu = 0.15\,\text{eV}, 0.3\,\text{eV}, 0.6\,\text{eV}$. I start my calculations at $r_0 = 10^{-3}\,\text{Mpc}/h$ and end them at a distance of $r = 10\,\text{Mpc}/h$ from the halo centre. With the choice of halo virial masses $M_{\text{vir}} = 10^{12}\,M_\odot \rightarrow 10^{15}\,M_\odot$ I can get both number densities in halos of galaxies and clusters of galaxies. The present matter density parameter is chosen to be $\Omega_{m,0} = 0.3$ and the Hubble parameter to be $h = 0.7$.

Both bound and unbound neutrino number densities are calculated and then added to give a total number density at the given distance r from the halo center. Bound particles are defined to be the particles that are caught within the gravitational potential, thus having velocities (momenta) less than the escape velocity (escape momentum) of the NFW potential. The unbound particles are then the neutrinos with greater velocities (momenta) than the escape velocity (momentum). When neutrinos experience a gravitational potential they lose momentum and thus energy and since the capturing of the relic neutrinos are slowly changing the gravitational potential we are working with an adiabatic invariant (Binney and Tremaine, 1987).

We're filling up the potential very slowly, thus the energy needs to be an adiabatic invariant. This is because, neutrinos affected by a gravitational potential lose momentum and therefore also energy. The potential will be filled up the neutrinos with lowest momentum first, $p \simeq 0$, hence $f \simeq 0.5$. We're therefore able to write the number density as

$$\begin{aligned} n_\nu &= n_{\nu,\text{bound}} + n_{\nu,\text{unbound}} \\ &= \frac{4\pi\gamma}{h_p^3}\left(0.5\int_0^{p_{\text{esc}}} p^2 \mathrm{d}p + \int_{p_{\text{esc}}}^{\infty} \frac{p^2}{e^{\frac{pc}{kT_{\nu,0}}} + 1}\mathrm{d}p\right) \end{aligned}$$

We're only able to approximate the Fermi-Dirac distribution for the bound neutrinos to a constant value, since it's the energy that's the adiabatic invariant. We still need to integrate over the momentum phase-space for the bound neutrinos.

An interesting thing to examine is the total number of neutrinos in the halo, and hence the total mass the neutrinos will occupy in the halo. Again, both the total number of bound and unbound neutrinos are calculated separately and then added in the end. Since the number density n_ν is r dependent, it needs to be integrated with respect to r, thus

$$\#_\nu = \int_{r_0}^{r} 4\pi n_\nu(r')\, r'^2 \mathrm{d}r' \tag{2.20}$$

whence the total mass is calculated as

$$M_\nu = \#_\nu m_\nu \tag{2.21}$$

2.3.1 Results and discussion

All number densities are normalized to the average present value $\overline{n}_\nu$, which is calculated as all neutrinos in the entire momentum phase-space homogenously distributed, ie.

$$\begin{aligned}\overline{n}_\nu &= \frac{4\pi\gamma}{h_p^3}\int_0^\infty \frac{p^2}{\mathrm{e}^{\frac{pc}{kT_{\nu,0}}}+1}\mathrm{d}p \\ &= \frac{4\pi\gamma}{h_p^3}\left(\frac{kT_{\nu,0}}{c}\right)^3\int_0^\infty \frac{x^2}{\mathrm{e}^x+1}\mathrm{d}x \\ &\simeq 56\,\mathrm{cm}^{-3}\end{aligned} \tag{2.22}$$

since

$$\int_0^\infty \frac{x^2}{\mathrm{e}^x+1}\mathrm{d}x = \frac{3}{2}\zeta(3)$$

where $\zeta(3) \simeq 1.20206$ is the Riemann zeta function.

The results of the calculations are shown in figures 2.1 - 2.4. The plots show the neutrino number density normalized to the average present value $\overline{n}_\nu$ for all twelve configurations of $\{m_\nu, M_{\mathrm{vir}}\}$[3]. The original data from RW is also plotted for comparison. We see that as we crank up the mass of the halos, we get a larger clustering effect. This is due to the depth of the gravitational potential. A heavier halo results in a deeper potential well, which in the end causes a larger clustering effect. Also we note that the heavier the neutrinos are, the more they cluster. This effect is caused by the kinetical energy of the neutrinos. Light neutrinos will have a higher kinetic energy than heavy neutrinos with the same temperature $T_{\nu,0}$

[3]Only four configurations are plotted here. The rest are shown in appendix A.

and slow neutrinos will easier become bound than fast ones. In the lowest mass configuration, see figure 2.1, my data is roughly of the same value as the data from RW. By moving to heavier configurations we note that my data becomes larger than RW's and moves from roughly a factor ~ 1 to a factor of ~ 10 for the heaviest configuration, as seen in figure 2.4. A modern version of the Tremaine-Gunn bound (Tremaine and Gunn, 1979; Ringwald and Wong, 2004), which can be written as

$$\frac{n_\nu}{\overline{n}_\nu} < \frac{m_\nu^3}{9\zeta(3)(kT_{\nu,0})^3}\left[\frac{2GM_{\text{vir}}}{g(c(z))c^2}\frac{\ln\left(1+\frac{r}{r_s}\right)}{r}\right]^{3/2} \tag{2.23}$$

is also included in the plots.

So what are the main reasons for my data to differ from RW's data? (i), RW explicitly writes that they simply sum all neutrinos over the entire momentum space. They don't care whether or not the relic neutrinos form bound states. (ii), they do a simulation with initial redshift $z = 3$. (iii), they do all their simulations with a different reservoir of relic neutrinos: They take the neutrinos from as far away as they can travel before reaching $r = 10\,\text{Mpc}/h$ within the evolution of their simulations. This leads to the fact that a light halo gets to have a very large reservoir of neutrinos, while large halos has a small reservoir. (iv), RW uses the entire Fermi-Dirac distribution for all the relic neutrinos in their simulations, I've been using $f = 0.5$ for the bound neutrinos and the Fermi-Dirac distribution for the unbound neutrinos. The use of the entire Fermi-Dirac distribution will obviously lead to a drop in the normalized number densities (the overdensities) compared to my results, where a constant maximum value for the Fermi-Dirac distribution has been used for the bound neutrinos.

My results should also be compared to a modern version of the Tremaine-Gunn bound, which states that neutrinos must have masses larger than 20 eV if they are to constitute the dark matter of a galactic halo alone. This mass limit comes from the argumentation that the coarse-grained distribution should always be smaller than the maximum fine-grained distribution, if assuming a Maxwellian phase-space distribution. The fine-grained and coarse-grained distributions will be discussed in detail in chapter 4. The Tremaine-Gunn bound is a way to express the upper limit to the value the overdensity can take at given points in a halo, like the NFW halo. The original Tremaine-Gunn bound is only valid for neutrinos making up the dark matter of galactic halos, where the modern version allows for more than one type of matter as contributor to the total gravitational potential (Kull *et al.*, 1996).

We see that for the light configurations my data exceeds the Tremaine-Gunn bound. However, this can be explained. While the Tremaine-Gunn bound only takes the bound particles into account, I look at both bound and unbound parti-

cles. In the light configurations, the unbound neutrinos will consume more mass than the bound neutrinos, thus the unbound neutrinos will be the most important when looking at overdensities. When moving to heavier configurations, the bound neutrinos become more and more important to the overdensity. We also note that the Tremaine-Gunn data suddenly drops below my data for some of the configurations. This is due to the fact that the bound neutrinos are only most important out until a certain distance. When we're a certain distance away from the center of the halo, the unbound neutrinos become more important again, since the potential is filled with bound neutrinos, and the Tremaine-Gunn drops. In the lightest configuration, the Tremaine-Gunn isn't showing up on the plot at all. This is occuring because the Tremaine-Gunn bound allows for $\frac{n_\nu}{\overline{n}_\nu} < 1$. When taking the unbound neutrinos into account as well, the curve will take its minimum at $\frac{n_\nu}{\overline{n}_\nu} = 1$. In the heavier configurations, where the bound neutrinos are dominating heavily over the unbound neutrinos, we see that the Tremaine-Gunn bound is always exceeding my data. This is just as it should be, since the Tremaine-Gunn bound is, as mentioned, an upper limit to the overdensity at given points in a halo.

The RW data have overdensities that exceeds those from my calculations for the light configurations (the $M_{\text{vir}} = 10^{12}\, M_\odot$ NFW halo), but as we move to heavier halos the overdensities calculated from my program quickly begins to grow larger than those from RW. From the $10^{13}\, M_\odot$ halos where the overdensities from my calculations and from RW are roughly equal, to the heavy $10^{15}\, M_\odot$ halo where my data have grown roughly a factor ~ 10 larger than RW's data.

For the same sets of configuration $\{m_\nu\,, M_{\text{vir}}\}$ the total masses used at the corresponding radii are calculated and plotted. The plots are shown in figures 2.5 - 2.8. The physical masses of the NFW halos are also included in the graphs in order to check whether or not the total neutrino mass exceeds the halo mass. We see that this only happens for a few configurations and it's only at very large distances. If the total neutrino mass M_ν used in the halo had exceeded the physical halo mass or would have been comparable to it, then self-gravitation between the neutrinos would have to be taken into account as well. As already noted this isn't the case, hence we can ignore self-gravitation of the neutrinos. If we were to use heavier particles than neutrinos, the scenario would have been different. The total mass would then exceed the physical halo mass at a small distance, hence self-gravitation would play an important role.

The graphs also include curves of the total mass of the homogeneously distributed neutrinos. The curves show us that the unbound neutrinos can easily come from the homogeneously distributed neutrinos, since the mass curve for the homogeneously distributed neutrinos consequently have higher value than that of the unbound neutrinos. This is just as it very well should be since the unbound neutrinos are the ones having $p > p_{\text{esc}}$ and the homogeneous neutrinoes are all neutrinos with the full Fermi-Dirac distribution.

For the lightest configurations we note, that the bound neutrinos aren't the largest contributor to the total neutrino mass used. The unbound neutrinos are actually using more mass in the light NFW halo than the bound neutrinos. However, as we move to heavier configurations, we see that the bound neutrinos are becoming a lot more clustered and thus contributes more and more to the total neutrino mass used. In the heaviest of the configurations the total neutrino mass used is almost entirely "made" of bound neutrinos in the potential.

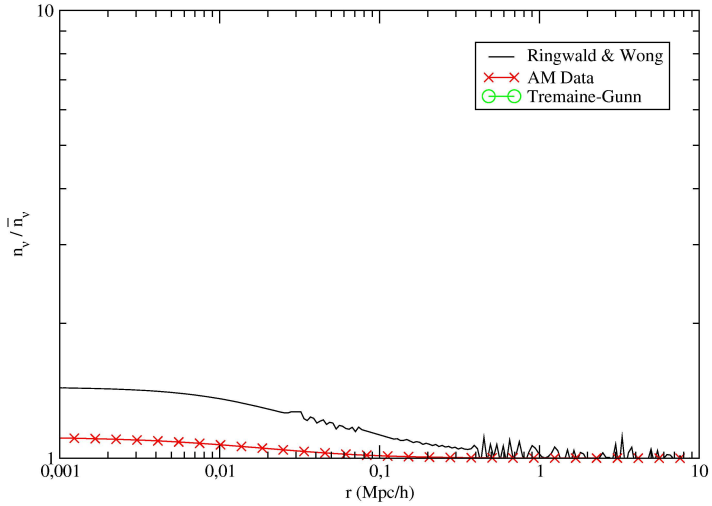

Figure 2.1: Number densities n_ν normalized to present average $\bar{n}_\nu$ for $m_\nu = 0.15\,\mathrm{eV}$ neutrinos in a $M_{\mathrm{vir}} = 10^{12}\,M_\odot$ halo. The solid line displays the data from RW, the X-line displays my numerical calculations and the O-line shows the Tremaine-Gunn bound.

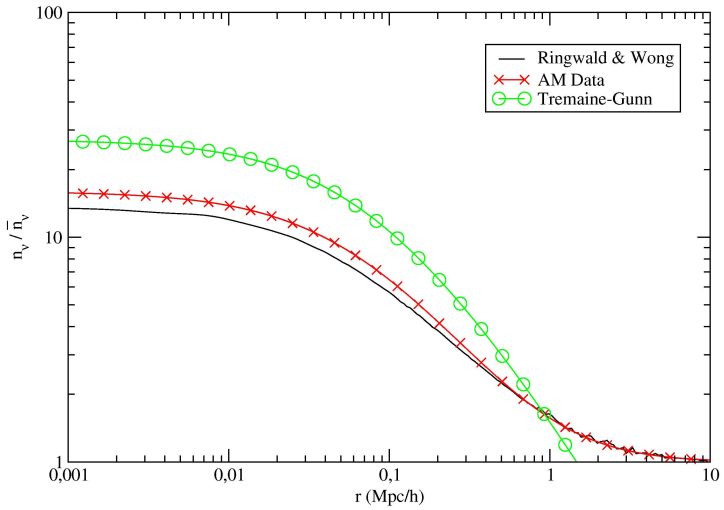

Figure 2.2: Number densities n_ν normalized to present average $\bar{n}_\nu$ for $m_\nu = 0.3\,\mathrm{eV}$ neutrinos in a $M_{\mathrm{vir}} = 10^{13}\,M_\odot$ halo. The solid line displays the data from RW, the X-line displays my numerical calculations and the O-line shows the Tremaine-Gunn bound.

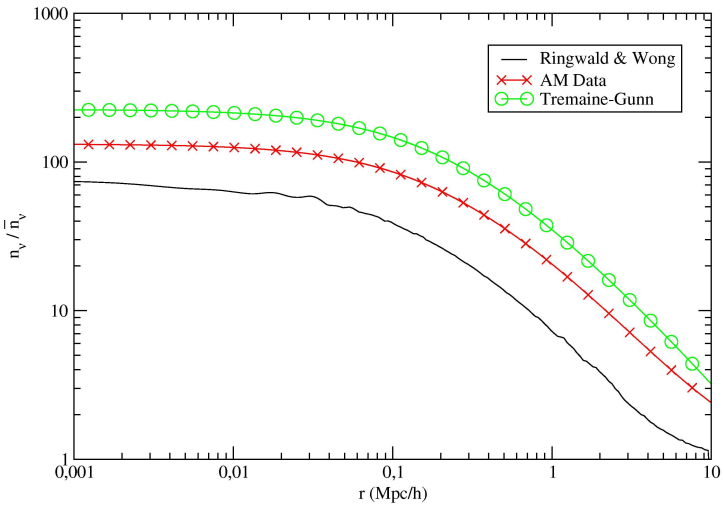

Figure 2.3: Number densities n_ν normalized to present average $\bar{n}_\nu$ for $m_\nu = 0.3\,\mathrm{eV}$ neutrinos in a $M_{\mathrm{vir}} = 10^{14}\,M_\odot$ halo. The solid line displays the data from RW, the X-line displays my numerical calculations and the O-line shows the Tremaine-Gunn bound.

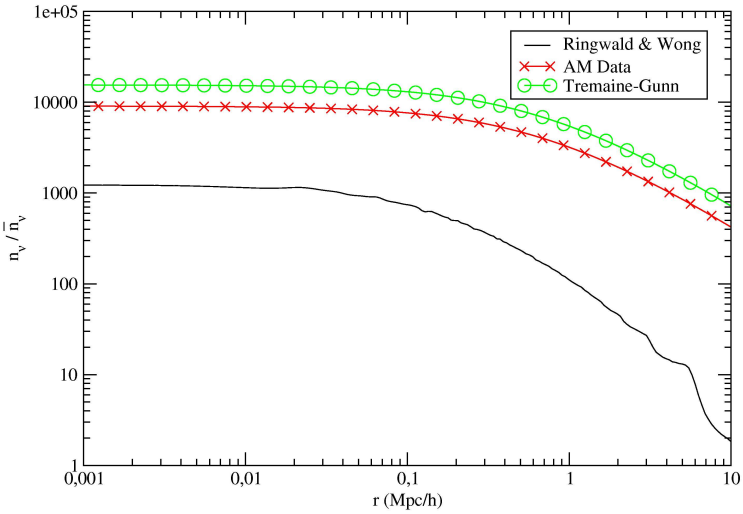

Figure 2.4: Number densities n_ν normalized to present average $\overline{n}_\nu$ for $m_\nu = 0.6\,\mathrm{eV}$ neutrinos in a $M_{\mathrm{vir}} = 10^{15}\,M_\odot$ halo. The solid line displays the data from RW, the X-line displays my numerical calculations and the O-line shows the Tremaine-Gunn bound.

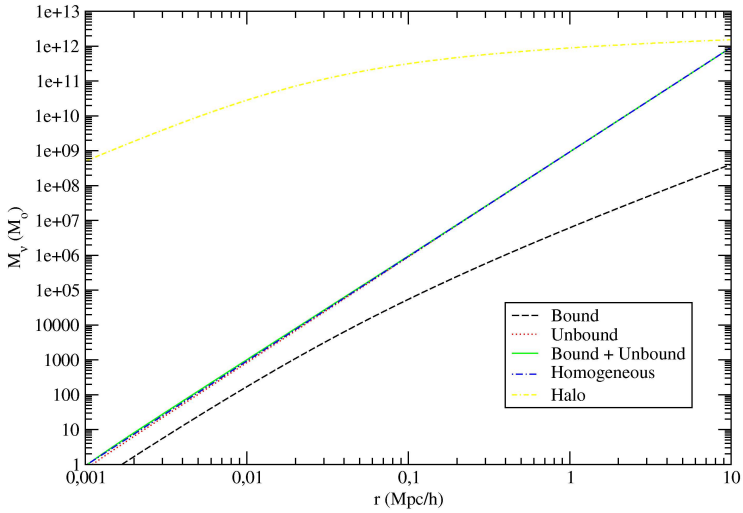

Figure 2.5: A complete plot of neutrino mass used in the halo for $m_\nu = 0.15\,\mathrm{eV}$ neutrino in a $M_{\mathrm{vir}} = 10^{12}\,M_\odot$ halo. The plot shows the total bound, the total unbound, and the total neutrino mass used. Furthermore the total homogeneously distributed mass as well as the NFW halo mass are plotted.

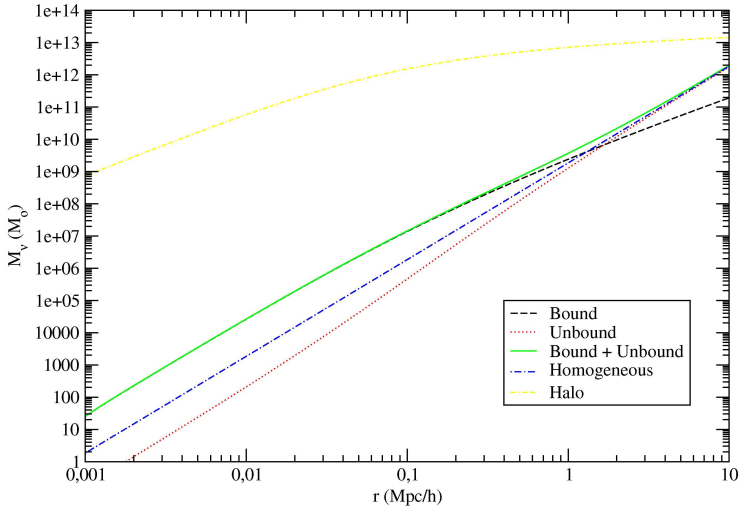

Figure 2.6: A complete plot of neutrino mass used in the halo for $m_\nu = 0.3\,\mathrm{eV}$ neutrino in a $M_{\mathrm{vir}} = 10^{13}\,M_\odot$ halo. The plot shows the total bound, the total unbound, and the total neutrino mass used. Furthermore the total homogeneously distributed mass as well as the NFW halo mass are plotted.

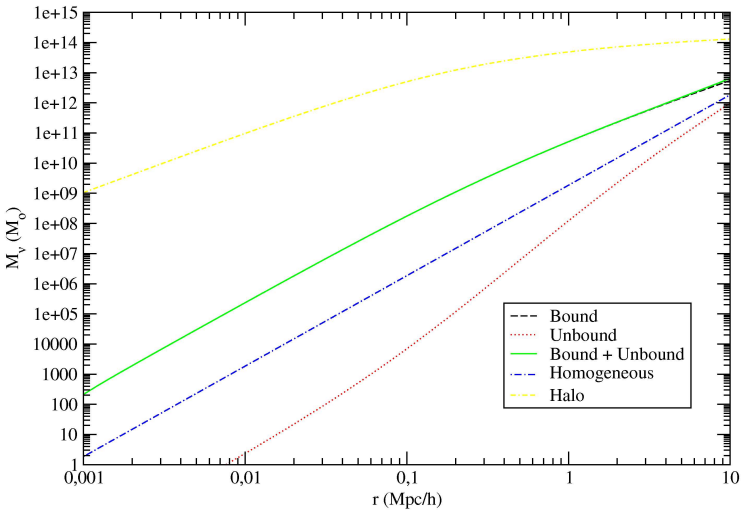

Figure 2.7: A complete plot of neutrino mass used in the halo for $m_\nu = 0.3\,\mathrm{eV}$ neutrino in a $M_{\mathrm{vir}} = 10^{14}\,M_\odot$ halo. The plot shows the total bound, the total unbound, and the total neutrino mass used. Furthermore the total homogeneously distributed mass as well as the NFW halo mass are plotted.

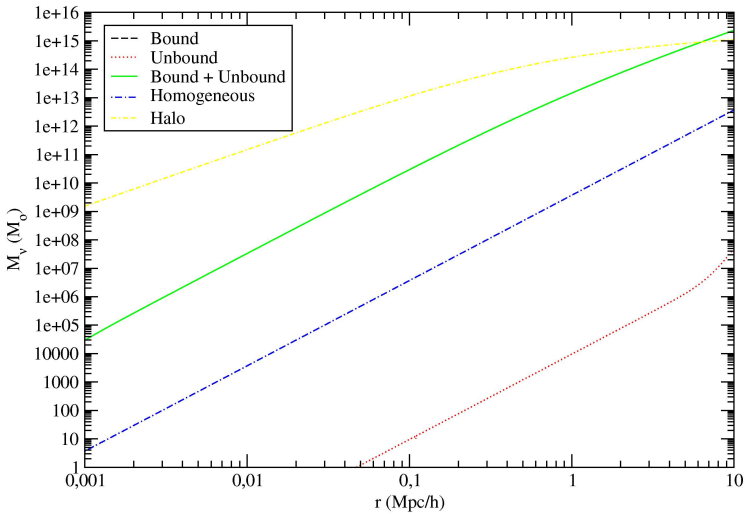

Figure 2.8: A complete plot of neutrino mass used in the halo for $m_\nu = 0.6\,\mathrm{eV}$ neutrino in a $M_{\mathrm{vir}} = 10^{15}\,M_\odot$ halo. The plot shows the total bound, the total unbound, and the total neutrino mass used. Furthermore the total homogeneously distributed mass as well as the NFW halo mass are plotted.

Chapter 3

Improvements for galactic halos

In this chapter I'll look deeper into the details of the theory and make enhancements in order to make the results more realistic, thus I'll be taking a step further than the original work done by RW. I'll be looking at the maximum allowed radius for which I'll be capturing neutrinos into my NFW potential. Also I'll make alterations concerning the unbound neutrinos by making their energy depend on the potential energy as well as the kinetic energy. Again I'll be doing numerical calculations for various neutrino masses and conclude with my results.

3.1 Estimation of galaxy radius

Until now we've assumed that we can capture neutrinos in the gravitational potential from a fixed radius of $10\,\mathrm{Mpc}/h$ for all halos. This assumption is very rough and only gives a vague image of the actual distribution, since it allows for neutrinos to be captured from far away from the galaxy itself. It could even be that we're capturing neutrinos from another galaxy halo, eg. if two galaxies, each having halos with a radius of $5\,\mathrm{Mpc}/h$, are lying right up against each other, then we allow for the galaxy we're looking at to capture all the neutrinos from the other galaxy halo as well. This needs to be adjusted. I will here describe a way that can give an estimate of the radius of a NFW galaxy.

The mass of a NFW halo with radius r_{galaxy} is given by equation (2.8), thus

$$M_{\text{NFW}}\left(r_{\text{galaxy}}\right) = 4\pi\rho_s a^3 r_s^3\left[\ln\left(1+\frac{r_{\text{galaxy}}}{r_s}\right)-\frac{r_{\text{galaxy}}}{r_s+r_{\text{galaxy}}}\right] \tag{3.1}$$

Within this NFW halo we have a homogeneous and spherical distribution of cold dark matter which have a mass given by

$$M_{\text{CDM}}\left(r_{\text{galaxy}}\right) = \frac{4}{3}\pi\overline{\rho}_{m,0} r_{\text{galaxy}}^3 \tag{3.2}$$

where $\overline{\rho}_{m,0}$, given by equation (2.5), is the mean matter density at the present day. If the NFW halo is to consist of cold dark matter the two masses must be equal to each other, hence we're able to find the radius of the NFW galaxy. That is, at $r = r_{\text{galaxy}}$ the following criteria must be fulfilled

$$\begin{aligned} M_{\text{CDM}}\left(r_{\text{galaxy}}\right) &= M_{\text{NFW}}\left(r_{\text{galaxy}}\right) \\ \frac{4}{3}\pi\overline{\rho}_{m,0} r_{\text{galaxy}}^3 &= 4\pi\rho_s a^3 r_s^3\left[\ln\left(1+\frac{r_{\text{galaxy}}}{r_s}\right)-\frac{r_{\text{galaxy}}}{r_s+r_{\text{galaxy}}}\right] \end{aligned}$$

Which reduces to

$$r_{\text{galaxy}}^3 = \frac{2M_{\text{vir}}G}{\Omega_{m,0}H^2}\frac{\left[\ln\left(1+\frac{r_{\text{galaxy}}}{r_s}\right)-\frac{r_{\text{galaxy}}}{r_s+r_{\text{galaxy}}}\right]}{\left[\ln(1+c)-\frac{c}{1+c}\right]} \tag{3.3}$$

Besides, at the center of the halo ($r_{\text{galaxy}} = 0$), equation (3.3) only has one solution which can be found numerically. In this way we've split all the cold dark matter in the universe up into NFW galaxies with virial mass M_{vir} and total mass $M_{\text{NFW}}\left(r_{\text{galaxy}}\right)$.

This of course again is a rough estimate of the cold dark matter distribution in the universe since the distribution of cold dark matter isn't completely homogeneous and spherical and since all cold dark matter isn't distributed into NFW

galaxies, but it will provide us with an image of the radius from which we can capture neutrinos. For the halo masses $\{10^{12}\,M_\odot, 10^{13}\,M_\odot, 10^{14}\,M_\odot, 10^{15}\,M_\odot\}$ we get the following radii $\{\sim 1.4\,\mathrm{Mpc}/h, \sim 3.0\,\mathrm{Mpc}/h, \sim 7.0\,\mathrm{Mpc}/h, \sim 15.5\,\mathrm{Mpc}/h\}$.

If two NFW halos are lying next to each other they will inevidently have neutrino flow between them, but the flow will most likely be in equilibrium. This means that the number of neutrinos going into a NFW halo is roughly the same as the number of neutrinos going out of the halo, thus making us capable of ignoring this effect.

3.2 Energy considerations for the unbound neutrinos

At the time of the neutrino decoupling one second after Big Bang the relic neutrinos were ultra relativistic. While the Universe expands the neutrinos will cool down, lose momentum and become non-relativistic. However, as stated in chapter 2 the Fermi-Dirac distribution is still of the form given in equation 2.18.

Far away from the gravitational potential the neutrinos will only have kinetic energy given by

$$E \simeq E_{\mathrm{kin}} = \frac{p^2}{2m} \tag{3.4}$$

Hence the momentum can be written as

$$p = (2mE)^{1/2} \tag{3.5}$$

As we move closer to the gravitational potential, the potential energy also starts to have effect on total energy of the unbound neutrinos. When taking the potential energy into account as well, equation (3.5) becomes

$$p = (2m(E_{\mathrm{kin}} + E_{\mathrm{pot}}))^{1/2} \tag{3.6}$$

where the potential energy is given as

$$E_{\mathrm{pot}} = m\Phi(r) \tag{3.7}$$

In chapter 2, I've only considered the unbound neutrinos to have kinetic energy and no potential energy. This is too big a simplification since the unbound neutrinos still will be attracted by the gravitational potential even though this is filled up by the bound neutrinos. Since the gravitational potential energy of the neutrinos will cause the potential to change slowly, the energy of the neutrinos is here

also an adiabatic invariant, whence the number density for the unbound neutrinos, when inserting equations (3.4) and (3.7) into equation (3.6), yields

$$n_{\nu,\text{unbound}} = \frac{4\pi\gamma}{h_p^3} \int_{p_{\text{esc}}}^{\infty} \frac{p^2}{e^{\frac{\left(p^2+2m^2\Phi(r)\right)^{1/2}c}{kT_{\nu,0}}} + 1} \, \mathrm{d}p \tag{3.8}$$

With these alterations at hand I'm able to write a more complete and realistic numerical program and I therefore repeat the numerical calculations from chapter 2 to see the change.

3.3 Results and discussion

As in chapter 2 I'll be doing numerical calculations for a set of NFW halos with virial masses in the range of $M_{\text{vir}} = 10^{12}\, M_\odot \rightarrow 10^{15}\, M_\odot$ and with the three neutrino masses $m_\nu = 0.15\,\text{eV},\ 0.3\,\text{eV},\ 0.6\,\text{eV}$.

I start out by looking at the neutrino overdensities for the various sets of halos and neutrinos. The results are shown in figures 3.1 - 3.4. By comparing these results with the results from chapter 2, which are also included in the plots as well as the RW data, we see that the energy considerations only had an impact close to the halo center on the lighter configurations. The impact however, is very modest. The largest alterations are seen in the lightest configurations, especially the $M_{\text{vir}} = 10^{12}\, M_\odot$ halo with $m_\nu = 0.15\,\text{eV}$ neutrinos. Here the overdensity grows a bit and becomes as the RW data. In the heavy configurations there's less and less alterations in my data compared to those from chapter 2. A large distances the inclusion of the gravitational potential energy for the unbound netrinos caused the total overdensity to rise, most observable for light neutrinos. This means that the introduction of the potential energy in the total energy caused the neutrinos to "flatten" out more compared to the calculations done in chapter 2, thus making the number density equal to the present average $\overline{n}_\nu$ at a further distance from the center of the halo.

We then look at the total unbound mass used in the halos for each configuration. The results are shown in figures 3.5 - 3.8. We quickly see that the unbound neutrinos are weighing more in total than they did in chapter 2, where we didn't include the potential energy. That makes a lot of sense since the gravitational potential, though filled up by the bound neutrinos, still will attract the unbound neutrinos and make them cluster up around the center of the halo. We also see that the largest difference in total mass of the unbound neutrinos from chapter 2 and now is around the center of the halo. As we go to further distances, we see that the mass of the unbound neutrinos in these calculations approach the results

from chapter 2 as it should be, since

$$\Phi(r) \to 0 \quad \text{for} \quad r \to \infty$$

Another important fact is that the total mass of the unbound neutrinos is exceeding that of the homogeneously distributed neutrinos. This is different from chapter 2 where it was the other way around. This is due to the fact, that we've changed the energy of the unbound neutrinos. More unbound neutrinos will be collected in the halo thus making the overdensity rise, that is the Fermi-Dirac occupation number will rise due to the extra energy term. This results in a higher total mass used by the unbound neutrinos. The homogeneously distributed neutrinos are still calculated over the entire Fermi-Dirac distribution, but only with kinetic energy. The small effect from the inclusion of the gravitational potential energy of the unbound neutrinos is enough to make the total mass of the unbound neutrinos exceed that of the homogeneously distributed.

The inclusion of the potential energy for the unbound neutrinos results in a larger amount of neutrinos being clustered up around the center of the halo. At large distances, from the center, the amount of unbound neutrinos approach the amount of neutrinos calculated without the potential energy.

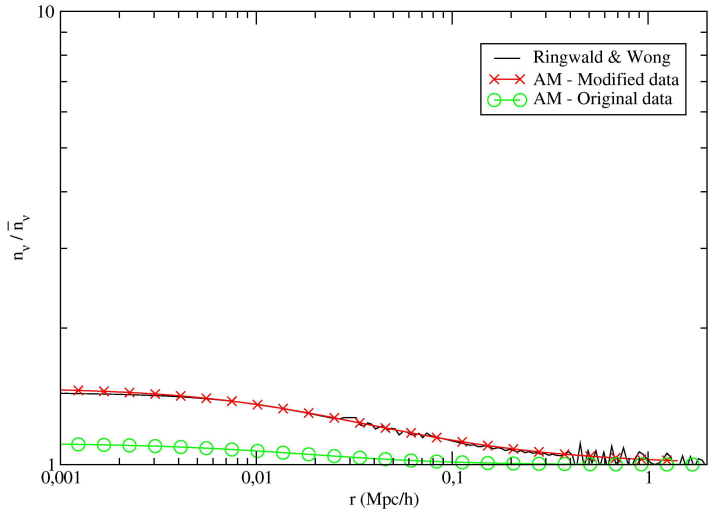

Figure 3.1: Number densities n_ν normalized to present average $\bar{n}_\nu$ for the $m_\nu = 0.15\,\text{eV}$ neutrino in a $M_{\text{vir}} = 10^{12}\,M_\odot$ halo. Included in the plot are the data from RW (solid line), original NFW data (O-line) and the energy modified data (X-line).

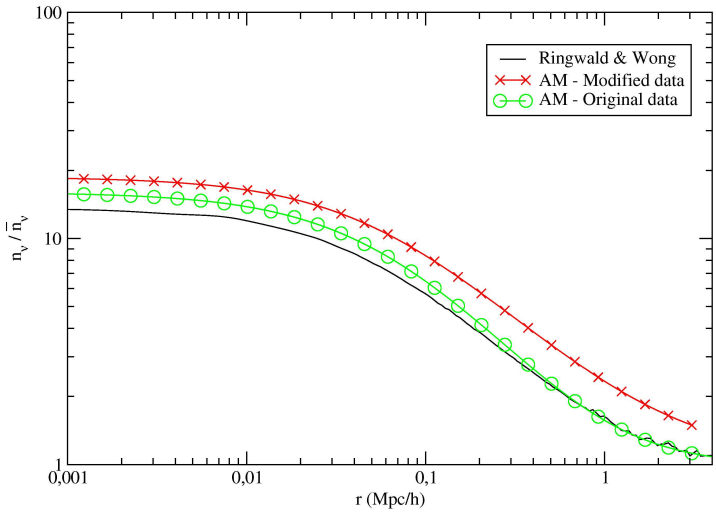

Figure 3.2: Number densities n_ν normalized to present average $\overline{n}_\nu$ for the $m_\nu = 0.3\,\text{eV}$ neutrino in a $M_{\text{vir}} = 10^{13}\,M_\odot$ halo. Included in the plot are the data from RW (solid line), original NFW data (O-line) and the energy modified data (X-line).

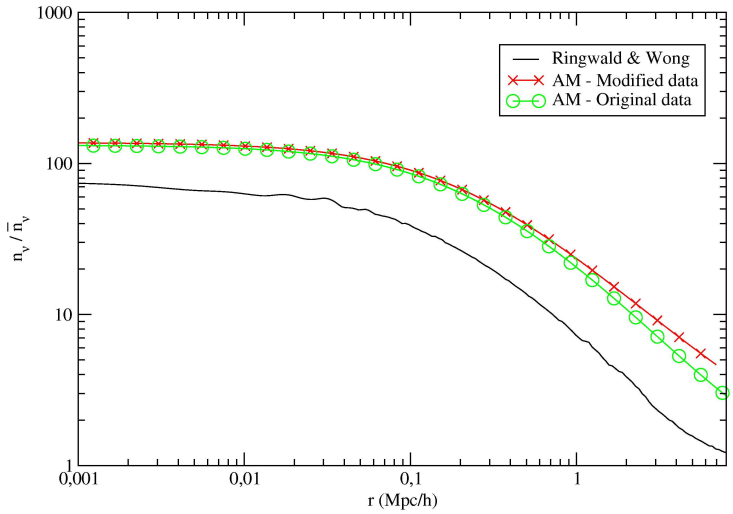

Figure 3.3: Number densities n_ν normalized to present average $\overline{n}_\nu$ for the $m_\nu = 0.3\,\text{eV}$ neutrino in a $M_{\text{vir}} = 10^{14}\,M_\odot$ halo. Included in the plot are the data from RW (solid line), original NFW data (O-line) and the energy modified data (X-line).

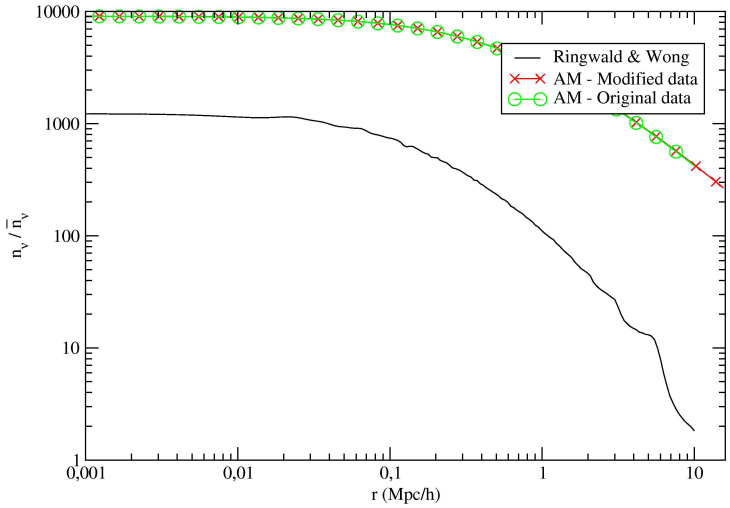

Figure 3.4: Number densities n_ν normalized to present average $\overline{n}_\nu$ for the $m_\nu = 0.6\,\mathrm{eV}$ neutrino in a $M_{\mathrm{vir}} = 10^{15}\,M_\odot$ halo. Included in the plot are the data from RW (solid line), original NFW data (O-line) and the energy modified data (X-line).

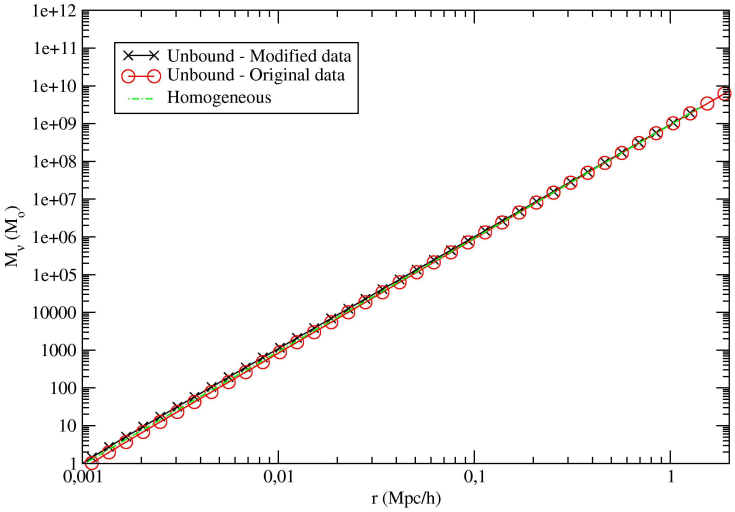

Figure 3.5: Unbound masses used in a $M_{\mathrm{vir}} = 10^{12}\,M_\odot$ NFW halo. Neutrino mass is $m_\nu = 0.15\,\mathrm{eV}$. The plot compares original NFW data (O-line) with the energy modified data (X-line). Dashed-line shows the homogeneously distributed neutrinos.

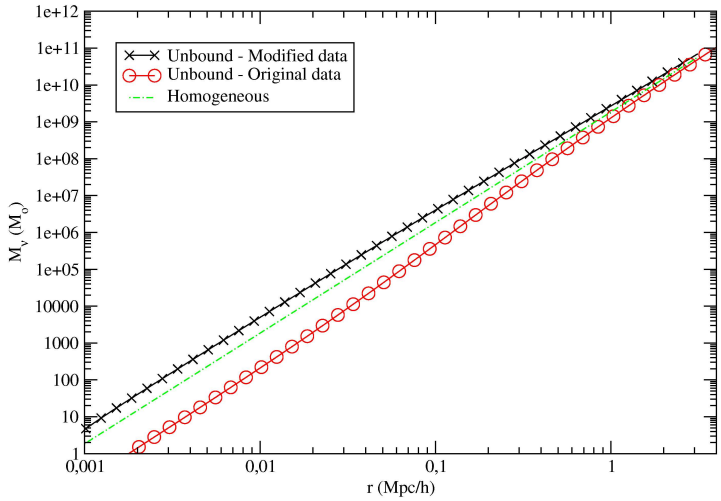

Figure 3.6: Unbound masses used in a $M_{\text{vir}} = 10^{13}\, M_{\odot}$ NFW halo. Neutrino mass is $m_{\nu} = 0.3\,\text{eV}$. The plot compares original NFW data (O-line) with the energy modified data (X-line). Dashed-line shows the homogeneously distributed neutrinos.

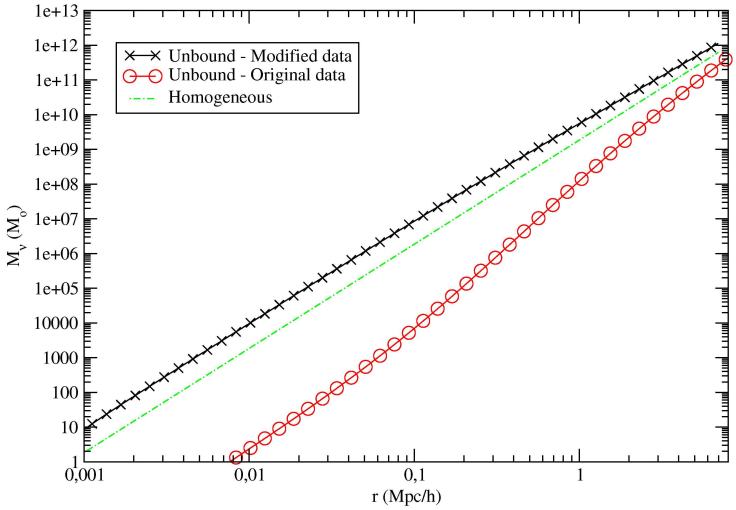

Figure 3.7: Unbound masses used in a $M_{\text{vir}} = 10^{14}\, M_{\odot}$ NFW halo. Neutrino mass is $m_{\nu} = 0.3\,\text{eV}$. The plot compares original NFW data (O-line) with the energy modified data (X-line). Dashed-line shows the homogeneously distributed neutrinos.

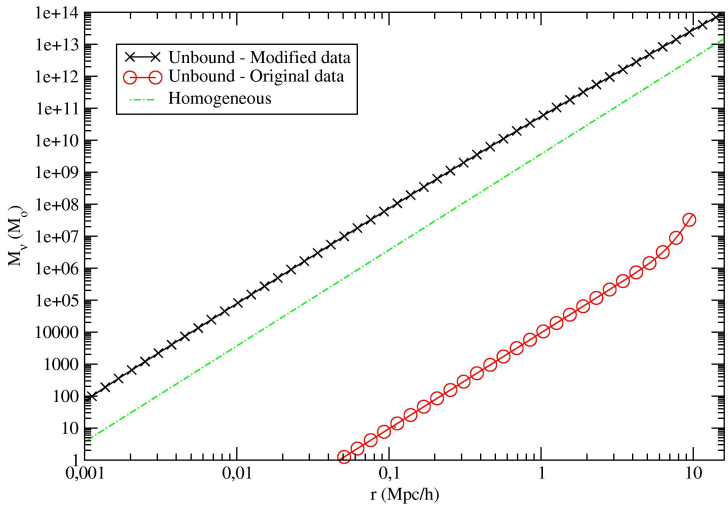

Figure 3.8: Unbound masses used in a $M_{\rm vir} = 10^{15}\,M_\odot$ NFW halo. Neutrino mass is $m_\nu = 0.6\,\text{eV}$. The plot compares original NFW data (O-line) with the energy modified data (X-line). Dashed-line shows the homogeneously distributed neutrinos.

Chapter 4

Phase-space considerations

Until now the bound neutrinos have been assumed to have a fine-grained distribution in the six-dimensional phase-space. A more correct approach to the bound neutrinos in the gravitational potential involves looking deeper into the phase-space discussion. Instead of looking at the microscopic phase-space (fine-grained) I'll look at the macroscopic phase-space (coarse-grained) in which I want to pack my neutrinos into lumps, each with the same coarse-grained occupation number, and thereby having a mean value for the coarse-grained distribution for my neutrinos. In this chapter I'll look at the connection between the fine-grained and coarse-grained distributions in the phase-space. I'll conclude with results and discussion of the results obtained from the numerical calculations.

4.1 Fine-grained and coarse-grained phase-space

During the expansion of the Universe the microscopic phase-space distribution given by equation (2.18) is conserved due to Liouville's theorem. If we assume that we have a homogeneous Universe then the momentum of the neutrinos p is proportional to $1 + z$, hence T_ν must be proportional to $1 + z$ as well in order to satisfy Liouville's theorem.

As stated in chapter 2, I've been using $f = 0.5$, which is the maximum allowed fine-grained phase-space occupation number as noted by (Tremaine and Gunn, 1979). In fact only a few neutrinos have $f \sim 0.5$ which can be seen from figure 4.1 (Madsen and Epstein, 1984). The curve is produced by finding the fraction $N(f)$ of neutrinos having fine-grained phase-space occupation number greater than f, that is

$$N(f) = \frac{\int_0^{p(f)} f(p')p'^2 \mathrm{d}p'}{\int_0^{\infty} f(p')p'^2 \mathrm{d}p'} \tag{4.1}$$

where $p(f)$ is obtained from equation (2.18), hence

$$p(f) = \frac{kT_{\nu,0}}{c} \ln\left(\tfrac{1}{f} - 1\right) \tag{4.2}$$

We quickly see that we can write equation (4.1) as

$$N(f) = \frac{2}{3\zeta(3)} \int_0^{q(f)} \frac{x^2}{e^x + 1} \, \mathrm{d}x \tag{4.3}$$

with

$$q(f) = \ln\left(\tfrac{1}{f} - 1\right) \tag{4.4}$$

While the fine-grained (microscopic) phase-space occupation number is conserved, the coarse-grained (macroscopic) phase-space occupation number can undergo change as low-density phase-space is intermixed with high-density phase-space as noted by (Madsen, 1985; Tremaine *et al.*, 1986).

Let $M(\theta)$ be the mass and $V(\theta)$ be the phase-space volume inside a region where the coarse-grained phase-space occupation number is higher than θ, that is

$$M(\theta) = \int \mathrm{d}\mathbf{x}\mathrm{d}\mathbf{v} F(\mathbf{x}, \mathbf{v}) H[F(\mathbf{x}, \mathbf{v}) - \theta] \tag{4.5a}$$

$$V(\theta) = \int \mathrm{d}\mathbf{x}\mathrm{d}\mathbf{v} H[F(\mathbf{x}, \mathbf{v}) - \theta] \tag{4.5b}$$

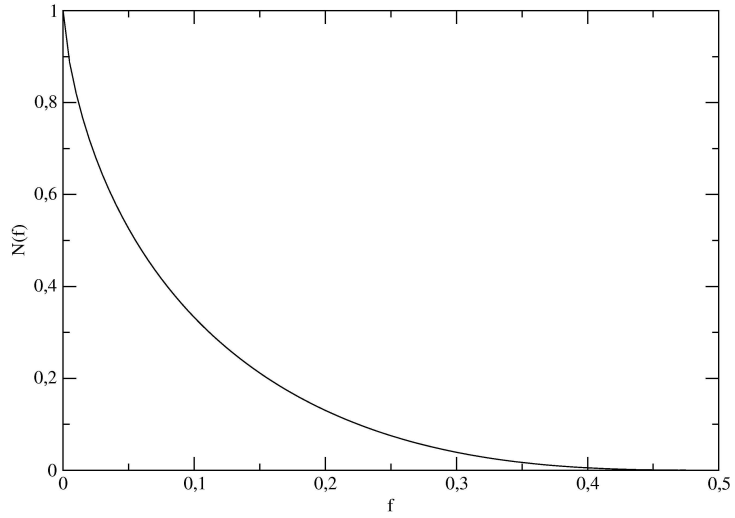

Figure 4.1: Fraction $N(f)$ of neutrinos with fine-grained phase-space occupation number greater than f (Madsen and Epstein (1984)).

Here H is the Heaviside function, which is defined as

$$H(x) = \begin{cases} 0 & x < 0 \\ \frac{1}{2} & x = 0 \\ 1 & x > 0 \end{cases}$$

and F is the particle distribution function. In the initial state both M and V are defined from the fine-grained phase-space distribution f. We define the coarse-grained phase-space occupation number ϕ as the mass per phase-space volume of the fine-grained phase-space distribution. From equations (4.5a) and (4.5b) we're able to find ϕ. The mass of the initial fine-grained region can be calculated as the fraction of neutrinos with fine-grained occupation number higher than f times the mean mass density $\overline{\rho}$ times the integral over the entire space. We calculate the phase-space volume as the volume in momentum phase-space of the neutrinos times the integral over the entire space, hence

$$\begin{aligned} \phi = \frac{M(f)}{V(f)} &= \frac{N(f)\overline{\rho}\int \mathrm{d}\mathbf{x}}{\frac{4}{3}\pi q(f)^3 \int \mathrm{d}\mathbf{x}} \\ &= \frac{9\zeta(3)}{2}\frac{N(f)}{\ln^3\left(\frac{1}{f}-1\right)}\frac{m_\nu}{h_p^3} \end{aligned} \tag{4.6}$$

From equation (4.6) we see that the maximal fraction of neutrinos $\mathcal{N}(\phi)$ able to obtain coarse-grained phase-space occupation number higher than ϕ is $N(f)$. By

calculation $\frac{M}{V}$ in units of $\frac{m_\nu}{h_p^3}$ we get the curve for $(\phi, \mathcal{N}(\phi))$ which can be seen on figure 4.2 as the upper curve. The lower curve represents the $(f, N(f))$ curve. In units of $\frac{m_\nu}{h_p^3}$ we can write equation (4.6) as

$$\phi = \frac{3}{q(f)^3} \int_0^{q(f)} \frac{x^2}{e^x + 1} \mathrm{d}x \tag{4.7}$$

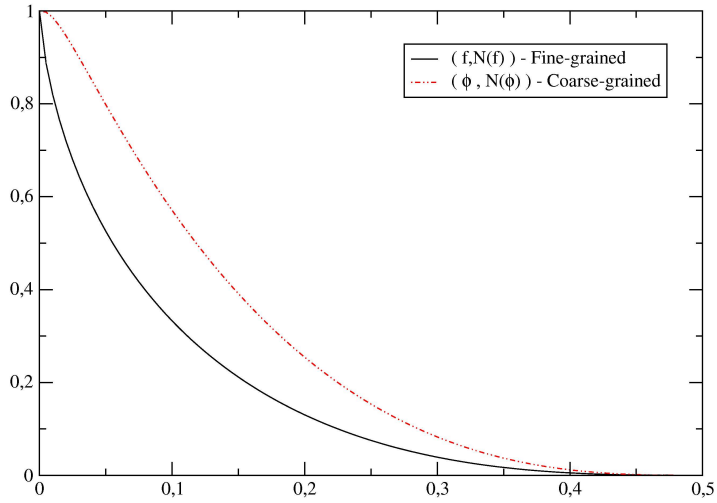

Figure 4.2: Maximal fraction $\mathcal{N}(\phi)$ of neutrinos able to obtain coarse-grained phase-space distribution higher than ϕ (Madsen (1985)).

In order to get a ”mean” value of the coarse-grained phase-space occupation number we first need to find the corresponding fine-grained occupation number. When having the fine-grained occupation number f we can get the coarse-grained ϕ from figure 4.2 by finding the $\mathcal{N}(\phi)$ that corresponds to the $N(f)$ value, hence obtaining ϕ, e.g. $N \simeq 30.4\%$ of the neutrinos have a fine-grained phase-space occupation number $f > 0.11$. A fine-grained phase-space occupation number of $f = 0.11$ corresponds to a coarse-grained phase-space occupation number of $\phi = 0.18$. Thus, the graph can be used as a visual tool of understanding the connection between the coarse-grained and the fine-grained phase-space occupation number.

The fraction of the coarse-grained phase-space occupation number can be expressed in terms of the fraction of the total bound neutrino mass $M_{\nu,\mathrm{bound}}$ in our gravitational potential, thus

$$\mathcal{N}(\phi) = \frac{M_{\nu,\mathrm{bound}}(r_{\mathrm{galaxy}})}{M_\nu(r_{\mathrm{galaxy}})}$$

Since we want to end up with the coarse-grained phase-space occupation number for the bound particles, we calculate the total mass of the bound neutrinos with ϕ

instead of f, which we've used in our numerical calculations until know, and let it be unknown, thus

$$M_{\nu,\text{bound}}(r_{\text{galaxy}}) = \phi\, M^*_{\nu,\text{bound}}(r_{\text{galaxy}}) \tag{4.8}$$

Define $\xi(r_{\text{galaxy}})$ as being

$$\xi(r_{\text{galaxy}}) \equiv \frac{M^*_{\nu,\text{bound}}(r_{\text{galaxy}})}{M_\nu(r_{\text{galaxy}})} \tag{4.9}$$

hence

$$\xi(r_{\text{galaxy}}) = \frac{\mathcal{N}(\phi)}{\phi} \tag{4.10}$$

We know that the fraction of the coarse-grained occupation number is equal to the fraction of the fine-grained occupation number at the f value that corresponds to the ϕ value, hence

$$\begin{aligned}\xi(r_{\text{galaxy}}) &= \frac{N(f)}{\phi} \\ &= \frac{2\phi \ln^3\left(\frac{1}{f} - 1\right)}{9\zeta(3)\phi}\end{aligned}$$

where $N(f)$ is found from equation (4.6) with ϕ in units of $\frac{m_\nu}{h_p^3}$. We see here that the coarse-grained phase-space occupation number drops out, leaving us with the fine-grained phase-space occupation number as long as $\xi(r_{\text{galaxy}})$ is know, which by definition (equation (4.9)) is easily calculated. We therefore end up with the fine-grained phase-space occupation number given as

$$f = \frac{1}{e^{\left(\frac{9\xi(r_{\text{galaxy}})\zeta(3)}{2}\right)^{1/3}} + 1} \tag{4.11}$$

From here we can calculate the coarse-grained phase-space occupation number by inserting equation (4.11) into equation (4.7). We've hereby found the mean coarse-grained occupation number which we'll use in the calculations from now on. We've packed our fine-grained distributed neutrinos into lumps of coarse-grained distributed neutrinos in our phase-space. In our gravitational potential we might have low ϕ values at one point, high ϕ values at another and maybe these will mix, but since we've found a mean value for ϕ in our gravitational potential, we can ignore whether the bound neutrinos mix or stay in regions with the same coarse-grained occupation number.

With these considerations at hand I rerun my numerical calculations and compare them with the results from chapters 2 and 3. In the following section a discussion of the numerical results is made.

4.2 Results and discussion

As before, I repeat my numerical calculations with exactly the same 12 possible configurations of virial mass and neutrino mass. Again I start out by looking at the overdensities for each configuration and compare them with the results from chapter 2.

The results from my new and adjusted numerical calculations can be seen in figures 4.3 - 4.6. We quickly see that the introduction of the mean coarse-grained phase-space occupation number is causing the bound neutrino overdensity to drop. Eventhough the introduction of the potential energy for the unbound neutrinos in chapter 3 caused the total overdensity to rise a bit, the introduction of the mean coarse-grained phase-space occupation number is causing the total overdensity to fall close to the center of the halo, compared to the "simple" scenario in chapter 2. This effect of less clustering of the neutrinos around the center of the halo is observed for the following configurations $\{m_\nu, M_{\rm vir}\} = (\{0.6\,{\rm eV}, 10^{12}\,M_\odot\}\,, \{0.3\,{\rm eV}, 10^{13}\,M_\odot\}\,, \{0.6\,{\rm eV}, 10^{13}\,M_\odot\})$ and all the configurations for the two heavier halos. The rest of the configurations have higher overdensities around the center of the halo. More neutrinos are clustering up together in the heart of the gravitational potential for the light NFW halos compared with the results in chapter 2. This is because the unbound neuntrinos became much more important for the light configurations after introducing gravitational potential energy in their total energy. For the heaviest halos we see that the overdensities have dropped quite a lot, roughly between a factor ~ 1.5 for the $m_\nu = 0.15\,{\rm eV}$ neutrinos in a $10^{14}\,M_\odot$ halo and $\sim 20 - 30$ for the $m_\nu = 0.6\,{\rm eV}$ neutrinos in a $10^{15}\,M_\odot$ halo, compared to the results from chapter 2. Even at large distances from the center of the halo, the overdensities are well below the number densities calculated in chapter 2.

We again turn to the scenario with the total used masses in the halo. The results of the numerical calculations can be seen in figures 4.7 - 4.10.

We quickly note that the total mass of the bound neutrinos has dropped below the mass calculated in chapter 2. In the light $10^{12}\,M_\odot$ halo the bound neutrinos are roughly taking up the same amount of mass as they did in chapter 2, but as we move to heavier halos the mass used by the bound neutrinos drops down to around a factor ~ 500 less than the masses used in chapter 2. This is a clear consequence of the introduction of the mean coarse-grained phase-space occupation number. We saw from figure 4.1 that only a very small percentage of the neutrinos would have an fine-grained occupation number with the value 0.5, hence we found the mean coarse-grained occupation number which describes the system more realistically from a macroscopic point of view. We see that the heavier configurations cause a bigger alteration in the total bound neutrino mass compared with chapter 2. From the lightest configuration with $m_\nu = 0.15\,{\rm eV}$ and $M_{\rm vir} = 10^{12} M_\odot$ to the heaviest with $m_\nu = 0.6\,{\rm eV}$ and $M_{\rm vir} = 10^{15} M_\odot$ we see that the drop in the total

bound mass is between a factor ≈ 2 for the lightest configuration and a factor ≈ 500 for the heaviest configuration. Thus the introduction of the coarse-grained phase-space occupation number had the biggest influence on the heavier configurations in my numerical calculations. The consequences of this influence will be discussed further in chapter 8 where detection of relic neutrinos will be discussed.

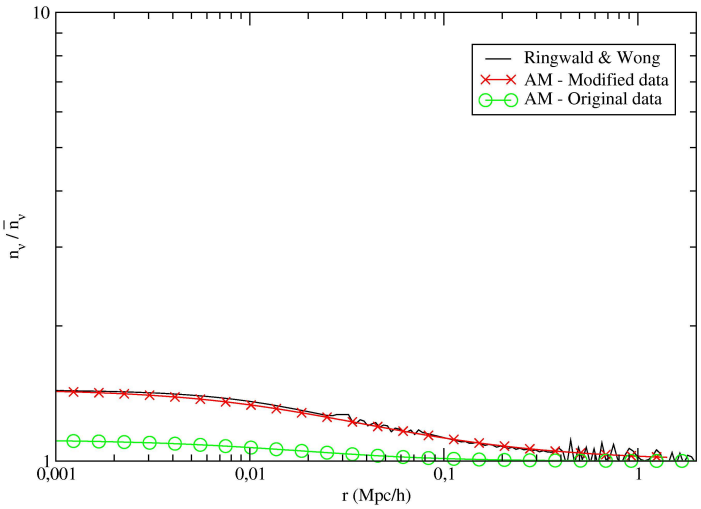

Figure 4.3: Number densities n_ν normalized to present average $\overline{n}_\nu$ for the $m_\nu = 0.15\,\mathrm{eV}$ neutrino in a $M_{\mathrm{vir}} = 10^{12}\,M_\odot$ NFW halo. Included in the plot are the data from RW (solid line), original NFW data (O-line) and the phase-space modified data (X-line).

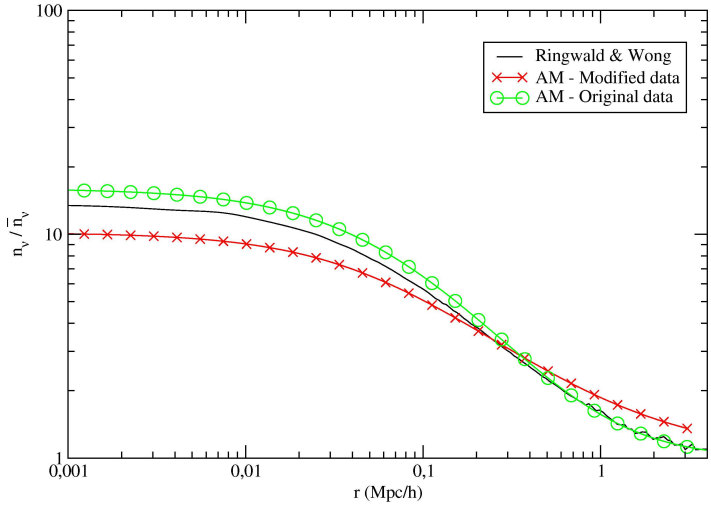

Figure 4.4: Number densities n_ν normalized to present average $\bar{n}_\nu$ for the $m_\nu = 0.3\,\mathrm{eV}$ neutrino in a $M_{\mathrm{vir}} = 10^{13}\,M_\odot$ NFW halo. Included in the plot are the data from RW (solid line), original NFW data (O-line) and the phase-space modified data (X-line).

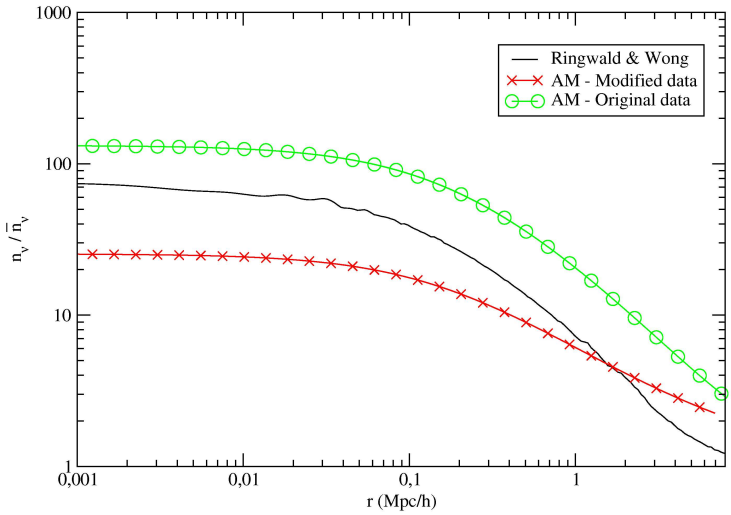

Figure 4.5: Number densities n_ν normalized to present average $\bar{n}_\nu$ for the $m_\nu = 0.3\,\mathrm{eV}$ neutrino in a $M_{\mathrm{vir}} = 10^{14}\,M_\odot$ NFW halo. Included in the plot are the data from RW (solid line), original NFW data (O-line) and the phase-space modified data (X-line).

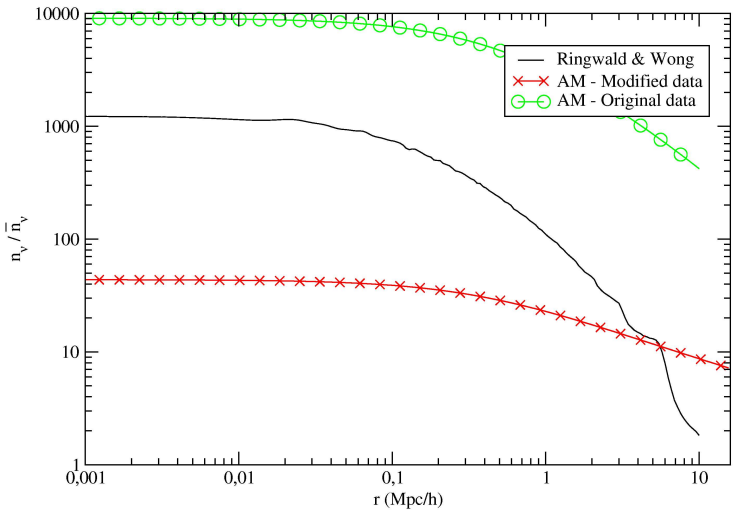

Figure 4.6: Number densities n_ν normalized to present average $\bar{n}_\nu$ for the $m_\nu = 0.6\,\mathrm{eV}$ neutrino in a $M_{\mathrm{vir}} = 10^{15}\,M_\odot$ NFW halo. Included in the plot are the data from RW (solid line), original NFW data (O-line) and the phase-space modified data (X-line).

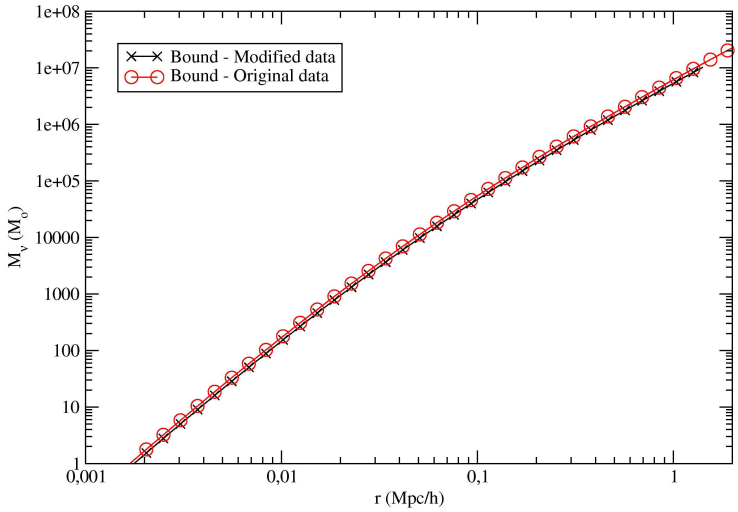

Figure 4.7: Bound masses used in a $M_{\mathrm{vir}} = 10^{12}\,M_\odot$ NFW halo. Neutrino mass is $m_\nu = 0.15\,\mathrm{eV}$. The plot compares original NFW data (O-line) with the phase-space modified data (X-line).

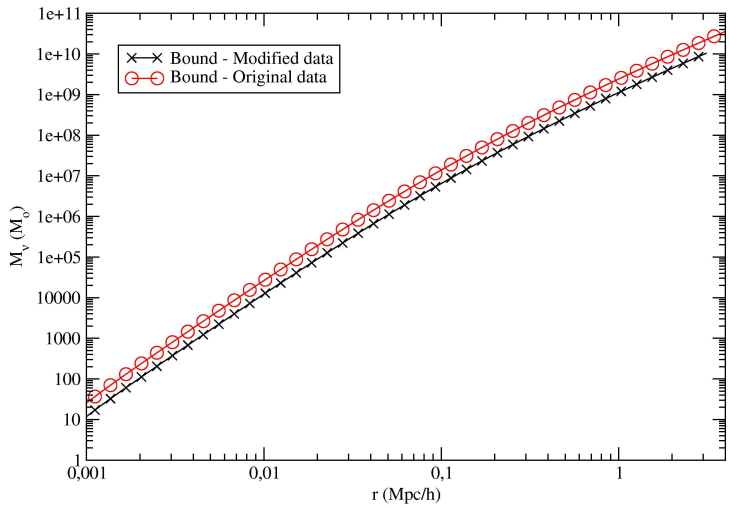

Figure 4.8: Bound masses used in a $M_{\rm vir} = 10^{13}\,M_\odot$ NFW halo. Neutrino mass is $m_\nu = 0.3\,\mathrm{eV}$. The plot compares original NFW data (O-line) with the phase-space modified data (X-line).

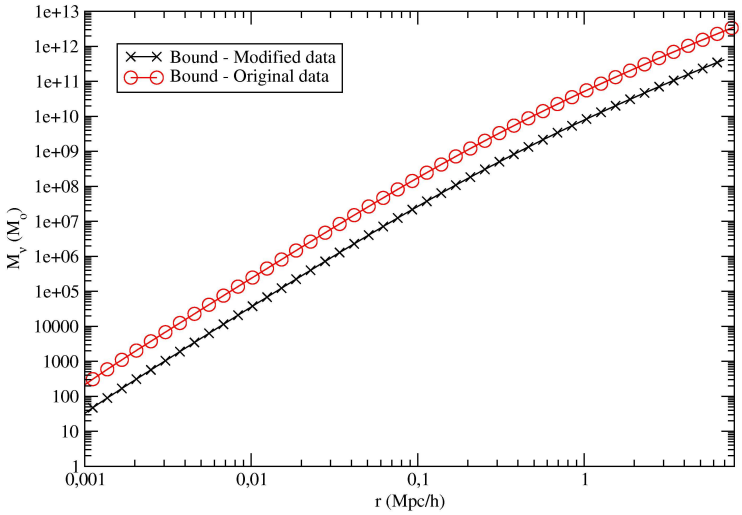

Figure 4.9: Bound masses used in a $M_{\rm vir} = 10^{14}\,M_\odot$ NFW halo. Neutrino mass is $m_\nu = 0.3\,\mathrm{eV}$. The plot compares original NFW data (O-line) with the phase-space modified data (X-line).

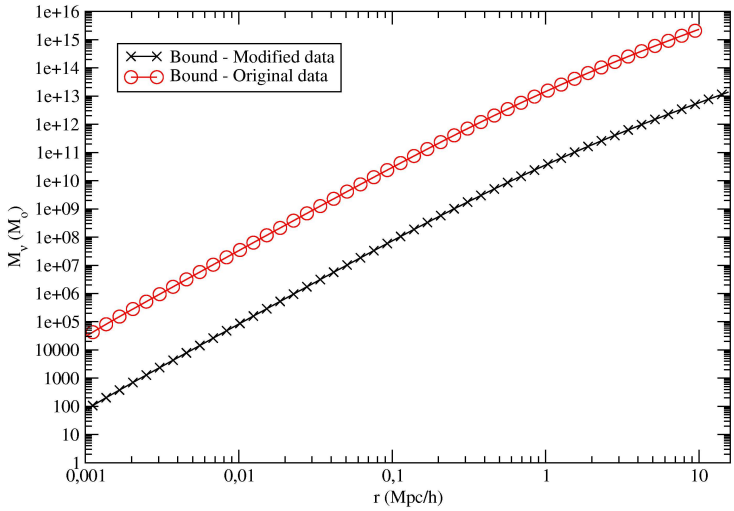

Figure 4.10: Bound masses used in a $M_{\rm vir} = 10^{15}\,M_\odot$ NFW halo. Neutrino mass is $m_\nu = 0.6\,\mathrm{eV}$. The plot compares original NFW data (O-line) with the phase-space modified data (X-line).

Chapter 5

Black holes

Until now I've been looking at neutrino clustering in NFW galactic halos. I now turn to look at clustering in a point mass gravitational potential like the gravitational potential around a black hole. I start out with the theory of the point mass potential and the considerations I've made regarding the implementation of this potential in my numerical calculations. I conclude with the results from my numerical calculations.

5.1 History of the black holes

As early as in 1783, when the British geologist and astronomer John Michell[1] wrote in an article to the Royal Society that a star, with radius 500 times larger than the radius of the Sun and with the same density as the Sun, would have a gravitational field so strong on the surface that the escape velocity would exceed the speed of light, the main points of the later named black holes have been known. 13 years later, in 1796, Laplace published Michell's ideas and calculated that a star with radius 250 times larger than the Sun and with density equal to the density of the Earth would have an escape velocity exceeding the speed of light. But not until Einstein published his General theory of relativity in 1915 was the idea given any further thought.

Already the year after, in 1916, Karl Schwarzschild derived a general relativistic solution from Einstein's field equations in vacuum[2] for the gravitational field surrounding a spherical mass. Schwarzschild's solution, which is the only spherical symmetric vacuum solution to Einstein's field equations, turned out to be a complete description of a spherical, eletrically neutral, non-rotating black hole. Schwarzschild's solution is today known as the Schwarzschild metric.

After Chandrasekhar in 1930 discovered the existence of the upper mass limit for complete degenerate matter, Eddington quickly noted that the formation of black holes would have to be the inevitable fate of massive stars. But he didn't think that nature worked in that way and wrote the whole thing off by modifying the equation of state of a degenerate relativistic gas so that equilibrium would exist for stars of arbitrary mass.

In 1939 came the first calculation that demonstrated the formation of a black hole. This calculation was made by Oppenheimer and Snyder. With their calculations of the collaps of a homogeneous sphere of pressureless gas in general relativity, they showed that the sphere becomes cut from all communication with the rest of the Universe, which is one of the key proporties with black holes.

In 1963 Roy Kerr found an exact family of charge-free solutions to Einstein's vacuum field equations for charge-free rotating systems. But it wasn't until 1968, in a lecture given by Wheeler, that the black holes got their name. Before that time they were called frozen stars and dark stars. (Shapiro and Teukolsky, 1983).

Today black holes are widely accepted as real and existing objects in the Universe. It is believed that most galaxies have a super-massive black hole located in the center.

[1] (Carrol and Ostlie, 1996) claims that his name was George Michell and that he was an English clergyman and amateur astronomer.

[2] This solution is *only* valid *outside* the object itself.

5.2 Theory

Eventhough black holes are very complex, they can be completely described by the three measurable parameters, mass M_{BH}, charge Q and angular momentum J. The most simple black holes are the so-called Schwarzschild black holes which are non-rotating, charge-free black holes, that is $J = Q = 0$. To describe this type of black hole we turn to the schwarzschild metric, which is given as:

$$\mathrm{d}s^2 = \left(1 - \frac{2GM_{\mathrm{BH}}}{c^2 r}\right) c^2 \mathrm{d}t^2 - \left(1 - \frac{2GM_{\mathrm{BH}}}{c^2 r}\right)^{-1} \mathrm{d}r^2 - r^2 \Omega^2 \tag{5.1}$$

where the angular part of the Schwarzschild metric is defined as

$$\mathrm{d}\Omega^2 \equiv \mathrm{d}\theta^2 + \sin^2(\theta)\mathrm{d}\phi^2 \tag{5.2}$$

We note that the Schwarzschild metric is singular at

$$r = R_s = \frac{2GM_{\mathrm{BH}}}{c^2} \tag{5.3}$$

which is known as the Schwarzschild radius (d'Inverno, 1992). This radius denotes the size of a black hole. I'll be doing purely classical calculations and thus considering the black hole as a point mass. My calculations will therefore be very unrelativistic. For a comprehensive study of how to do the strictly relativistic calculations, I refer to (Shapiro and Teukolsky, 1983). A good distance from R_s of a black hole the black hole will pretty much behave as a point mass, hence I'm able to simply generalize my study to that of the point mass potential.

From classical mechanics we know the gravitational potential from a black hole is given by the point mass potential,

$$\Phi(r) = -\frac{GM_{\mathrm{BH}}}{r} \tag{5.4}$$

hence the escape velocity becomes

$$v_{\mathrm{esc}}(r) = \sqrt{2\left|\frac{-GM_{\mathrm{BH}}}{r}\right|} \tag{5.5}$$

5.3 Setup for numerical calculations

In my numerical calculations I'm looking at a single black hole with a gravitational potential given by equation (5.4). I'm starting my calculations at $2R_s$ and I end them at a distance of $r = 10\,\mathrm{pc}$ away from the singularity of the black hole.

The temperature of the neutrinos is again taking to be the present day neutrino temperature $kT_{\nu,0} = 1.676 \cdot 10^{-4}\,\text{eV}$.

I run my numerical calculations with different configurations of masses both for the neutrinos and for the black hole. I use the same neutrino masses as in the previous chapters about the NFW halos. The black hole masses, M_{BH}, used will be $10^6\,M_\odot$ (the central black hole in our Milky Way galaxy, Sagitarius A*, is $\sim 3.7 \cdot 10^6\,M_\odot$ (Ghez *et al.*, 2005)), $10^7\,M_\odot$ (central black hole of the NGC 4258 galaxy, which can be found in the constellation of Canes Venatici ("Hunting Dogs"), with a mass of $M_{\text{BH}} \sim 3.9 \cdot 10^7\,M_\odot$ (Herrnstein *et al.*, 1999)), $10^8\,M_\odot$ (central black hole in the satellite galaxy NGC 4486b[3], which is roughly $M_{\text{BH}} \sim 5.0 \cdot 10^8\,M_\odot$ (Magorrian *et al.*, 1998)) and $10^9\,M_\odot$ (the central black hole in M87 is $\sim 3.2 \cdot 10^9\,M_\odot$ (Macchetto *et al.*, 1997)).

As in the previous chapter I'll calculate both the total overdensities for the neutrinos and the total mass which the neutrinos use. I'll be looking at the total configuration consisting of both bound and unbound neutrinos. Experiences with the phase-space considerations from chapter 4 tells us that the fine-grained phase-space occupation number f is equal to the coarse-grained phase-space occupation number ϕ with the value $f \simeq \phi \simeq 0.5$. I'll still use the coarse-grained phase-space though. The unbound neutrinos will again be calculated using the entire phase-space distribution $f(p)$.

5.4 Results and discussion

With the theory for the point mass potential at hand, I reprogram my numerical calculations program and run the twelve different configurations.

When looking at the overdensities we quickly note that the there's a very high concentration of neutrinos close to the black hole, but that it drops rapidly as the distance to the black hole is increased. This tremendeous clustering effect is a direct consequence of the infinite gravitational well created by the black hole. The results of the numerical calculations for the overdensities are shown in figures 5.1 - 5.4. For the "light" $10^6\,M_\odot$ and $10^7\,M_\odot$ black holes there are large separations between the three neutrino masses in the plots, but as the mass of the black hole is raised the separation becomes smaller and smaller. For the heavy $10^9\,M_\odot$ the $m_\nu = 0.3\,\text{eV}$ and $m_\nu = 0.6\,\text{eV}$ neutrinos have the same overdensity out until $\sim 0.1\,\text{pc}$ away from the black hole.

In figures 5.5 - 5.8 we see the total masses used in the gravitational potential of the black hole for which we're looking. If we look at figures 5.1 - 5.4 again, we note the number density drops to the average present value $\overline{n}_\nu$. If we then again

[3]The NGC 4486b is a satellite galaxy of M87, which is also known as NGC 4486.

turn to mass plots, we now see that, at the point where the number density becomes equal to $\overline{n}_\nu$, there's a small bend upwards in the curve and the total neutrino mass is increasing quite fast from that point on. It might seem a bit odd that the total mass of the neutrinos used suddenly increases rapidly far from the black hole, but this can easily be explained after giving it some thought. When moving away from the black hole, the total neutrino number density drops until it reaches the average present value $\overline{n}_\nu$, whereafter it becomes constant. When the overdensity is constant, the total mass will increase constantly as r^3, but when the overdensity drops closer to the black hole, the increase in mass will have to be less than r^3 and it can't be constant. Therefore, we have a more flat mass curve until we reach the point where the number density becomes equal to $\overline{n}_\nu$. From here on the total mass will increase constantly by r^3. We also note that this effect means that the total mass close to the black hole will be larger than it would if the mass increased constantly with r^3. We note this by expanding the r^3 part of the curve backwards. This line drops heavily below the present curve.

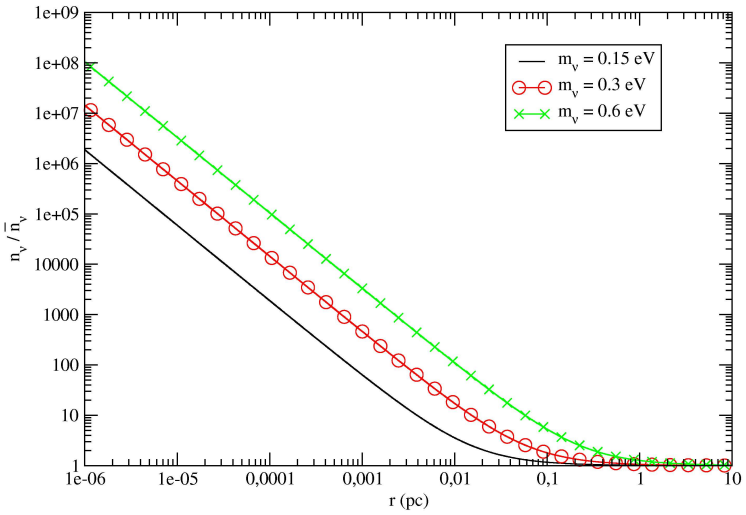

Figure 5.1: Number densities n_ν normalized to present average $\overline{n}_\nu$ around a $M_{\mathrm{BH}} = 10^6\, M_\odot$ black hole. Solid line denotes $m_\nu = 0.15\,\mathrm{eV}$, O-line $m_\nu = 0.3\,\mathrm{eV}$ and X-line $m_\nu = 0.6\,\mathrm{eV}$

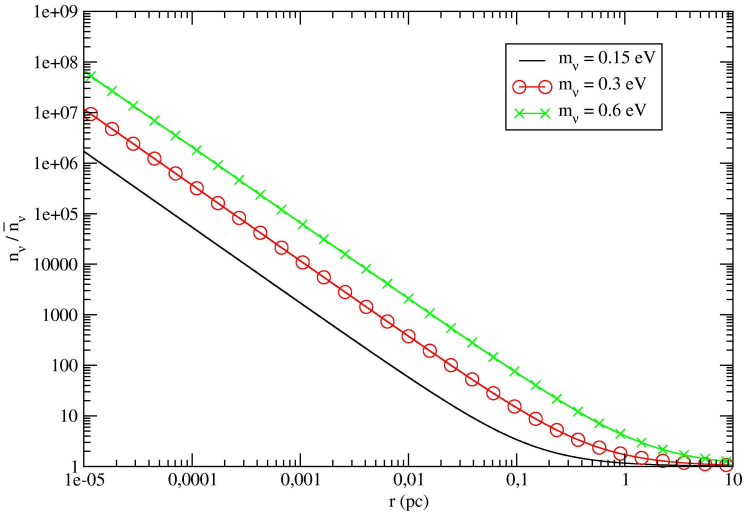

Figure 5.2: Number densities n_ν normalized to present average $\bar{n}_\nu$ around a $M_{\mathrm{BH}} = 10^7\, M_\odot$ black hole. Solid line denotes $m_\nu = 0.15\,\mathrm{eV}$, O-line $m_\nu = 0.3\,\mathrm{eV}$ and X-line $m_\nu = 0.6\,\mathrm{eV}$

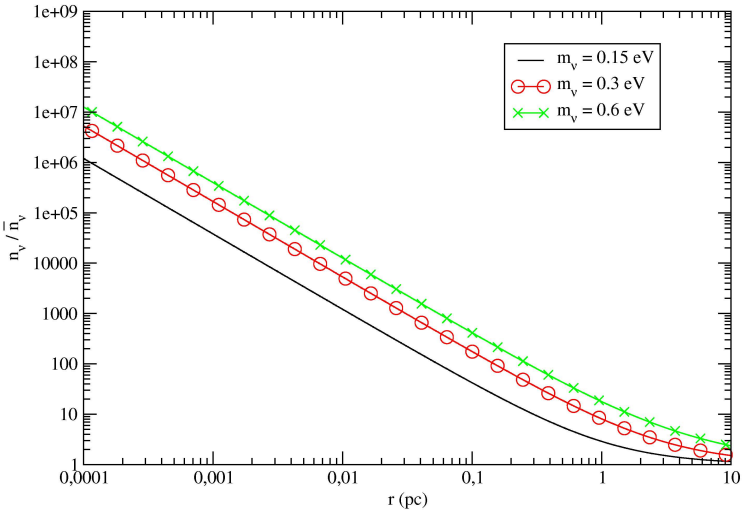

Figure 5.3: Number densities n_ν normalized to present average $\bar{n}_\nu$ around a $M_{\mathrm{BH}} = 10^8\, M_\odot$ black hole. Solid line denotes $m_\nu = 0.15\,\mathrm{eV}$, O-line $m_\nu = 0.3\,\mathrm{eV}$ and X-line $m_\nu = 0.6\,\mathrm{eV}$

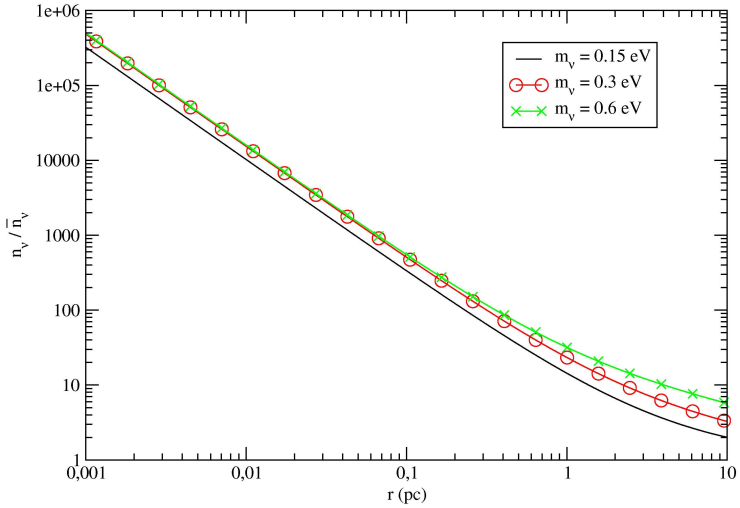

Figure 5.4: Number densities n_ν normalized to present average $\bar{n}_\nu$ around a $M_{\mathrm{BH}} = 10^9\, M_\odot$ black hole. Solid line denotes $m_\nu = 0.15\,\mathrm{eV}$, O-line $m_\nu = 0.3\,\mathrm{eV}$ and X-line $m_\nu = 0.6\,\mathrm{eV}$

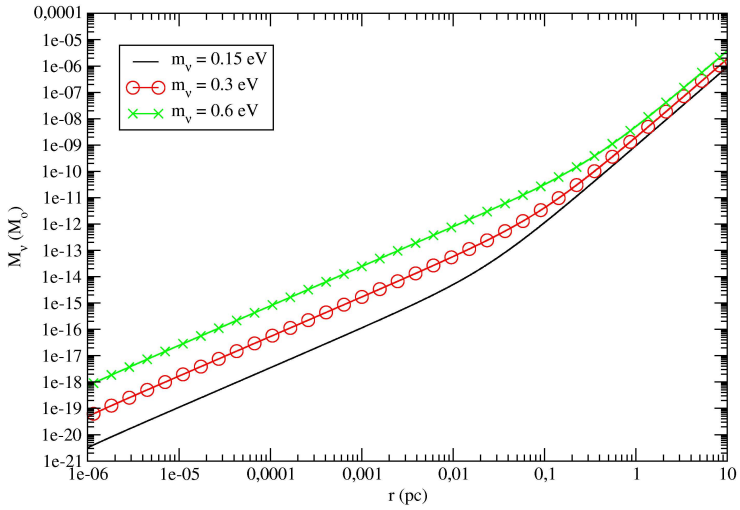

Figure 5.5: Masses used in the gravitational potential of a $M_{\mathrm{BH}} = 10^6\, M_\odot$ Black Hole. Solid line denotes $m_\nu = 0.15\,\mathrm{eV}$, O-line $m_\nu = 0.3\,\mathrm{eV}$ and X-line $m_\nu = 0.6\,\mathrm{eV}$

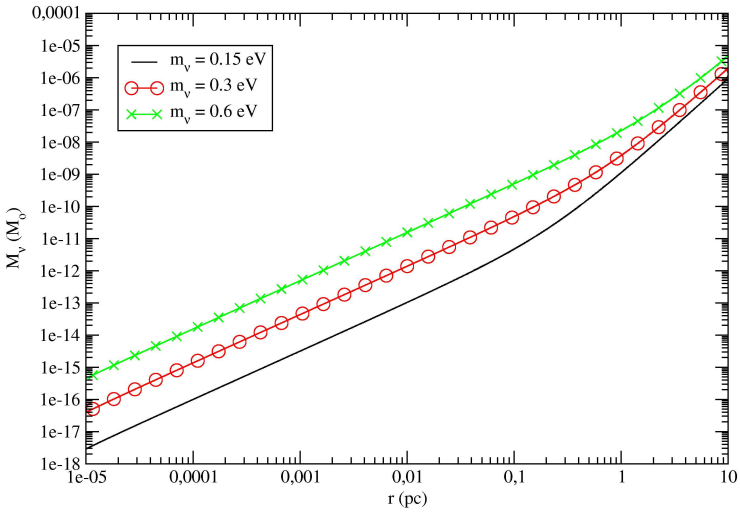

Figure 5.6: Masses used in the gravitational potential of a $M_{\rm BH} = 10^7\,M_\odot$ Black Hole. Solid line denotes $m_\nu = 0.15\,$eV, O-line $m_\nu = 0.3\,$eV and X-line $m_\nu = 0.6\,$eV

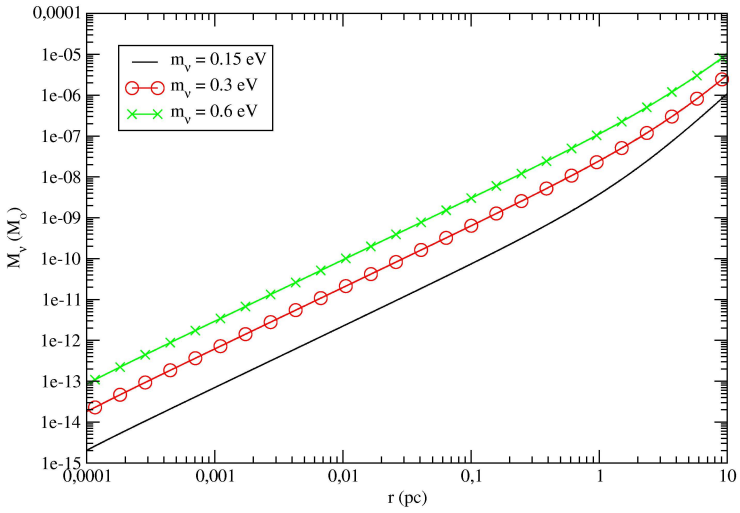

Figure 5.7: Masses used in the gravitational potential of a $M_{\rm BH} = 10^8\,M_\odot$ Black Hole. Solid line denotes $m_\nu = 0.15\,$eV, O-line $m_\nu = 0.3\,$eV and X-line $m_\nu = 0.6\,$eV

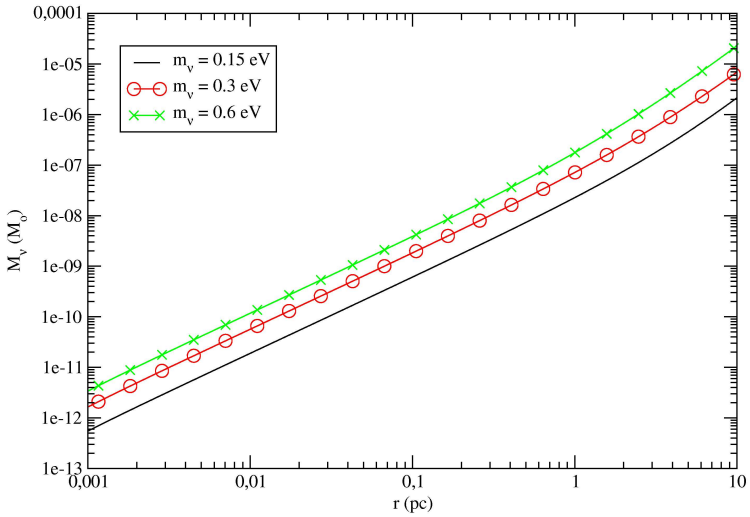

Figure 5.8: Masses used in the gravitational potential of a $M_{\mathrm{BH}} = 10^9\, M_\odot$ Black Hole. Solid line denotes $m_\nu = 0.15\,\mathrm{eV}$, O-line $m_\nu = 0.3\,\mathrm{eV}$ and X-line $m_\nu = 0.6\,\mathrm{eV}$

Chapter 6

NFW halos with central black hole

So far galaxies and black holes have been separated from each other and I've only looked at the effects of gravitational potentials individually. An obvious choice of a gravitational potential will be to combine the black hole potential with the NFW potential, since most galaxies are believed to be the home of supermassive black holes which are located at the halo centers. By combining the knownledge gathered from the previous numerical calculations, I create a new type of gravitational potential and redo my numerical calculations.

6.1 The galactic potential

In chapter 2, I introduced the gravitational potential for a cold dark matter halo, the so-called NFW potential $\Phi_{\text{NFW}}(r)$, as suggested by (Navarro *et al.*, 1996) and in chapter 5, I introduced the well-known classical gravitational potential for a single black hole (the point mass potential) $\Phi_{\text{BH}}(r)$.

By combining the two potentials we create a new gravitational potential in which a black hole is located in the center of a NFW galaxy. We recall that the NFW potential and the point mass potential is given as, respectively

$$\Phi_{\text{NFW}}(r) = -4\pi G\rho_s \frac{r_s^3}{r}\left(\ln\left(1+\frac{r}{r_s}\right)\right)$$

$$\Phi_{\text{BH}}(r) = -\frac{GM_{\text{BH}}}{r}$$

Thus giving us the gravitational potential

$$\begin{aligned}\Phi(r) &= \Phi_{\text{NFW}}(r) + \Phi_{\text{BH}}(r) \\ &= -4\pi G\rho_s \frac{r_s^3}{r}\left(\ln\left(1+\frac{r}{r_s}\right)\right) - \frac{GM_{\text{BH}}}{r}\end{aligned} \tag{6.1}$$

This new gravitational potential, which obeys the Poisson equation, gives rise to the exact same density profile as for the NFW potential alone. Only at the exact center of this new potential, does the density profile differ. Here it becomes infinite due to the behavior of the point mass potential when $r = 0$. Of course the influence of a central black hole would have caused the density profile of the fitted NFW halo to look differently, but I assume that the NFW density profile and thus the general expressions for M_{halo}, r_s, ρ_s etc. introduced in chapter 2 are valid for this type of potential as well.

If we look at the graphical representation of the potential, we find that it resembles that of the point mass potential a great deal. But a further examination reveals that the newly created mixture potential has a more ”flat” profile around the black hole. The potential itself is depicted in a three dimensional illustration in figure 6.1

Since the same density profile is valid for this potential as well as for the NFW potential, we can reuse the parameters as mentioned in chapters 2, 3 and 4. But because we can use the parameters and profiles for the NFW galaxies we expect the central black hole, which total mass is $10^3 - 10^9$ times smaller than that of the NFW halo, only to have a small effect on the total mass of the neutrinos captured in the gravitational potential. The effect would of course be massive close to the

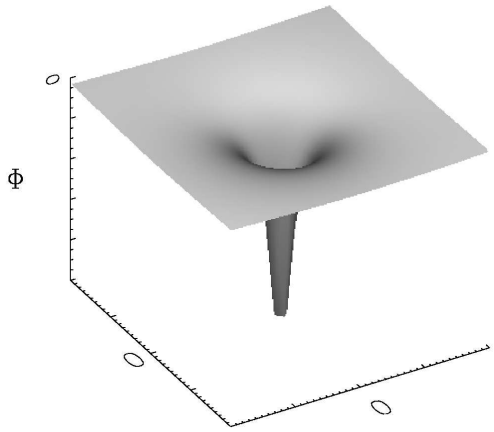

Figure 6.1: Graphical representation of the combined NFW and point mass potential.

black hole, but as we move out into the halo, the influence of the black hole will decrease rapidly and we expect to end up with results very close to those of the pure NFW galaxies from chapter 4. We would also expect that the mass of the black hole should be close to that of the halo itself at distances close to the center of the halo. If we for instance have a $10^6\,M_\odot$ black hole and look at a $10^{13}\,M_\odot$ virial mass NFW galaxy at a distance of 1 kpc from the center, the weight of the halo itself is $\sim 10^9\,M_\odot$. The black hole, therefore, is roughly a factor 10^3 lighter than the NFW halo, hence we wouldn't expect to see any effect on the results from the black hole. But if we instead have a $10^9\,M_\odot$ black hole, the halo mass would roughly equal that of the black hole, hence it would cause alterations in the calculations compared to those of chapter 4.

Since we again are working with large halo masses, in the range of $M_{\rm vir} = 10^{12} \rightarrow 10^{15}\,M_\odot$, we need to coarse-grain the our phase-space, since practically none of the neutrinos in the NFW halos have a fine-grained phase-space occupation number of $f = 0.5$. So we need to pack the neutrinos into lumps, each with the same mean coarse-grained phase-space occupation number. We found the connection between the fine-grained and the coarse-grained phase-space in chapter 4, thus we can easily do the transformations in phase-space by reusing our program code already developed.

6.2 Setup for the calculations

The experience from chapter 5 told us, that already at a distance of $r \sim 1 - 10$ pc away from the black hole the overdensity would equal 1 for most of the black hole scenarios. Only the super massive $M_{\rm BH} = 10^9\,M_\odot$ still have an effect at

that distance. Combined with the above mentioned fact that only black holes with masses similar to that of the NFW halo itself will have any effect on the gravitational potential, I therefore choose only to include a black hole with a mass of $3.2 \cdot 10^9\, M_\odot$ (equal to that of the central black hole of the M87 galaxy) in my combined NFW + Black Hole potential. The other black holes wouldn't have any substantial influence on the neutrino clustering, except if we move really close to the center of the gravitational potential, of course.

Also I begin my plotting closer to the center of the NFW halo instead of just from $r = 1\,\mathrm{kpc}/h$ as I did in chapter 4. In this way I get to the point where the mass of the black hole actually exceeds that of the NFW halo, which should cause a noticable alteration in the numerical calculations compared to those of earlier ones where I only looked at a "pure" NFW galactic halo.

6.3 Results and discussion

I ran my numerical calculations program with the same virial NFW masses as previous and with the same neutrino masses. To examine the impact from the black hole on the calculations I decided to begin my plots at the distance of $1\,\mathrm{pc}/h$ away from the center of the gravitational potential. Experiences from the results in chapter 4 told me that I needed to go around a factor 10 closer to the center in order to have the mass of the smallest black hole equal that of the NFW halo, since the mass of the halo is roughly proportional to r^3 for small distances (see equation (2.8)). But also the experiences from the studies of the single black hole in chapter 5 told me that the number densities for the $10^6\, M_\odot$ black holes starts to equal the present average value $\overline{n}_\nu$ around a distance of $1\,\mathrm{pc}$. Thus I needed to go at least back to $r = 1\,\mathrm{pc}/h$ in order to see the effects from the central black hole in the heaviest configuration, that is $\{m_\nu\,,\, M_{\mathrm{BH}}\,,\, M_{\mathrm{vir}}\} = \left\{0.6\,\mathrm{eV}\,,\, 3.2 \cdot 10^9\, M_\odot\,,\, 10^{15}\, M_\odot\right\}$.

In figures 6.2 - 6.5 the overdensities are plotted. We see that the influence from the black hole in the lightest configuration is causing the overdensity to increase radically. In fact at the distance of $r \sim 1\,\mathrm{pc}/h$ the overdensity is raised by a factor of ~ 100. But as noted in chapter 5, we see that the overdensity also drops rapidly as we move out into the galaxy, which is caused by the declining influence of the central black hole.

If we then turn to the heaviest $10^{15}\, M_\odot$ NFW halo with the heaviest $0.6\,\mathrm{eV}$ neutrinos, which is plotted in figure 6.5, we quickly see that the central black hole never gets to have any major influence on the number density, only in the distance of $r \sim 1\,\mathrm{pc}/h$ to $r \sim 10\,\mathrm{pc}/h$ is the influence noticable (roughly a factor ~ 4 larger number density at $r \sim 1\,\mathrm{pc}/h$.

We can now look at how much mass, compared with that of the pure NFW

halo, this perticular gravitational potential with a M87 size central super-massive is able to capture. This results in the plots shown in figures 6.6 - 6.9.

As can be seen from the figures, none of the configurations suffers large alterations from the central black hole. Only close to the center do we have a more massive clustering of neutrinos, and only for the two lightest halos do we see a noticeably effect. When we're around $r = 1\,\mathrm{kpc}/h$ away from the center of the halo the influence of the central black hole is neglitable, hence the addition of a central black hole to the NFW gravitational potential only results in more clustering of neutrinos around the center of this particular halo. For the lightest of the halos, the $M_{\mathrm{vir}} = 10^{12}\,M_{\odot}$ halo, we see that, at a distance of $r = 1\,\mathrm{pc}/h$ from the center, the central black hole causes the total neutrino mass used to be around 10^3 times larger than that of the pure NFW halo. But as we move outwards in the halo the effect of the black hole quickly declines and the mass used in this potential quickly equals that of the NFW halo alone.

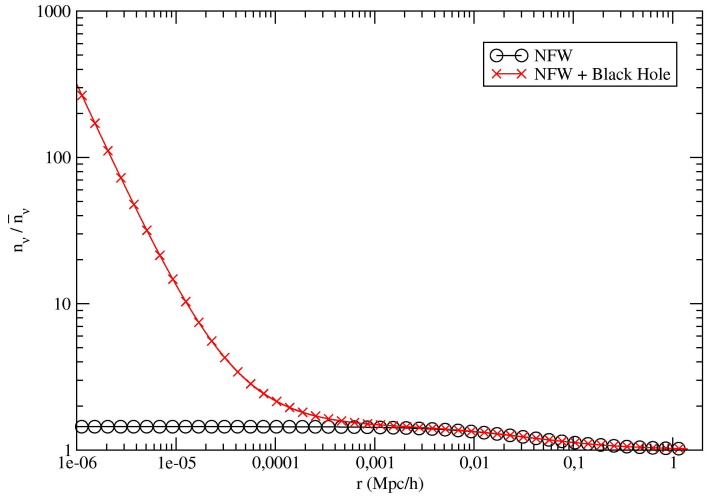

Figure 6.2: Normalized number density in a $M_{\mathrm{vir}} = 10^{12}\,M_{\odot}$ NFW halo with a central $3.7 \cdot 10^9\,M_{\odot}$ black hole. Neutrino mass is $m_\nu = 0.15\,\mathrm{eV}$. The plot compares the clean phase-space modified NFW (O-line) with the phase-space modified NFW + Black Hole (X-line).

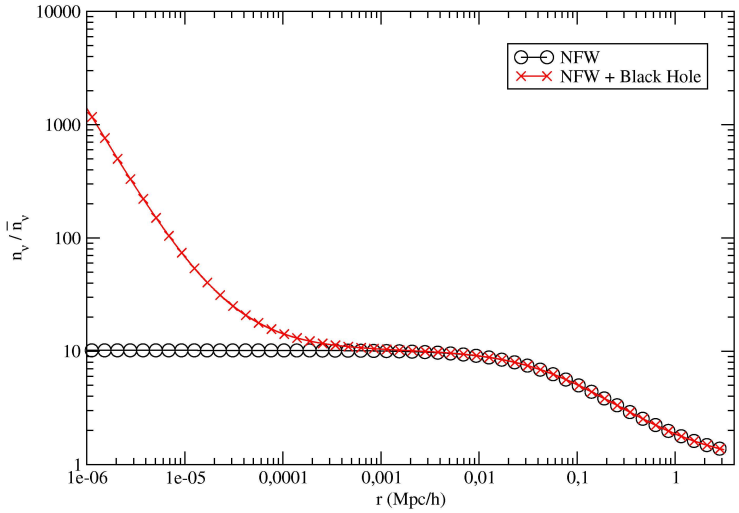

Figure 6.3: Normalized number density in a $M_{\rm vir} = 10^{13}\,M_\odot$ NFW halo with a central $3.7 \cdot 10^9\,M_\odot$ black hole. Neutrino mass is $m_\nu = 0.3\,\text{eV}$. The plot compares the clean phase-space modified NFW (O-line) with the phase-space modified NFW + Black Hole (X-line).

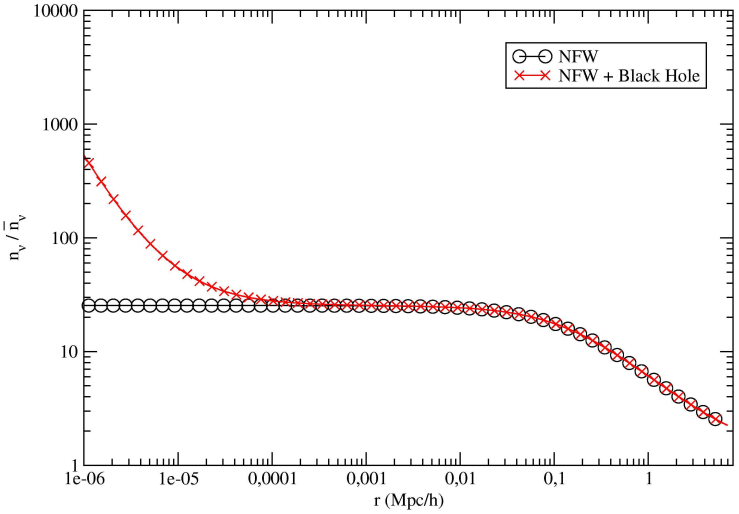

Figure 6.4: Normalized number density in a $M_{\rm vir} = 10^{14}\,M_\odot$ NFW halo with a central $3.7 \cdot 10^9\,M_\odot$ black hole. Neutrino mass is $m_\nu = 0.3\,\text{eV}$. The plot compares the clean phase-space modified NFW (O-line) with the phase-space modified NFW + Black Hole (X-line).

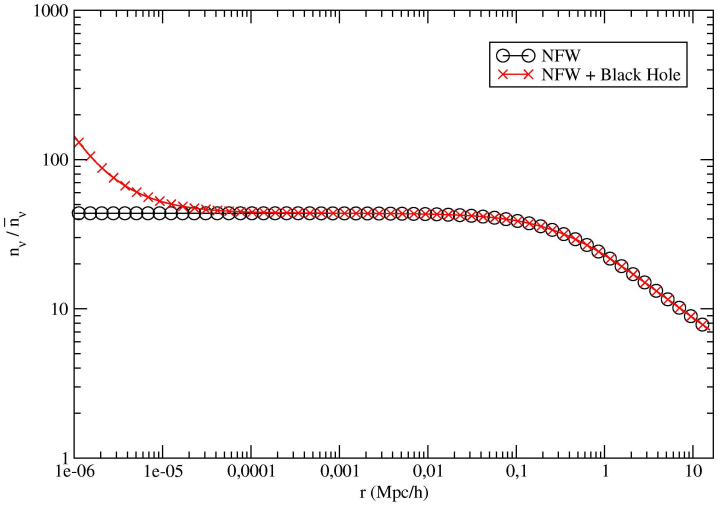

Figure 6.5: Normalized number density in a $M_{\text{vir}} = 10^{15}\,M_{\odot}$ NFW halo with a central $3.7 \cdot 10^{9}\,M_{\odot}$ black hole. Neutrino mass is $m_{\nu} = 0.6\,\text{eV}$. The plot compares the clean phase-space modified NFW (O-line) with the phase-space modified NFW + Black Hole (X-line).

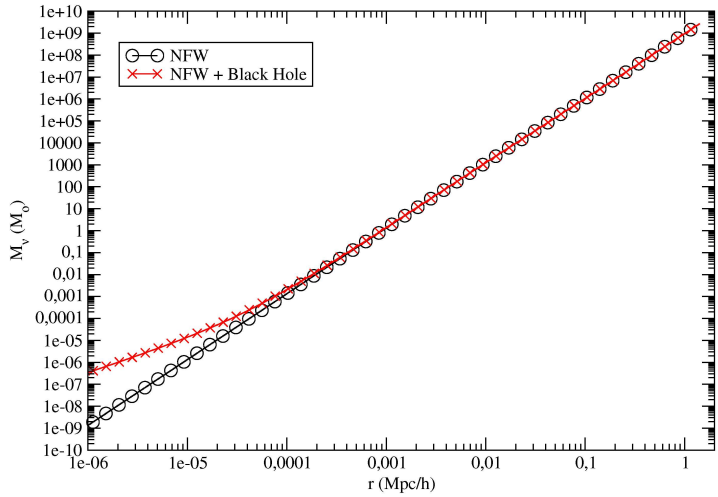

Figure 6.6: Total masses used in a $M_{\text{vir}} = 10^{12}\,M_{\odot}$ NFW halo with a central $3.7 \cdot 10^{9}\,M_{\odot}$ black hole. Neutrino mass is $m_{\nu} = 0.15\,\text{eV}$. The plot compares the clean phase-space modified NFW (O-line) with the phase-space modified NFW + Black Hole (X-line).

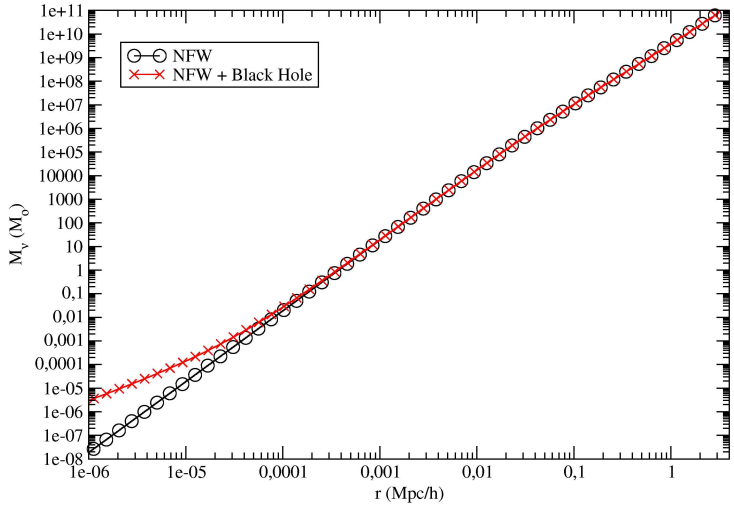

Figure 6.7: Total masses used in a $M_{\text{vir}} = 10^{13}\,M_{\odot}$ NFW halo with a central $3.7 \cdot 10^{9}\,M_{\odot}$ black hole. Neutrino mass is $m_{\nu} = 0.3\,\text{eV}$. The plot compares the clean phase-space modified NFW (O-line) with the phase-space modified NFW + Black Hole (X-line).

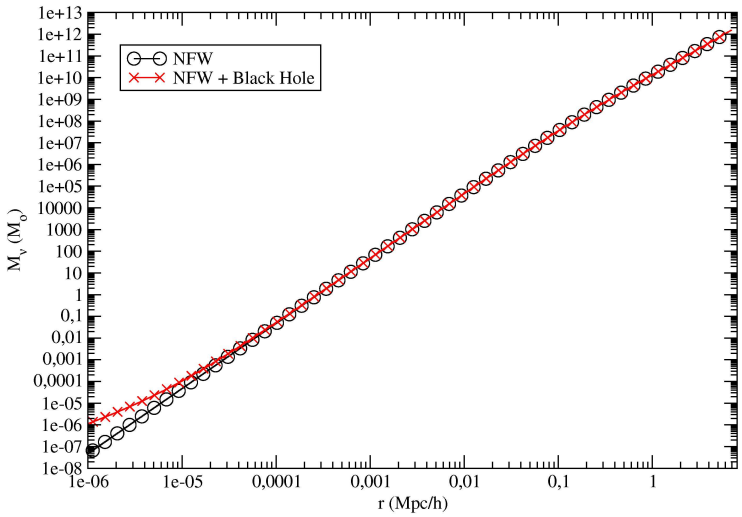

Figure 6.8: Total masses used in a $M_{\text{vir}} = 10^{14}\,M_{\odot}$ NFW halo with a central $3.7 \cdot 10^{9}\,M_{\odot}$ black hole. Neutrino mass is $m_{\nu} = 0.3\,\text{eV}$. The plot compares the clean phase-space modified NFW (O-line) with the phase-space modified NFW + Black Hole (X-line).

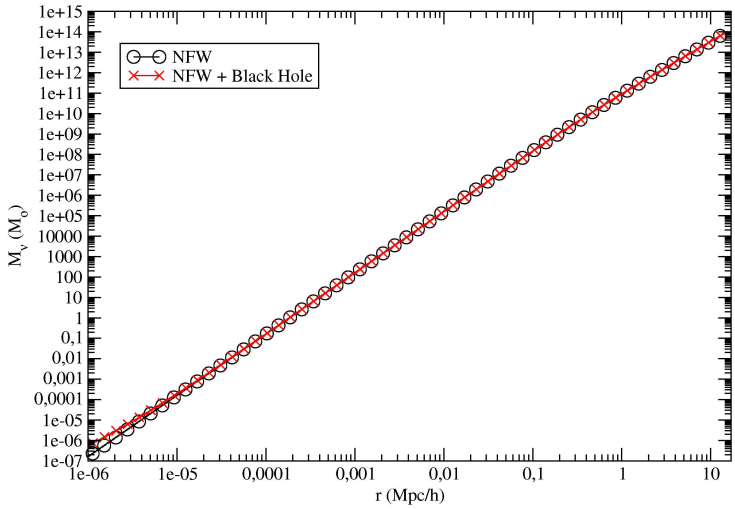

Figure 6.9: Total masses used in a $M_{\mathrm{vir}} = 10^{15}\,M_{\odot}$ NFW halo with a central $3.7 \cdot 10^{9}\,M_{\odot}$ black hole. Neutrino mass is $m_{\nu} = 0.6\,\mathrm{eV}$. The plot compares the clean phase-space modified NFW (O-line) with the phase-space modified NFW + Black Hole (X-line).

Chapter 7

Solar and Earth based calculations

So far I've investigated neutrino clustering in large scale systems like NFW halos and black hole systems. The latter was described by a simple classical point mass gravitational potential. In this chapter, I'll be doing calculations for the point mass potential again, but this time with objects like the Sun and the Earth instead of a massive black hole. It's interesting to see how big an influence our Sun and our Earth has on neutrino clustering and on possible future detections thereof. I've therefore dedicated a small chapter to Solar and Earth based calculations of overdensities. We need to keep in mind though, that these data is based on calculations of the same sort as in earlier chapters. When looking in the Solar System we need to beware of the fact that neutrinos of all sorts of course already exists here as bound neutrinos. My data will merely be an addition to the clustering of the already existing neutrinos in the Solar System.

7.1 Solar

When simulating how neutrinos will cluster around a star like our Sun, we can use a simple classical point mass gravitational potential, just as we did for the black holes in chapter 6. Of course the Sun isn't a point mass, but when we're a distance away from the Sun itself, the gravitational potential behaves just like that of a point mass.

To see whether we experience any kind of neutrino clustering around the Sun we need to go to smaller distances, hence I'll be using the astronomical unit (AU) as a unit for the distances. Since I'll be simulating the clustering of neutrinos around the Sun the mass will be set to $M = M_\odot$. Again I'll look at the same three neutrino masses as earlier, that is $m_\nu = \{0.15\,\text{eV}, 0.3\,\text{eV}, 0.6\,\text{eV}\}$. When plotting my results I'll plot them from $r \simeq R_\odot \simeq 4.65 \cdot 10^{-3}\,\text{AU}$ to $r = 10\,\text{AU}$, which is on the other side of Saturn.

7.1.1 Results

Figure 7.1 shows the three scenarios of neutrino overdensities around the Sun.

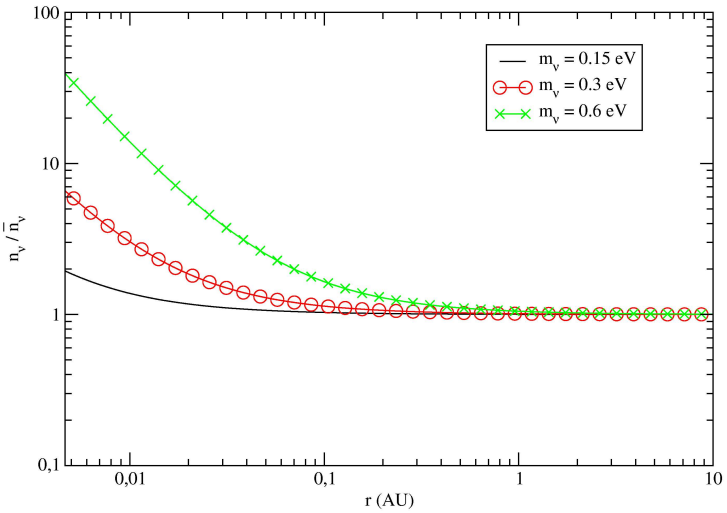

Figure 7.1: Overdensities of each neutrino around the Sun.

We clearly see that the lightest neutrino, the $m_\nu = 0.15\,\text{eV}$ neutrino, only cluster up at the surface of the Sun. When we move beyond the surface of the Sun, the number density quickly declines and becomes equal to that of the present neutrinos $\overline{n}_\nu$. If we instead go to the $m_\nu = 0.3\,\text{eV}$ neutrino, we see that the overdensity here is somewhat larger than that of the $m_\nu = 0.15\,\text{eV}$ neutrino. But already at a distance of $r \simeq 0.1\,\text{AU}$ from the center of the Sun, the number density has dropped to that

of the present neutrinos. The only neutrino with a relatively high overdensity is the heavies $m_\nu = 0.6\,\text{eV}$ neutrino. At the surface of the Sun the number density is around $n_\nu \simeq 40\overline{n}_\nu$. However, this number rapidly drops as we move away from the surface of the Sun. Around the location of the Earth in our Solar System, the number density again has dropped to the present value $\overline{n}_\nu$. What implications this has on possible detections of relic neutrinos will be discussed in detail in chapter 8.

7.2 Earth

Let us now turn to the area around the Earth and see what the Earth's gravitational potential can do to neutrino clustering. Again we'll be approximating the Earth's gravitational potential to that of a point mass potential. This will give us an idea of the clustering around the Earth.

Now we'll need to go to even smaller distances. I, therefore, do my calculations using the Earth's radius ($R_\oplus$) as the unit of distances. The mass of the Earth needs to be in the unit of $M_\odot$ which yields $M_\oplus \simeq 3 \cdot 10^{-6} M_\odot$. Again I'll begin my plot from the surface $r = R_\oplus$ and stop when I've reached $r = 10R_\oplus$. Since pratically no influence from the Sun was seen on the neutrinos, we should suspect the neutrinos around the Earth almost not to cluster up at all.

7.2.1 Results

A plot of the neutrino overdensities around the Earth can be seen in figure 7.2.

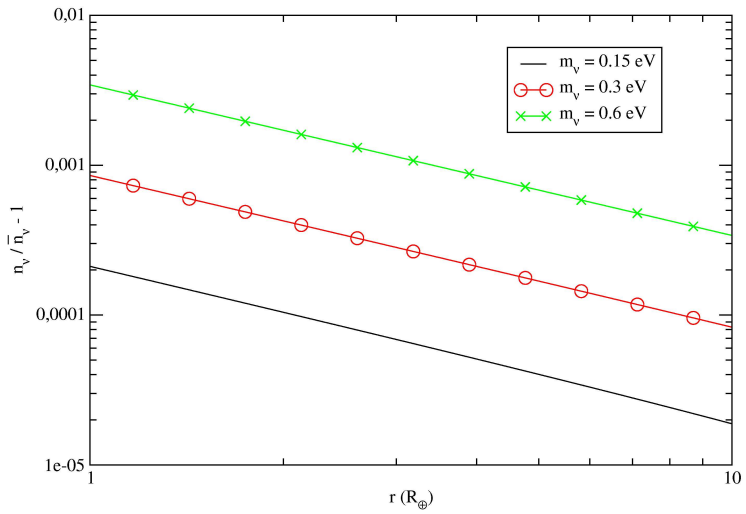

Figure 7.2: Overdensities for the three neutrinos around the Earth.

We quickly note that the Earth practically doesn't have any influence at all on the neutrinos at it's surface. In order to reveal the small effect from the Earth, I've plotted $\frac{n_\nu}{\overline{n}_\nu} - 1$ as a function of r. Here all three neutrinos have number densities that almost equal the average present value $\overline{n}_\nu$. If we were to try and move inside the Earth and look at clustering effects here, we would need a better potential. The point mass potential is completely wrong in this case, since

$$\Phi_{\text{Point}}(r) \to -\infty \text{ for } r \to 0$$

If we were to think of the Earth as a homogeneous sphere the potential would instead behave as

$$\Phi_{\text{Homogeneous}}(r) \to 0 \text{ for } r \to 0$$

However, this new potential would only increase the clustering effect slightly and we would therefore still not get any significant clustering even if we looked inside the Earth. Again, we need to note that these results only apply to relic neutrinos, which would enhance the overall neutrino overdensity in the Solar System (Solar neutrinos, atmospheric neutrinos etc). The Super-Kamiokande and other experiments have detected different types of neutrinos, but the relic are still to be detected.

We can, therefore, conclude that the gravitational pull from the Earth alone or from the Sun doesn't really strengthen the neutrino clustering from our Galaxy. We need to rely on the gravitational potential from the Milky Way in our quest for relic neutrino detection.

Chapter 8

Detection of relic neutrinos

After having looked at clustering of relic neutrinos in NFW halos, around massive black holes, around the Sun and around the Earth, I'll now try to investigate what these results implicate in the quest for neutrino detections. I'll look at different types of detections, namely via flux detection, using accelerators on Earth and via cosmic rays. This work is based on the calculations done by RW. I'll examine what consequences my numerical calculations have on the detections compared to the data from RW.

NFW version	$\frac{n_\nu}{\overline{n}_\nu}\,(m_\nu = 0.15\,\mathrm{eV})$	$\frac{n_\nu}{\overline{n}_\nu}\,(m_\nu = 0.3\,\mathrm{eV})$	$\frac{n_\nu}{\overline{n}_\nu}\,(m_\nu = 0.6\,\mathrm{eV})$
Original	~ 1.1	~ 2.1	~ 12.6
Energy modified	~ 1.4	~ 3.2	~ 15.1
Phase-space modified	~ 1.4	~ 2.7	~ 8.9
Ringwald & Wong	1.4	3.1	12

Table 8.1: Overdensities at Earth's location in an $10^{12}\,M_\odot$ NFW halo. "Original" refers to chapter 2, "Energy modified" refers to chapter 3 and "Phase-space modified" refers to chapter 4.

8.1 Flux detection

When the relic neutrinos move through the Earth they can produce a "wind force" with an acceleration given by (Duda *et al.*, 2001; Ringwald and Wong, 2004)

$$a_t \simeq 2 \cdot 10^{-28} \left(\frac{n_\nu}{\overline{n}_\nu}\right) \left(\frac{10^{-3}c}{v_{\mathrm{rel}}}\right) \left(\frac{\rho_t}{\mathrm{g/cm^3}}\right) \left(\frac{r_t}{\hbar/(m_\nu v_{\mathrm{rel}})}\right)^3 \mathrm{cm/s^2} \tag{8.1}$$

where ρ_t is the density of the target that experiences the acceleration, r_t is the radius of the target and v_{rel} is the mean velocity of the relic neutrinos in the rest system of the target. v_{rel} can be expressed in terms of a reduced de Broglie wavelength $\lambda\!\!\!^{-}$ given by

$$\lambda\!\!\!^{-} = \frac{\hbar}{m_\nu v_{\mathrm{rel}}} = \frac{\hbar}{\langle p \rangle} \tag{8.2}$$

where $\langle p \rangle$ denots the average momentum of the relic neutrinos. RW defines a dimensionless "escape momenta" y_{esc} as

$$y_{\mathrm{esc}} \equiv \frac{m_\nu v_{\mathrm{esc}} c}{k T_{\nu,0}} \tag{8.3}$$

where $v_{\mathrm{esc}} = \sqrt{2|\Phi(r_\oplus)|} \simeq 430\,\mathrm{km/s}$ is the escape velocity from Earth's location in the NFW halo. This yields the following "escape momenta" $\{y_{\mathrm{esc}}\} = \{1.3\,,\, 2.6\,,\, 5.1\}$ for the corresponding neutrinos $\{m_\nu\} = \{0.15\,\mathrm{eV}\,,\, 0.3\,\mathrm{eV}\,,\, 0.6\,\mathrm{eV}\}$. If we calculate the average dimensionless "momenta" $\langle y \rangle$ it can be used to express the average momentum as

$$\langle p \rangle = \frac{\langle y \rangle\, k T_{\nu,0}}{c}$$

which yields the reduced de Broglie wavelength

$$\lambda\!\!\!^{-} = \frac{\hbar c}{\langle y \rangle \, kT_{\nu,0}} \tag{8.4}$$

If we now combine equations (8.2) and (8.4), we see that we can express v_{rel} as

$$v_{\text{rel}} = \frac{\langle y \rangle \, kT_{\nu,0}}{cm_{\nu}} \tag{8.5}$$

Inserted in the equation for the acceleration experienced by a target due to the relic neutrino wind (8.1) we get

$$a_t \simeq 2 \cdot 10^{-28} \left(\frac{n_{\nu}}{\overline{n}_{\nu}}\right) \left(\frac{10^{-3} c^2 m_{\nu}}{\langle y \rangle \, kT_{\nu,0}}\right) \left(\frac{\rho_t}{\text{g/cm}^3}\right) \left(\frac{r_t \, \langle y \rangle \, kT_{\nu,0}}{\hbar c}\right)^3 \text{cm/s}^2 \tag{8.6}$$

In order to compare my data with the data from RW, we need to have the overdensities from my $10^{12}\, M_{\odot}$ NFW halos at hand. These can be found in table 8.1. I've included all three "versions" of the NFW halos which I've been looking at. We quickly note that the overdensities in my case is close to the ones found by RW (eg. table 8.1) and also that my calculated esacpe velocity, and thus "escape momenta", for the relic neutrinos in the $10^{12}\, M_{\odot}$ NFW halo, at the location of Earth, is sligthly smaller than the ones found by RW, but only by a few decimals. Hence my results for the neutrino wind acceleration will vary very little from the results produced by RW. For Cavendish-type torsion balances[1] the smallest measurable acceleration is in the order of $a_t \simeq 10^{-13}\,\text{cm/s}^2$, which will still be around 13 orders of magnitude off compared to the neutrino wind acceleration, when using tungsten spheres on the Cavendish torsion balacens ($\rho_t = 19.25\,\text{g/cm}^3$), $\frac{v_{\text{rel}}}{c} = 10^{-3}$ and $r_t = \lambda\!\!\!^{-}$. It's therefore highly unlikely that a direct measurement of the neutrino wind acceleration will be possible in a near future. We need to develop a ultra sensitive "acceleration measurements apperatus". But until this has been developed, we can safely rule out this way of detecting the relic neutrinos.

8.2 Using accelerators

The two forthcoming[2] accelerators LHC[3] and VLHC[4] will have beams with energies in the TeV range, hence interactions with relic neutrinos will have relatively

[1] Apperatus used to measure very small accelerations. It's also used by make very precise measurements of the acceleration due to gravity **g**

[2] Whether the VLHC accelerator becomes a reality or simply stays on the drawing board is still up to debate.

[3] Large Hadron Collider , http://lhc-new-homepage.web.cern.ch/lhc-new-homepage

[4] Very Large Hadron Collider , http://vlhc.org

Accelerator	N	A	Z	E_N (TeV)	L (km)	I (A)	$R^*_{\nu^A_Z N}$ (yr^{-1})
LHC	p	1	1	7	26.7	$5.8 \cdot 10^{-1}$	$1.6 \cdot 10^{-7}$
	Pb	208	82	574	26.7	$6.1 \cdot 10^{-3}$	$7.1 \cdot 10^{-5}$
VLHC	p	1	1	87.5	233	$5.7 \cdot 10^{-2}$	$1.7 \cdot 10^{-6}$
	Pb	208	82	7280	233	$5.7 \cdot 10^{-4}$	$7.3 \cdot 10^{-4}$
ULHC	p	1	1	10^7	$4 \cdot 10^4$	$1.0 \cdot 10^{-1}$	58

Table 8.2: Beam parameters for the LHC, VLHC and ULHC accelerators. The $R^*_{\nu^A_Z N}$ denotes the scattering rate calculated by RW.

large cross section, thus perhaps making detection of relic neutrinos possible. This won't be a direct detection of a relic neutrino though, but a detection of the remnants of an inverse beta decay

$$ {}^A_Z N + \nu_e \rightarrow {}^A_{Z+1} N + e^- $$

The target beam, eg. a proton beam p, will lose it's charge and become neutron n. The trajectory of the neutron will differ from that of the beam and can be detected. This would indicate that a neutrino was involved. The scattering rate $R_{\nu^A_Z N}$ for a beam of particles ${}^A_Z N$ is given by (Müller, 1987; Melissinos, 1999; Weiler, 2001; Ringwald and Wong, 2004)

$$ R_{\nu^A_Z N} \simeq 2 \cdot 10^{-8} \left(\frac{n_\nu}{\overline{n}_\nu}\right) \left(\frac{m_\nu}{\text{eV}}\right) \frac{A^2}{Z} \left(\frac{E_N}{10\,\text{TeV}}\right) \left(\frac{L}{100\,\text{km}}\right) \left(\frac{I}{0.1\,\text{A}}\right) \text{yr}^{-1} \qquad (8.7) $$

where E_N is the beam energy, L is the length of the accelerator and I is the current. The beam parameters for the different accelerators are shown in table 8.2. Both parameters for proton (p) beams as well as lead (Pb) beams are shown. The table also includes a very optimistic and futuristic accelerator called the ULHC (Ultimate Large Hadron Collider). This accelerator will have a circumference equal to that of the Earth $L \simeq 4 \cdot 10^4$ km. Furthermore, this accelerator will have energies at $E_N \simeq 10^7$ TeV. The last column in this table shows the scattering rate $R^*_{\nu^A_Z N}$ calculated by RW using their $m_\nu = 0.6$ eV overdensity data from table 8.1.

To make the most optimistic assumptions about whether or not we're able to detect relic neutrinos using any of these detectors let us now look at the number density for the heaviest of the three neutrinos in the $M_{\text{vir}} = 10^{12}\, M_\odot$ NFW halo. Our own galaxy the Milky Way is a $M_{\text{MW}} \simeq 10^{12}\, M_\odot$ galaxy. Since we're located at a distance of $r \simeq 8$ kpc away from the Galactic Center, we'll look at the overdensity for the neutrino at that distance. We'll then simply calculate the scattering

Accelerator	$R_{\nu_Z^A N}$ (yr^{-1})
LHC	$1.6 \cdot 10^{-7}$
	$7.5 \cdot 10^{-5}$
VLHC	$1.8 \cdot 10^{-6}$
	$7.7 \cdot 10^{-4}$
ULHC	60

Table 8.3: Expected scattering rates with relic neutrinos. Data from original NFW calculations.

rate, which tells us the number of interactions we can expect to see from relic neutrinos per year. I'll start out by looking at my original data from chapter 2 in section 8.2.1, then move on to look at the modified data from chapter 3 in section 8.2.2 and then conclude with the results from my phase-space modified data of the NFW halos from chapter 4 in section 8.2.3.

8.2.1 Original NFW

The data from the original NFW halo is gathered in table 8.3. By comparing my data with the ones from RW, $R^*_{\nu_Z^A N}$ shown in table 8.2, we see that my data allows for higher scattering rates. I'm able to detect a few more interactions per year in all of the accelerators, but even the extremely energetic VLHC with a Pb target we can only expect a little less than one interaction every millennium! Only with the ULHC are we able detect any interactions, around 60 per year.

8.2.2 Energy modified NFW

The data for the energy modified NFW halo can be seen in table 8.4. When taking into account that the unbound neutrinos also will have gravitational potential energy we will, as expected, get a higher scattering rate. But again we'll have to wait more then a millinium for just one interaction with the Pb beam in the VLHC. Again only the ULHC would provide us with enough interactions to detect relic neutrinos.

Accelerator	$R_{\nu_Z^A N}$ (yr^{-1})
LHC	$2.0 \cdot 10^{-7}$
	$8.9 \cdot 10^{-5}$
VLHC	$2.1 \cdot 10^{-6}$
	$9.2 \cdot 10^{-4}$
ULHC	72

Table 8.4: Expected scattering rates with relic neutrinos. Data from energy modified NFW halo calculations.

Accelerator	$R_{\nu_Z^A N}$ (yr^{-1})
LHC	$1.2 \cdot 10^{-7}$
	$5.3 \cdot 10^{-5}$
VLHC	$1.2 \cdot 10^{-6}$
	$5.4 \cdot 10^{-4}$
ULHC	43

Table 8.5: Expected scattering rates with relic neutrinos. Data from phase-space modified NFW calculations.

8.2.3 Phase-space modified NFW

The most realistic model of a 10^{12} $M_\odot$ NFW halo is the phase-space modified. The scattering rate data is gathered in table 8.5. This model also includes the energy modifications as before. However, since I've coarse-grained the occupation number of the bound neutrinos, the overdensity will automaticaly drop compared to that of the fine-grained bound neutrinos. This will, of course, play an important role on the scattering rate since this is proportional to the overdensity, see equation (8.7). This results in a lower scattering rate than the one RW have calculated. It seems that without the ULHC we will never be able to detect any interactions between an accelerator beam and relic neutrinos.

8.2.4 Solar based

As calculated in chapter 7, the overdensity for neutrinos around the Sun isn't reaching a high enough level at the location of the Earth in order for us to detect them using any of the above accelerators, apart from the ULHC of course. Could we, however, somehow send a satellite close to the Sun[5] we might be able to detect interactions with neutrinos. Unfortunately, only the $m_\nu = 0.6\,\text{eV}$ neutrino is able to cause a relatively large clustering. More realistic neutrino masses like the $m_\nu = 0.15\,\text{eV}$ never result in any noticable clustering.

8.2.5 Earth based

As we've seen, the Earth's gravitational pull isn't large enough to be the cause of any worth mentioning neutrino clustering. As noted in chapter 7, the gravitational potential of the Earth is assumed to be that of a point mass, which of course isn't a correct assumption. It only makes sense to talk about the Earth as a point mass when we're some distance away from the Earth. The closer we move to the Earth, the more incorrect the assumption becomes. However, if we were to apply the gravitational potential of a homogeneous sphere (as we to a good approximation can assume the Earth to be), we would be able to move inside the Earth and examine the clustering effects. But as mentioned in chapter 7, this would only cause the clustering of the relic neutrinos to increase slightly, hence the reward for detecting relic neutrinos inside the Earth would be negligible. In other words, it wouldn't help us to look for the relic neutrinos with detectors inside the Earth.

8.3 Cosmic rays

So far it doesn't seem that detection of relic neutrinos will be possible with any of the above mentioned methods, except if the ULHC is constructed. Another method we could investigate is using extremely energetic cosmic rays (Singh and Ma, 2003). Cosmic rays have been observed with energies up to $E_{\text{cr}} \sim 10^{20}\,\text{eV}$. This corresponds to a center of mass energy $\sqrt{s}$ given as

$$\sqrt{s} = \sqrt{m_\nu E_{\text{cr}}} \simeq 14 \left(\frac{m_\nu}{\text{eV}}\right)^{1/2} \left(\frac{E_{\text{cr}}}{10^{20}\,\text{eV}}\right)^{1/2} \text{GeV}$$

when interacting with relic neutrinos. A center of mass energy of that size is not too far from the resonances of the W and Z bosons, respectively $\sim 80.5\,\text{GeV}$ and $\sim 91.2\,\text{GeV}$ (Particle Data Group *et al.*, 2004). If extremely energetic cosmic

[5] We need to go very close to the Sun. The orbit of Mercury still isn't subject to any noticable neutrino clustering due to the gravitational potential of the Sun.

netrinos (EECν) react with relic anti-neutrinos (and vice versa) they annihilate and create Z-bosons (Weiler, 1982). On resonance the energy yields

$$E_\nu^{\text{res}} = \frac{m_Z^2}{2m_\nu} \simeq 4 \cdot 10^{21} \left(\frac{\text{eV}}{m_\nu}\right) \text{eV}$$

This energy is well beyond the GZK cut-off of $E_{\text{GZK}} \sim 10^{19}$ eV (Greisen, 1966; Zatsepin and Kuzmin, 1966). The GZK cut-off is the energy limit above which no cosmic rays should be observed. If a cosmic ray have energy greater than E_{GZK} it would interact with cosmic microwave background (CMB) photons until the energy of the cosmic ray would fall below the GZK cut-off threshold. It should therefore be impossible to detect cosmic rays with energies exceeding the GZK cut-off. The above mentioned cosmic ray energy E_{cr} is in clear contradiction with this limit. A way to explain this "GZK paradox" is to have EECν interact with local non-relativistic relic anti-neutrinos. This annihilation could lead to a resonance energy of the size mentioned above, which then leads to a mean free path of

$$l_\nu \simeq 1.4 \cdot 10^5 \,\text{Mpc}$$

According to RW this corresponds to a probability of $2 - 3\,\%$ for annihilation between relic anti-neutrinos and EECν. So how can we exploit this probability and possibly detect the relic neutrinos?

When relic anti-neutrinos and EECν annihilate the spectrum of the EECν will show a dip at the resonance energy (absorption dips) (Weiler, 1982). A number of neutrino detectors which operate with energies above 10^{21} have been planned. However, as stated by RW, the depths of the absorption dips are determined by number densities, thus at present day there are no striking dips in the EECν spectrum since relic neutrino clustering doesn't become significant until after $z \lesssim 2$. The number densities will be significantly higher at large redshifts $z \gg 1$. It, therefore, doesn't seem likely that these absorption dips will be observed in the near future.

Another effect that can be exploited is emission spectroscopy. When relic anti-neutrinos and EECν annihilate they produce Z-bosons which quickly decays into proton - anti-proton pairs and photons (Z-bursts), eg. (Fodor *et al.*, 2002; Fargion *et al.*, 1999), as can be seen in figure[6] 8.1. However, also the emission rate is strenghtened by the relic neutrino overdensity in the local universe. With local universe is ment $z \lesssim 0.01$ which corresponds to a sphere with radius $r_{\text{GZK}} \lesssim 50\,\text{Mpc}$. In the local universe the overdensity is $\frac{n_\nu}{\bar{n}_\nu} \lesssim 2$ (Ringwald and Wong, 2004), hence the emission rate can't be strengthened by clustering of relic neutrinos in our local universe.

[6] http://www.cerncourier.com/main/article/42/5/2/1

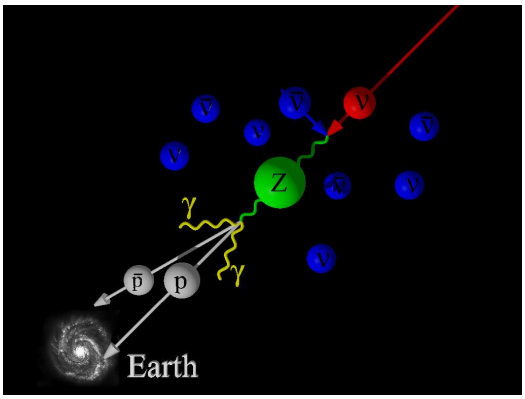

Figure 8.1: An EECν (red) reacts with a relic anti-neutrino (blue) and annihilates into a Z-boson (green), which decays into a proton - anti-proton pair (grey) and photons (yellow). The galaxy in the lower left corner corresponds to Earth.

But there's still a way to exploit the local universe. If we have a "neutrino telescope" with a good angular resolution, it would be possible to probe some of the local clusters of galaxies in the GZK zone (sphere with radius r_{GZK}). Some of these clusters ($M \gtrsim 10^{14}\, M_{\odot}$) have large clustering of relic neutrinos. If we choose the Virgo cluster ($M_{\mathrm{vir}} \simeq 8 \cdot 10^{14}\, M_{\odot}$), which spans around 10° across the sky, the AGASA[7], having an angular resolution of $\sim 2°$, would be able to resolve the internal structures of the cluster. From the original data from RW the average overdensity is estimated to be ~ 45 for $m_{\nu} = 0.6\,\mathrm{eV}$ neutrinos and ~ 5 for $m_{\nu} = 0.15\,\mathrm{eV}$ neutrinos. If we compare the overdensities from the $M_{\mathrm{vir}} = 10^{15}\, M_{\odot}$ configurations in RW and my calculations, we see that my data is either higher or lower depending on which of the NFW versions we're using (see the figures in chapters 2, 3,4 and appendix A).

If we're looking at my original NFW, we've seen in chapter 2 that my data is roughly a factor ~ 2 for $m_{\nu} = 0.15\,\mathrm{eV}$ neutrinos and ~ 8 for $m_{\nu} = 0.6\,\mathrm{eV}$ neutrinos higher than the RW data. This results in my average overdensities to be the corresponding factors higher. Thus, it'll enhance the emission rate in the Virgo cluster quiet significantly and therefore strengthen the possibility of detecting relic neutrinos.

The same enhancement is seen in the energy modified NFW from chapter 3. The effect of the inclusion of the gravitational potential energy for the unbound neutrinos didn't have a large impact on the total overdensities in the $10^{15}\, M_{\odot}$ halos. Only at large distances in the halo did we see a small enhancement of the over densities, as described in chapter 3.

If we, however, turn to the phase-space modified NFW from chapter 4, we see

[7] Akemo Giant Air Shower Array - http://www-akeno.icrr.u-tokyo.ac.jp/AGASA/

that the data isn't strengthened anymore, but is weakened instead, as previously described. For the light $m_\nu = 0.15\,\mathrm{eV}$ neutrinos the drop factor is roughly ~ 3 while it's as high as $\sim 20 - 30$ for heavy $m_\nu = 0.6\,\mathrm{eV}$ neutrinos. This means that the average overdensity will drop to around $\lesssim 2$ for both the light and the heavy neutrinos.

So if assuming a mean coarse-grained phase-space distribution of the relic neutrinos, it isn't likely that detection would be possible using a neutrino detector like the AGASA with a high angular resolution. It seems that relic neutrinos won't be detected using any of the above mentioned methods in the near future. Experimental techniques needs to be improved if we want to detect relic neutrinos. Of course detection would be enhanced if the neutrino weighed more. However, (Tegmark *et al.*, 2004) states that none of the three known neutrino types can weigh more than $m_\nu = 0.6\,\mathrm{eV}$.

Chapter 9

Conclusion

Detection of relic neutrinos is highly depend on clustering effects in the galactic halos. A large clustering of relic neutrino is crucial for all techniques which are being used and proposed in our effots for their detection.

I've studied relic neutrino clustering in NFW halos with the purpose of extending the ideas this thesis was build on. Futhermore, I've discussed some of the techniques of detection which have been studied and proposed.

In the conclusion I'll briefly summarize what has been done and what results have been obtained in this thesis. The question "What implacations does my study have on the continuing quest for the detection of the relic neutrino?" will be discussed as well.

9.1 Conclusion

With the introduction of the cold dark matter NFW halos, numerical calculations of neutrino clustering were carried out. Both bound and unbound relic neutrinos were accounted for. However, the bound neutrinos were assumed to have a constant maximum fine-grained phase-space occupation number of $f = 0.5$ given the argument that filling of the gravitational potential would be done by the slowest neutrinos, all with $p \simeq 0$. Furthermore, gravitational potential energy of the unbound relic neutrinos were ignored completely. This setup proved to keep within a modern version of the Tremaine-Gunn bound, which is a limit for the overdensity taken by neutrinos in a cold dark matter halo. For very light configurations, however, the Tremaine-Gunn bound was exceeded due to the fact that unbound neutrinos where the dominant type of neutrinos. A comparison, between my data and the data provided by RW, revealed a larger clustering effect in most of my data. Reasons were discussed. Besides looking at overdensities in NFW halos, calculations of the mass occupied by relic neutrinos in each halo were carried out. This was done to examine whether or not self-gravitation of the neutrinos should be included as well. If the total mass of the neutrinos exceeded the physical mass of the NFW halo this would be crucial. However, it was seen that self-gravitation wasn't needed in the calculations.

One thing was needed in the calculations though: An inclusion of the gravitational potential energy for the unbound neutrinos. Eventhough the gravitational potential would be filled by bound neutrinos, unbound neutrinos would still be attracted and cluster up around the center of the NFW halo. An increase in overdensity for the unbound neutrinos was seen as a result of this. This lead to an increase in the mass used by the unbound neutrinos. Also, a calculation of a maximum radius of the NFW halos in question was made in order to get a more realistic image of the NFW halos.

Phase-space for the bound neutrinos was discussed in detail and a switch from fine-grained $f = 0.5$ neutrinos to a mean coarse-grained occupation number was made. By introducing the coarse-grained phase-space occupation number to the bound neutrinos, a sudden drop was seen in the overdensity as well as in the enhancement of observing these relic neutrinos using cosmic rays.

Clustering around massive black holes such as the ones residing in the center of many galaxies was also briefly discussed with the intention of combining an NFW halo with a massive black hole. However, it was shown that the influence of these black holes only was sizeable a limited distance. By combining NFW halos with super-massive central black holes the overdensities were studied. This told us that no large enhancement was seen in the clustering of relic neutrinos once we were a certain distance away. At the location of the Earth no enhancement would have been seen.

A short trip to our Solar System was made as well. This just to see how much effect the gravitational potential from our Sun (and the Earth) would have on relic neutrinos. This effect would be an enhancement of the local overdensity of neutrinos already residing here (eg. solar neutrinos). The Earth proved to have no effect on the relic neutrinos while the Sun had some clustering around itself. This clustering, however, declined rapidly as we moved out into the Solar System.

After discussing relic neutrino clustering in graviational potentials, I turned to look at what effect the clustering had on our chances of detecing the relic neutrinos.

Detection using a present day Cavendish torsion balance is out of the question even if clustering were dramatically higher. An increase in the order of 10^{13} is needed just to get the acceleration of the neutrino wind up to level with the present day minimum measurable acceleration.

With the present colliders such as LHC and the proposed VLHC we still would be far from detection of relic neutrinos. Only around once per millinium would we expect to see a reaction caused by a relic neutrino. Unless a ULHC is constructed we'll have to rely on the study of cosmic ray detection and the proposed Z-burst scenario in our quest for the detection of relic neutrinos.

The detection of extremely energetic reaction products, in form of cosmic rays, from annihilation of EECν and local non-relativistic relic anti-neutrinos (and vice versa) seems like the only possible way of detecting relic neutrinos. However, it seems that relic neutrinos won't be detected in a nearby future if they indeed do have a mean coarse-grained phase-space as stated in this thesis.

9.1.1 RW vs. AM

So which study is the correct and most realistic? The study carried out by Ringwald & Wong or this thesis?

RW uses a time-evolving numerical simulation in which they run from an initial redshift $z = 3$ to the present day $z = 0$. I only look at the present day neutrinos with $z = 0$. An inclusion of time-evolution is preferable in the talk of relic neutrinos clustering, since clustering is effective at $z \sim 2 \rightarrow 0$.

Instead of calculating the total Fermi-Dirac distribution for bound neutrinos I find a mean coarse-grained occupation number, where RW uses the entire distribution. In light halos this doesn't result in large differences between the two methods. However, in heavy halos the mean coarse-grained occupation number becomes very low, which indicats that very fast neutrinos are bound to the halo. This seems like a simplification of the true situation where the slow neutrinos would be bound to the halo first. Also, to assume that only the slowest neutrinos with the lowest momenta ($p \sim 0$) becomes bound, which yield the Fermi-Dirac occupation number $f = 0.5$, seems like a too large simplification. However, for

light halos such as the $10^{12}\ M_{\odot}$ halo the mean coarse-grained phase-space probably gives the most realistic image of how the bound neutrinos are packed in the halo.

RW don't distinguish between bound and unbound neutrinos. They just sum all the neutrinos over the entire momentum space. I clearly distinguish between bound and unbound neutrinos and do different calculations depending on which of the two states we're dealing with. This is crucial since each of the two states behaves differently in the gravitational potential of the halos and point masses.

The matter of relic neutrino reservoir is also up for discussion. RW uses different reservoirs depending on which halo they're doing calculations of. The light halos have an almost infinite reservoir and the heavy halos have a relative small reservoir. I use a finite reservoir at all times, no matter if the halos are light or heavy. This seems more realistic since I directly calculate how far out the gravitational potential extends for the halo in question.

I think it's fair to conclude that neither of the studies are completely correct. Both add good and bad arguments to the discussion of relic neutrino clustering and their future detection. The subject of relic neutrino clustering isn't a closed chapter, the theories and simulations are still up for discussion.

9.2 Closing remarks

A more deep investigation and study of the detection of relic neutrinos using cosmic rays would have been preferable, however, time was against me. This field is a hot topic at the moment, new detectors are being planned and build and more research on the matter is being carried out. The quest continues.

Appendix A

Additional plots

Throughout this thesis only a few of the plots are shown in each chapter. This appendix is dedicated to the remaining plots from chapters 2, 3, 4 and 6.

A.1 Original NFW

Below are all the remaining plots from chapter 2

A.1.1 Number density

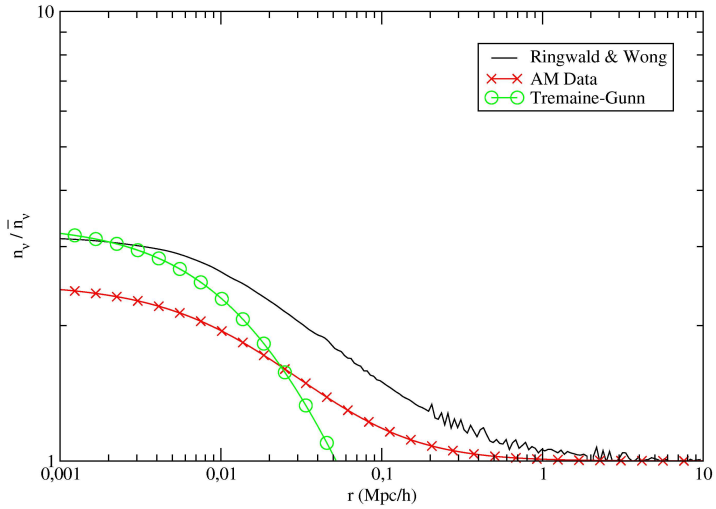

Figure A.1: Number densities n_ν normalized to present average $\bar{n}_\nu$ for $m_\nu = 0.3\,\mathrm{eV}$ neutrinos in a $M_{\mathrm{vir}} = 10^{12}\,M_\odot$ halo. The solid line displays the data from RW, the X-line displays my numerical calculations and the O-line shows the Tremaine-Gunn bound.

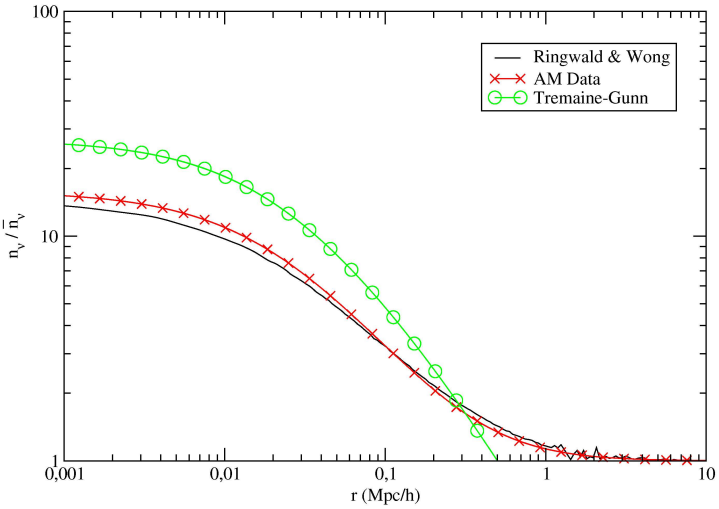

Figure A.2: Number densities n_ν normalized to present average $\overline{n}_\nu$ for $m_\nu = 0.6\,\mathrm{eV}$ neutrinos in a $M_{\mathrm{vir}} = 10^{12}\,M_\odot$ halo. The solid line displays the data from RW, the X-line displays my numerical calculations and the O-line shows the Tremaine-Gunn bound.

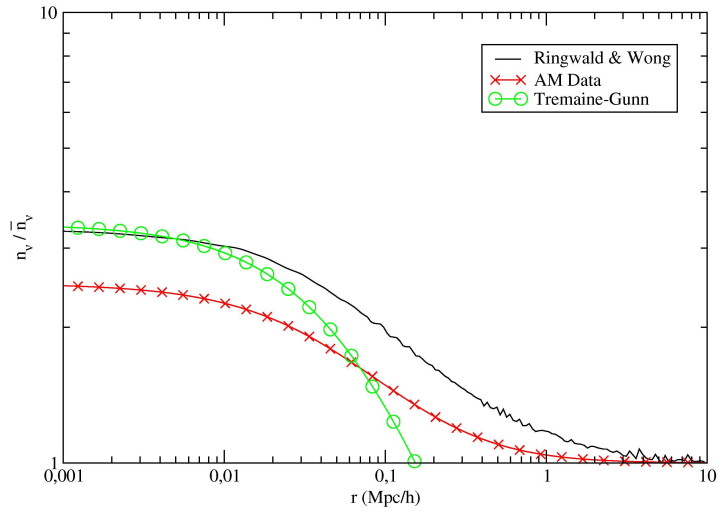

Figure A.3: Number densities n_ν normalized to present average $\overline{n}_\nu$ for $m_\nu = 0.15\,\mathrm{eV}$ neutrinos in a $M_{\mathrm{vir}} = 10^{13}\,M_\odot$ halo. The solid line displays the data from RW, the X-line displays my numerical calculations and the O-line shows the Tremaine-Gunn bound.

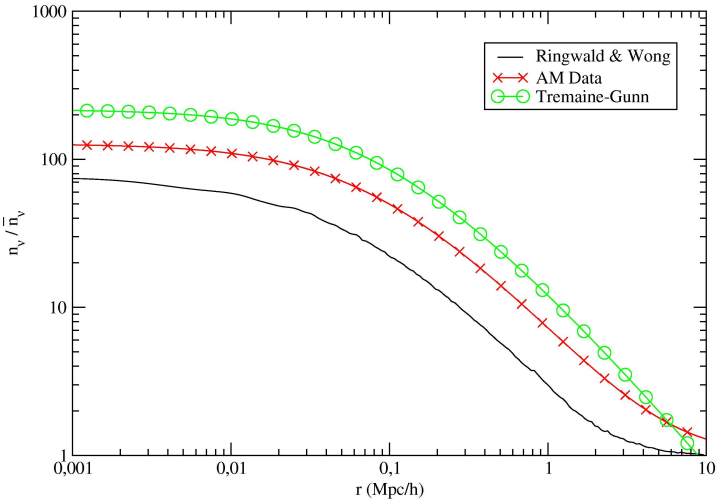

Figure A.4: Number densities n_ν normalized to present average $\overline{n}_\nu$ for $m_\nu = 0.6\,\mathrm{eV}$ neutrinos in a $M_{\mathrm{vir}} = 10^{13}\,M_\odot$ halo. The solid line displays the data from RW, the X-line displays my numerical calculations and the O-line shows the Tremaine-Gunn bound.

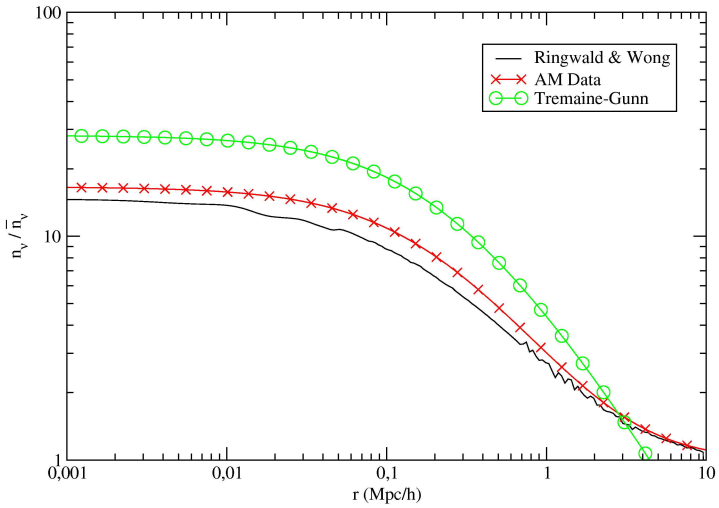

Figure A.5: Number densities n_ν normalized to present average $\overline{n}_\nu$ for $m_\nu = 0.15\,\mathrm{eV}$ neutrinos in a $M_{\mathrm{vir}} = 10^{14}\,M_\odot$ halo. The solid line displays the data from RW, the X-line displays my numerical calculations and the O-line shows the Tremaine-Gunn bound.

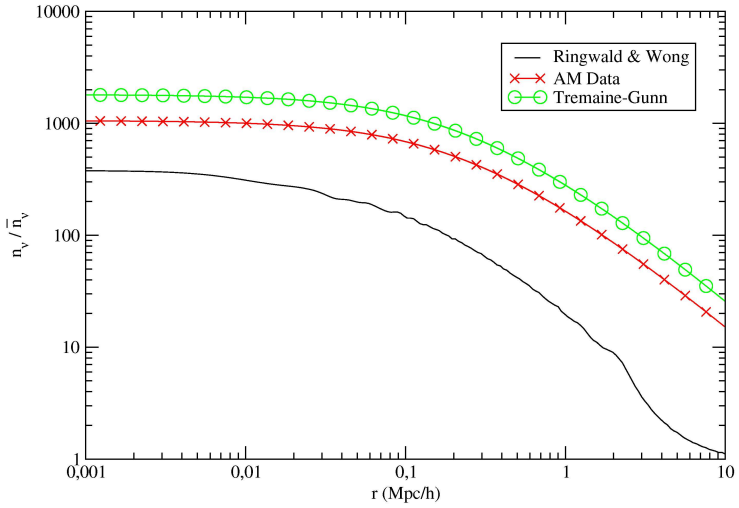

Figure A.6: Number densities n_ν normalized to present average $\overline{n}_\nu$ for $m_\nu = 0.6\,\mathrm{eV}$ neutrinos in a $M_{\mathrm{vir}} = 10^{14}\,M_\odot$ halo. The solid line displays the data from RW, the X-line displays my numerical calculations and the O-line shows the Tremaine-Gunn bound.

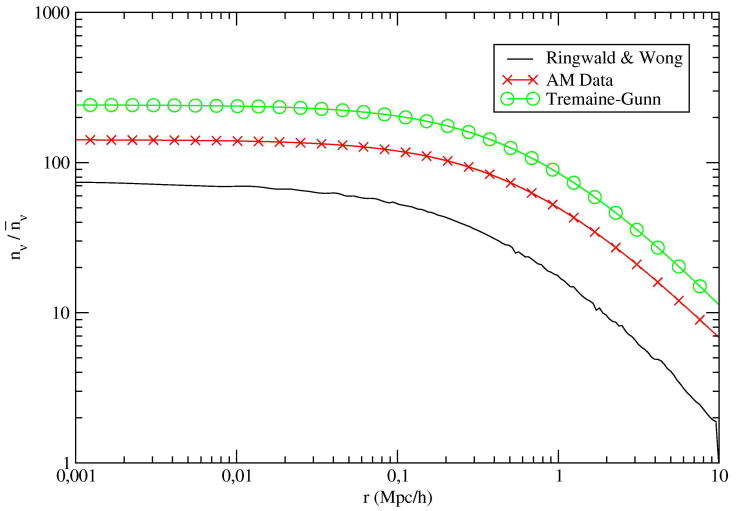

Figure A.7: Number densities n_ν normalized to present average $\overline{n}_\nu$ for $m_\nu = 0.15\,\mathrm{eV}$ neutrinos in a $M_{\mathrm{vir}} = 10^{15}\,M_\odot$ halo. The solid line displays the data from RW, the X-line displays my numerical calculations and the O-line shows the Tremaine-Gunn bound.

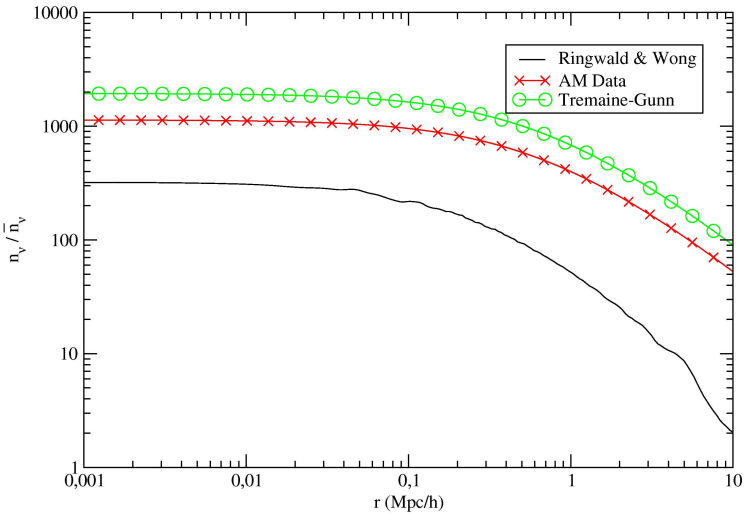

Figure A.8: Number densities n_ν normalized to present average $\bar{n}_\nu$ for $m_\nu = 0.3\,\mathrm{eV}$ neutrinos in a $M_{\mathrm{vir}} = 10^{15}\,M_\odot$ halo. The solid line displays the data from RW, the X-line displays my numerical calculations and the O-line shows the Tremaine-Gunn bound.

A.1.2 Mass

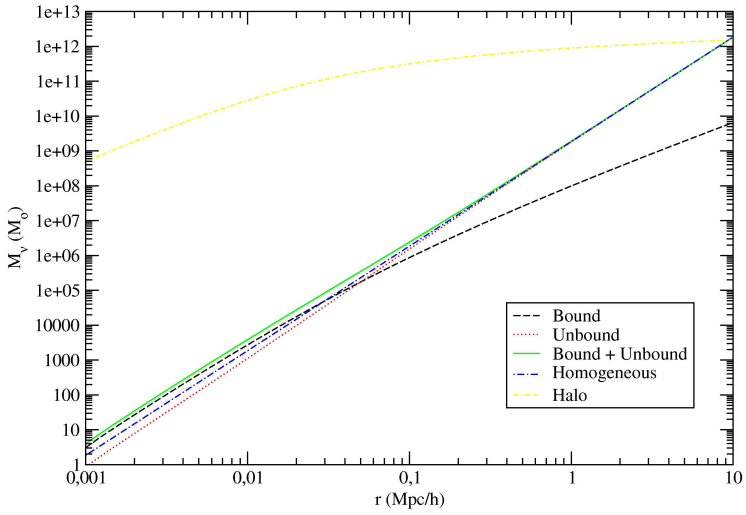

Figure A.9: A complete plot of neutrino mass used in the halo for $m_\nu = 0.3\,\mathrm{eV}$ neutrino in a $M_{\mathrm{vir}} = 10^{12}\,M_\odot$ halo. The plot shows the total bound, the total unbound, and the total neutrino mass used. Furthermore the total homogeneously distributed mass as well as the NFW halo mass are plotted.

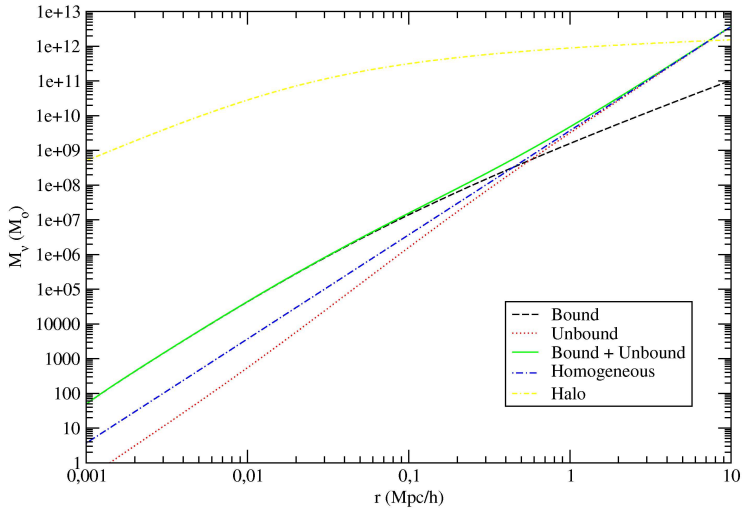

Figure A.10: A complete plot of neutrino mass used in the halo for $m_\nu = 0.6\,\mathrm{eV}$ neutrino in a $M_{\mathrm{vir}} = 10^{12}\,M_\odot$ halo. The plot shows the total bound, the total unbound, and the total neutrino mass used. Furthermore the total homogeneously distributed mass as well as the NFW halo mass are plotted.

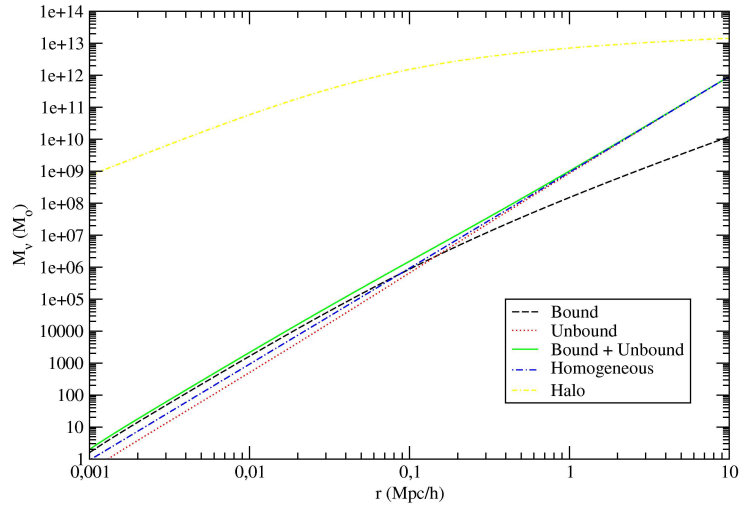

Figure A.11: A complete plot of neutrino mass used in the halo for $m_\nu = 0.15\,\mathrm{eV}$ neutrino in a $M_{\mathrm{vir}} = 10^{13}\,M_\odot$ halo. The plot shows the total bound, the total unbound, and the total neutrino mass used. Furthermore the total homogeneously distributed mass as well as the NFW halo mass are plotted.

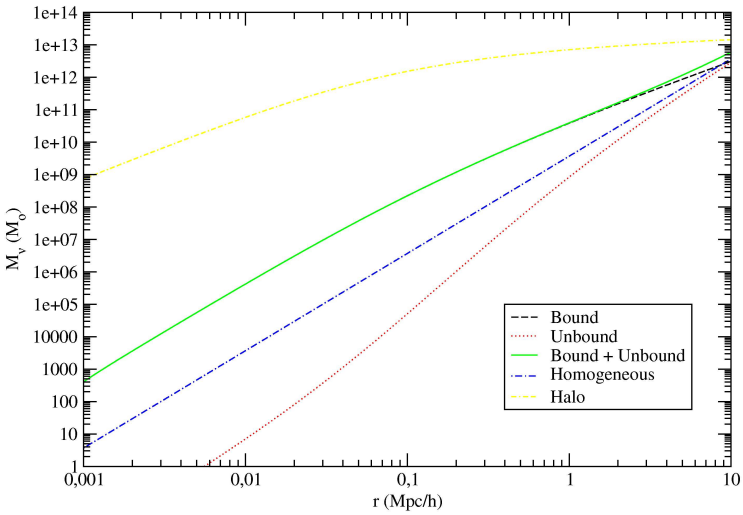

Figure A.12: A complete plot of neutrino mass used in the halo for $m_\nu = 0.6\,\mathrm{eV}$ neutrino in a $M_{\mathrm{vir}} = 10^{13}\,M_\odot$ halo. The plot shows the total bound, the total unbound, and the total neutrino mass used. Furthermore the total homogeneously distributed mass as well as the NFW halo mass are plotted.

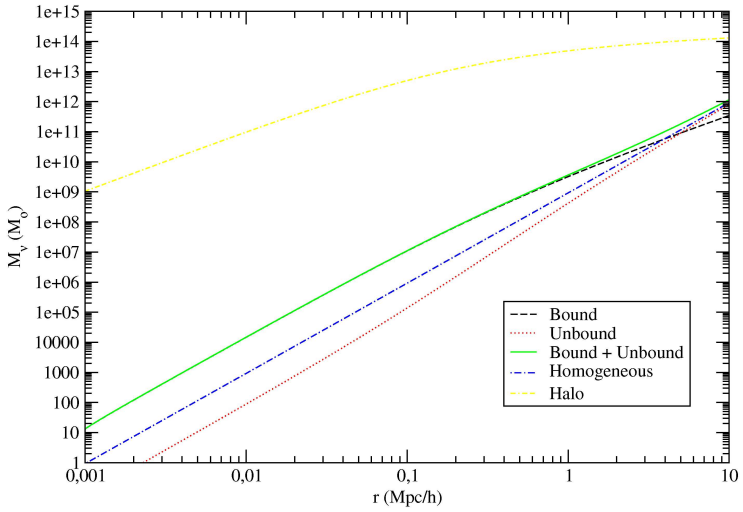

Figure A.13: A complete plot of neutrino mass used in the halo for $m_\nu = 0.15\,\mathrm{eV}$ neutrino in a $M_{\mathrm{vir}} = 10^{14}\,M_\odot$ halo. The plot shows the total bound, the total unbound, and the total neutrino mass used. Furthermore the total homogeneously distributed mass as well as the NFW halo mass are plotted.

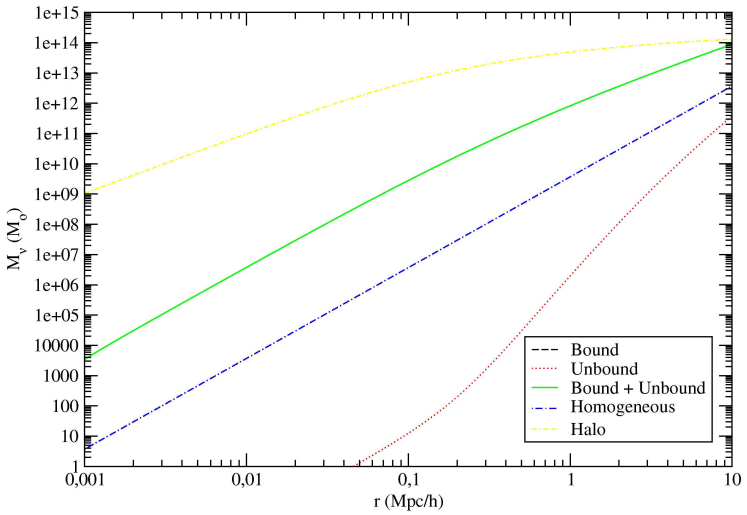

Figure A.14: A complete plot of neutrino mass used in the halo for $m_\nu = 0.6\,\mathrm{eV}$ neutrino in a $M_{\mathrm{vir}} = 10^{14}\,M_\odot$ halo. The plot shows the total bound, the total unbound, and the total neutrino mass used. Furthermore the total homogeneously distributed mass as well as the NFW halo mass are plotted.

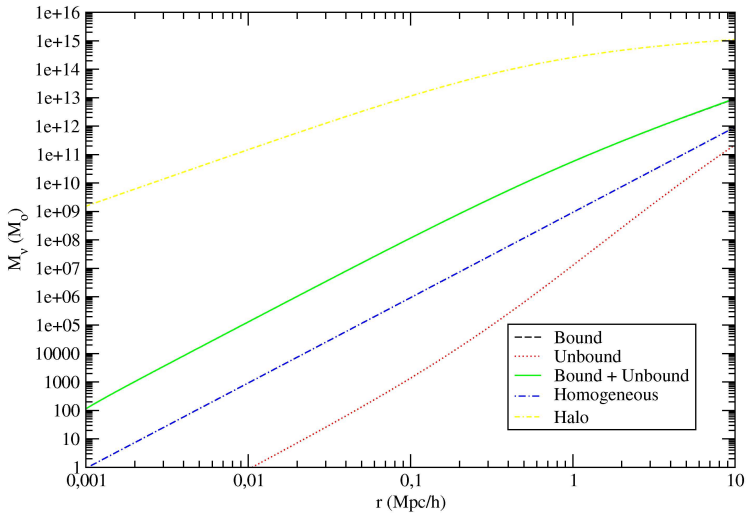

Figure A.15: A complete plot of neutrino mass used in the halo for $m_\nu = 0.15\,\mathrm{eV}$ neutrino in a $M_{\mathrm{vir}} = 10^{15}\,M_\odot$ halo. The plot shows the total bound, the total unbound, and the total neutrino mass used. Furthermore the total homogeneously distributed mass as well as the NFW halo mass are plotted.

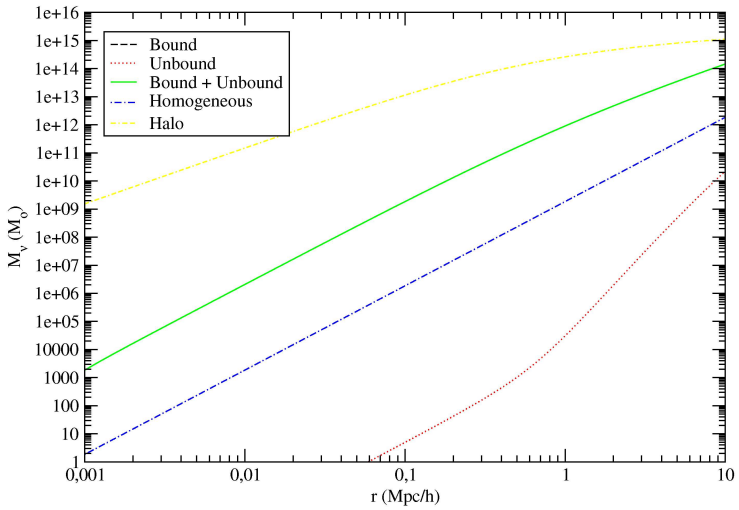

Figure A.16: A complete plot of neutrino mass used in the halo for $m_\nu = 0.3\,\mathrm{eV}$ neutrino in a $M_{\mathrm{vir}} = 10^{15}\,M_\odot$ halo. The plot shows the total bound, the total unbound, and the total neutrino mass used. Furthermore the total homogeneously distributed mass as well as the NFW halo mass are plotted.

A.2 Energy modified NFW

Below are all the remaining plots from chapter 3

A.2.1 Number density

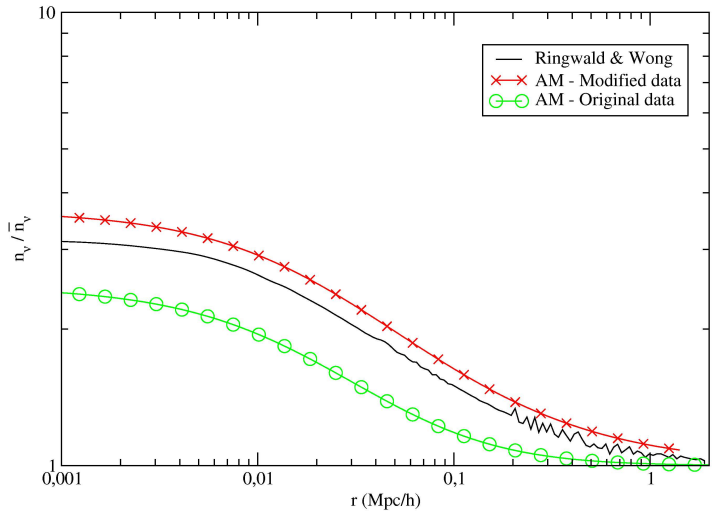

Figure A.17: Number densities n_ν normalized to present average $\overline{n}_\nu$ for the $m_\nu = 0.3\,\mathrm{eV}$ neutrino in a $M_{\mathrm{vir}} = 10^{12}\,M_\odot$ halo. Included in the plot are the data from RW (solid line), original NFW data (O-line) and the energy modified data (X-line).

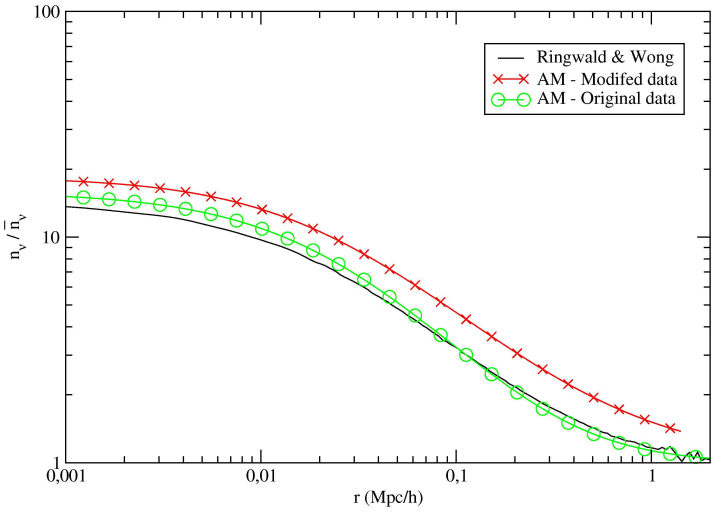

Figure A.18: Number densities n_ν normalized to present average $\overline{n}_\nu$ for the $m_\nu = 0.6\,\text{eV}$ neutrino in a $M_{\text{vir}} = 10^{12}\,M_\odot$ halo. Included in the plot are the data from RW (solid line), original NFW data (O-line) and the energy modified data (X-line).

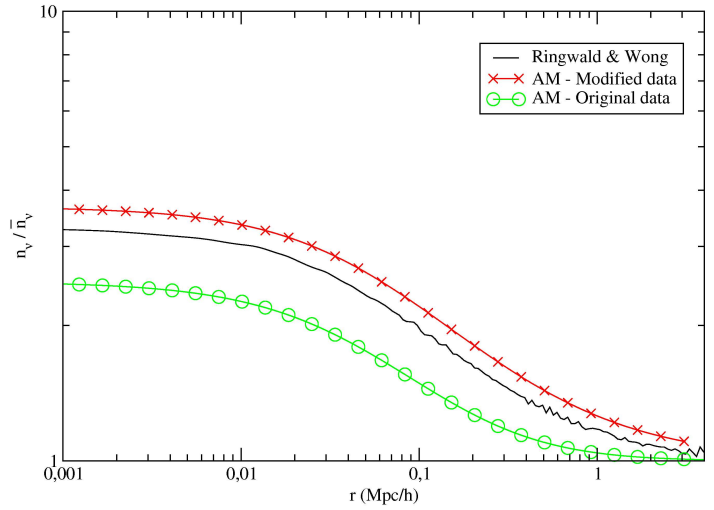

Figure A.19: Number densities n_ν normalized to present average $\overline{n}_\nu$ for the $m_\nu = 0.15\,\text{eV}$ neutrino in a $M_{\text{vir}} = 10^{13}\,M_\odot$ halo. Included in the plot are the data from RW (solid line), original NFW data (O-line) and the energy modified data (X-line).

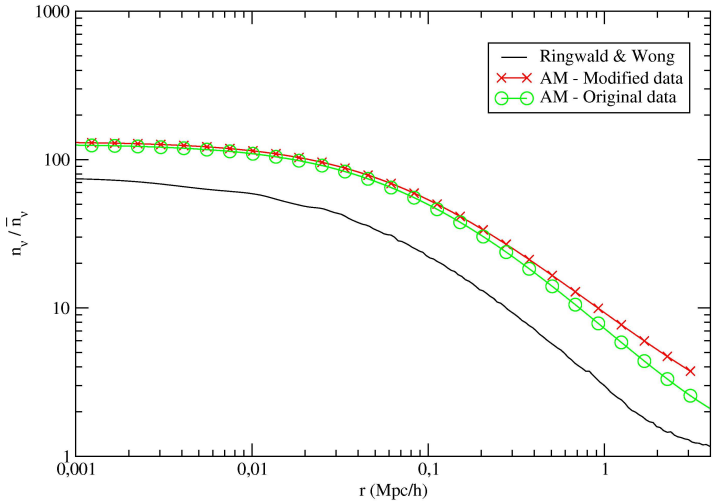

Figure A.20: Number densities n_ν normalized to present average $\overline{n}_\nu$ for the $m_\nu = 0.6\,\mathrm{eV}$ neutrino in a $M_{\mathrm{vir}} = 10^{13}\,M_\odot$ halo. Included in the plot are the data from RW (solid line), original NFW data (O-line) and the energy modified data (X-line).

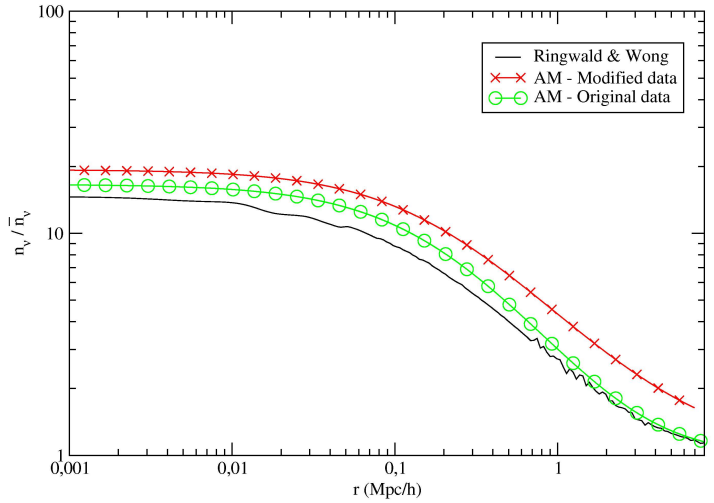

Figure A.21: Number densities n_ν normalized to present average $\overline{n}_\nu$ for the $m_\nu = 0.15\,\mathrm{eV}$ neutrino in a $M_{\mathrm{vir}} = 10^{14}\,M_\odot$ halo. Included in the plot are the data from RW (solid line), original NFW data (O-line) and the energy modified data (X-line).

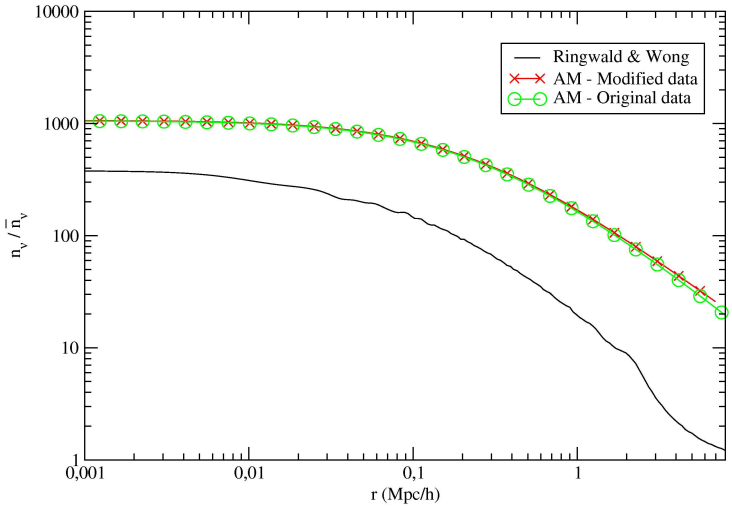

Figure A.22: Number densities n_ν normalized to present average $\overline{n}_\nu$ for the $m_\nu = 0.6\,\text{eV}$ neutrino in a $M_{\text{vir}} = 10^{14}\,M_\odot$ halo. Included in the plot are the data from RW (solid line), original NFW data (O-line) and the energy modified data (X-line).

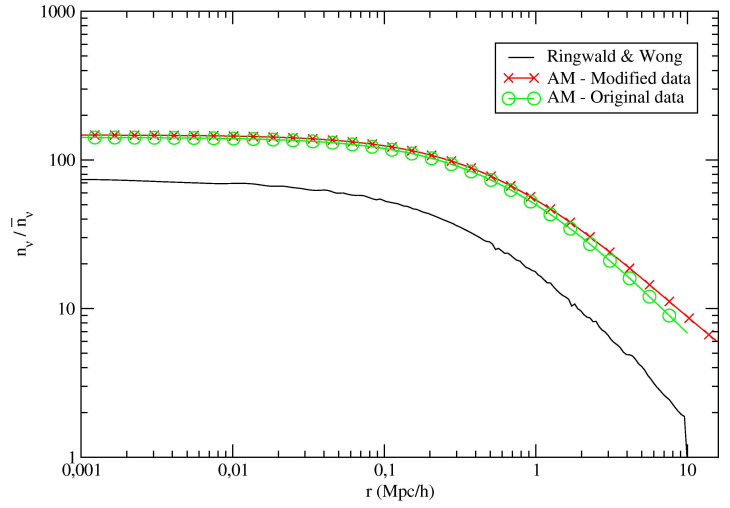

Figure A.23: Number densities n_ν normalized to present average $\overline{n}_\nu$ for the $m_\nu = 0.15\,\text{eV}$ neutrino in a $M_{\text{vir}} = 10^{15}\,M_\odot$ halo. Included in the plot are the data from RW (solid line), original NFW data (O-line) and the energy modified data (X-line).

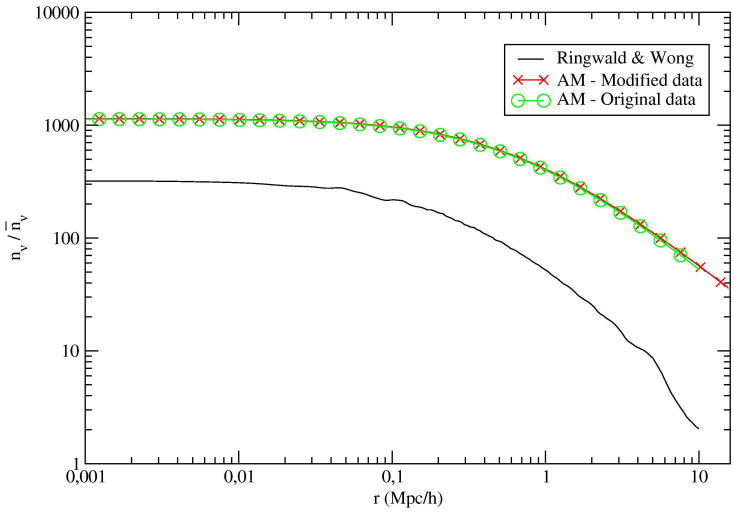

Figure A.24: Number densities n_ν normalized to present average $\bar{n}_\nu$ for the $m_\nu = 0.3\,\mathrm{eV}$ neutrino in a $M_{\mathrm{vir}} = 10^{12}\,M_\odot$ halo. Included in the plot are the data from RW (solid line), original NFW data (O-line) and the energy modified data (X-line).

A.2.2 Mass

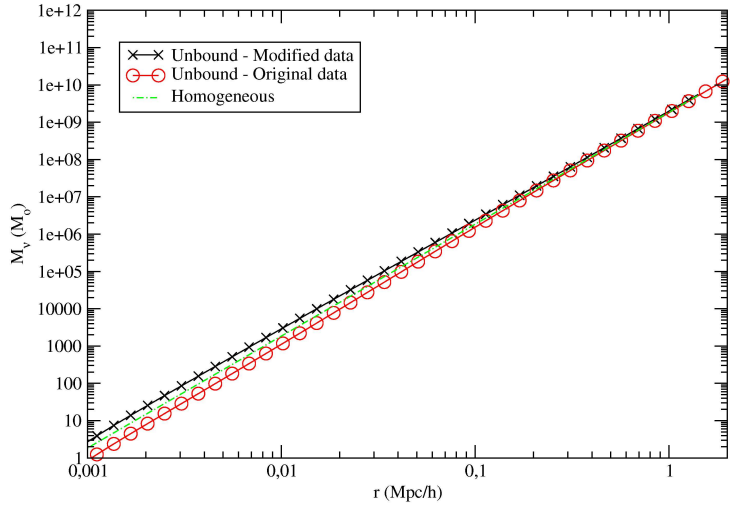

Figure A.25: Unbound masses used in a $M_{\mathrm{vir}} = 10^{12}\,M_\odot$ NFW halo. Neutrino mass is $m_\nu = 0.3\,\mathrm{eV}$. The plot compares original NFW data (O-line) with the energy modified data (X-line). Dashed-line shows the homogeneously distributed neutrinos.

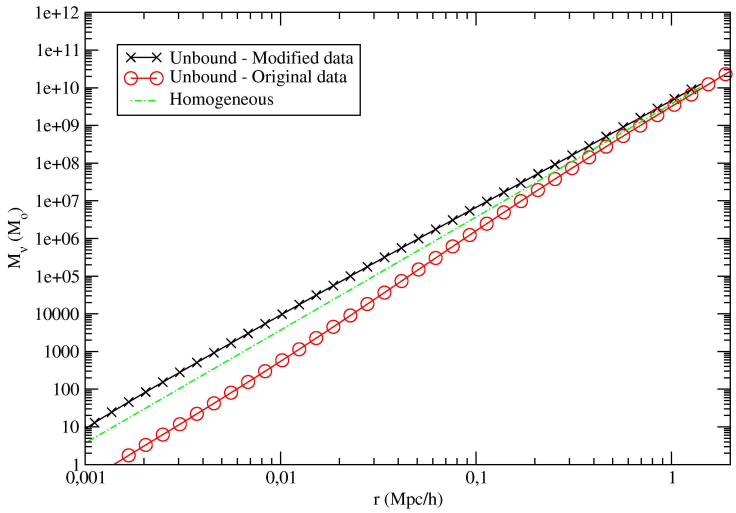

Figure A.26: Unbound masses used in a $M_{\text{vir}} = 10^{12}\, M_{\odot}$ NFW halo. Neutrino mass is $m_{\nu} = 0.6\,\text{eV}$. The plot compares original NFW data (O-line) with the energy modified data (X-line). Dashed-line shows the homogeneously distributed neutrinos.

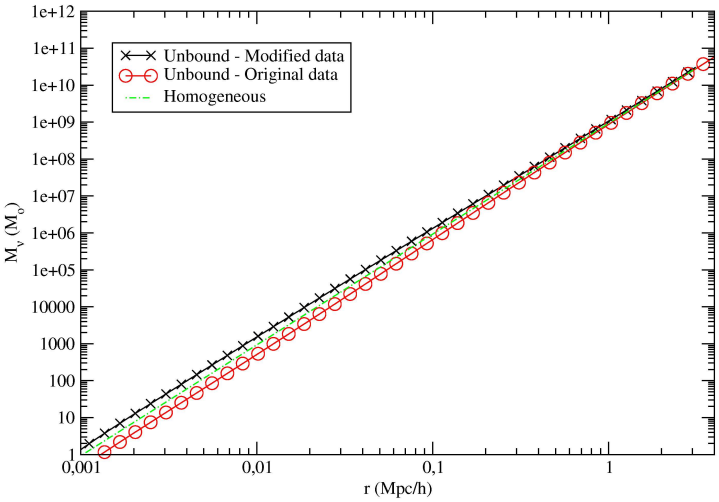

Figure A.27: Unbound masses used in a $M_{\text{vir}} = 10^{13}\, M_{\odot}$ NFW halo. Neutrino mass is $m_{\nu} = 0.15\,\text{eV}$. The plot compares original NFW data (O-line) with the energy modified data (X-line). Dashed-line shows the homogeneously distributed neutrinos.

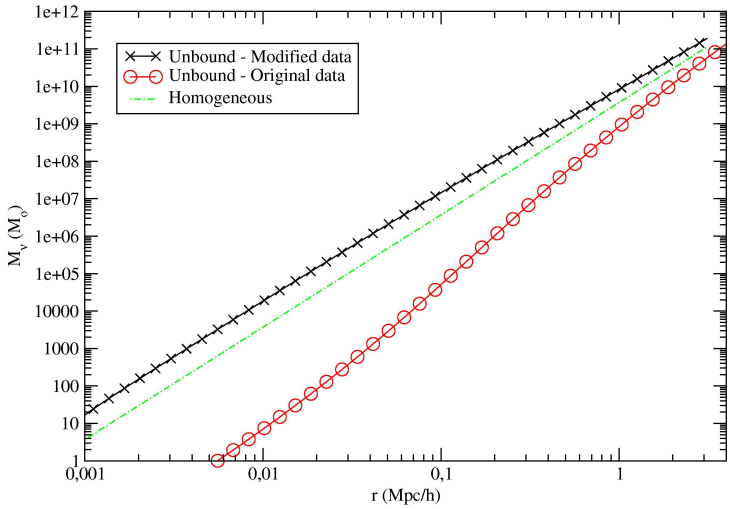

Figure A.28: Unbound masses used in a $M_{\rm vir} = 10^{13}\,M_\odot$ NFW halo. Neutrino mass is $m_\nu = 0.6\,\mathrm{eV}$. The plot compares original NFW data (O-line) with the energy modified data (X-line). Dashed-line shows the homogeneously distributed neutrinos.

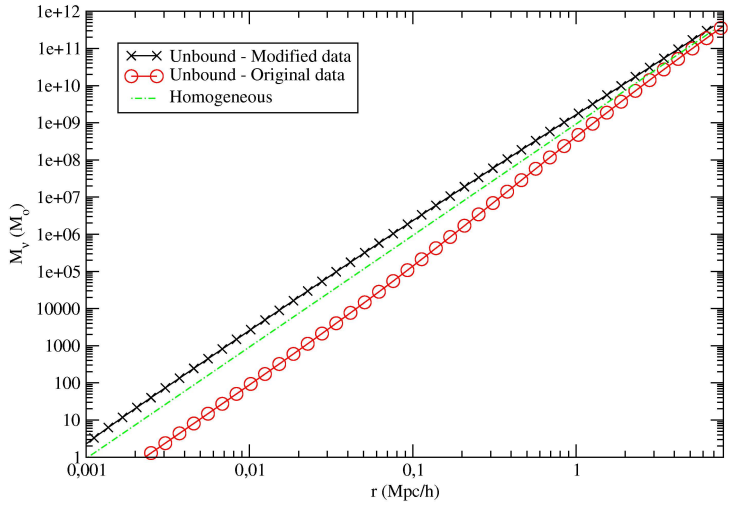

Figure A.29: Unbound masses used in a $M_{\rm vir} = 10^{14}\,M_\odot$ NFW halo. Neutrino mass is $m_\nu = 0.15\,\mathrm{eV}$. The plot compares original NFW data (O-line) with the energy modified data (X-line). Dashed-line shows the homogeneously distributed neutrinos.

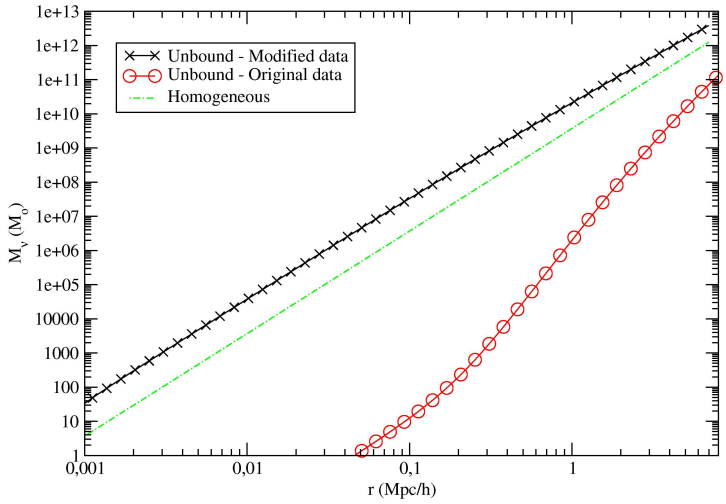

Figure A.30: Unbound masses used in a $M_{\text{vir}} = 10^{14}\, M_{\odot}$ NFW halo. Neutrino mass is $m_{\nu} = 0.6\,\text{eV}$. The plot compares original NFW data (O-line) with the energy modified data (X-line). Dashed-line shows the homogeneously distributed neutrinos.

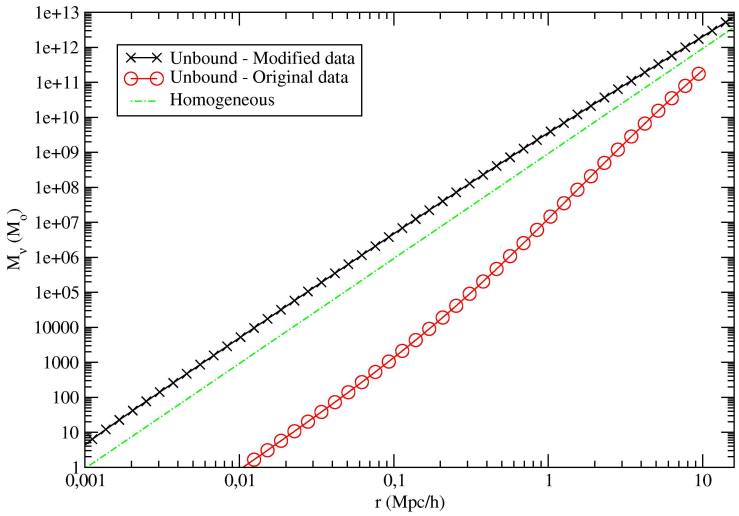

Figure A.31: Unbound masses used in a $M_{\text{vir}} = 10^{15}\, M_{\odot}$ NFW halo. Neutrino mass is $m_{\nu} = 0.15\,\text{eV}$. The plot compares original NFW data (O-line) with the energy modified data (X-line). Dashed-line shows the homogeneously distributed neutrinos.

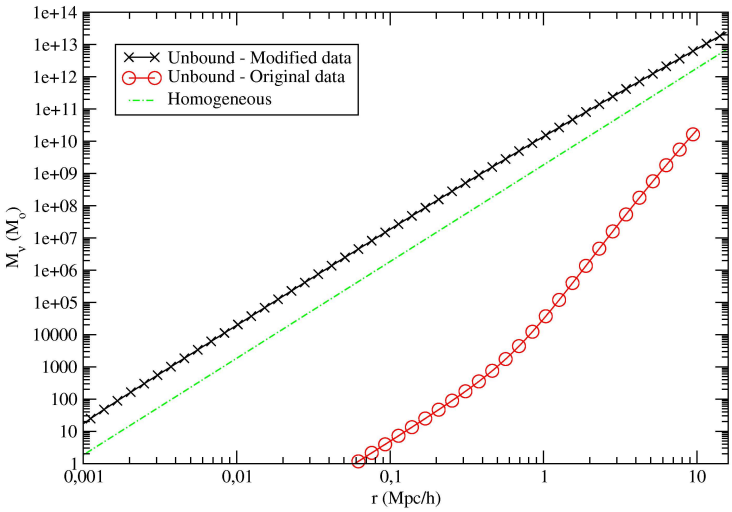

Figure A.32: Unbound masses used in a $M_{\rm vir} = 10^{15}\,M_\odot$ NFW halo. Neutrino mass is $m_\nu = 0.3\,\mathrm{eV}$. The plot compares original NFW data (O-line) with the energy modified data (X-line). Dashed-line shows the homogeneously distributed neutrinos.

A.3 Phase-space modified NFW

Below are all the remaining plots from chapter 4

A.3.1 Number density

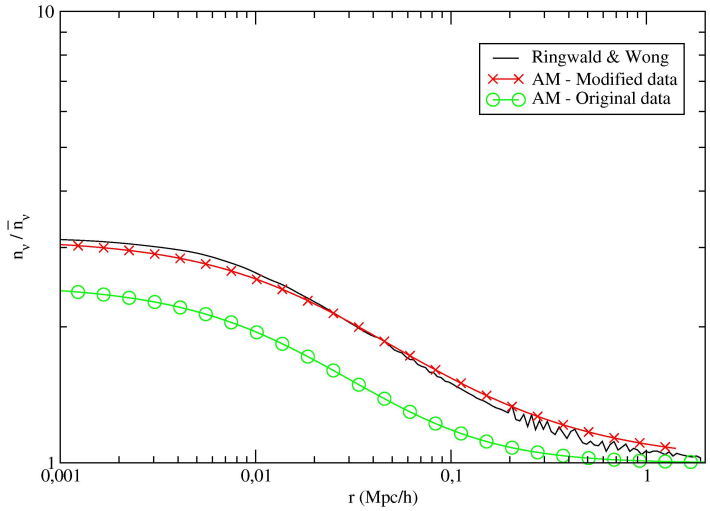

Figure A.33: Number densities n_ν normalized to present average $\bar{n}_\nu$ for the $m_\nu = 0.3\,\mathrm{eV}$ neutrino in a $M_{\mathrm{vir}} = 10^{12}\,M_\odot$ NFW halo. Included in the plot are the data from RW (solid line), original NFW data (O-line) and the phase-space modified data (X-line).

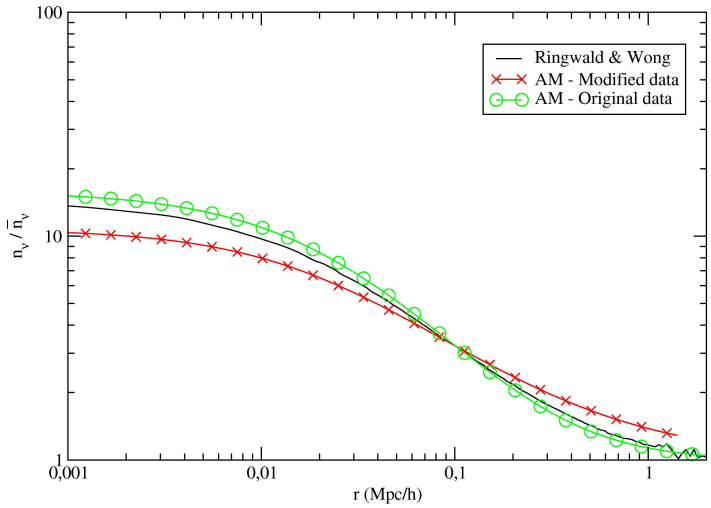

Figure A.34: Number densities n_ν normalized to present average $\bar{n}_\nu$ for the $m_\nu = 0.6\,\mathrm{eV}$ neutrino in a $M_{\mathrm{vir}} = 10^{12}\,M_\odot$ NFW halo. Included in the plot are the data from RW (solid line), original NFW data (O-line) and the phase-space modified data (X-line).

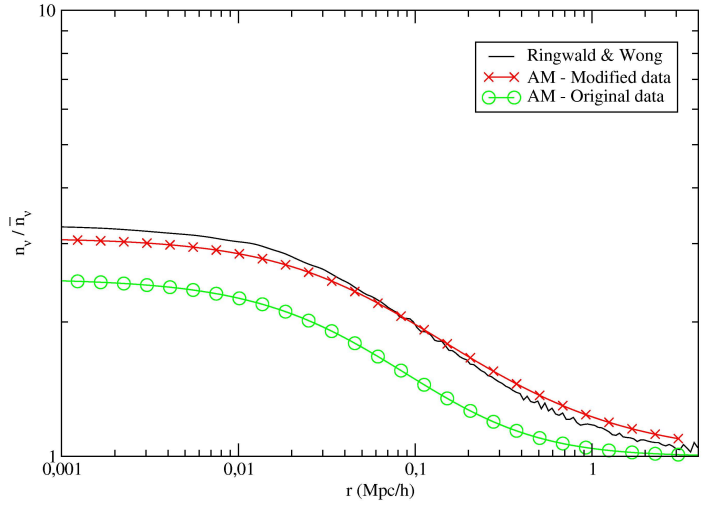

Figure A.35: Number densities n_ν normalized to present average $\bar{n}_\nu$ for the $m_\nu = 0.15\,\mathrm{eV}$ neutrino in a $M_{\mathrm{vir}} = 10^{13}\,M_\odot$ NFW halo. Included in the plot are the data from RW (solid line), original NFW data (O-line) and the phase-space modified data (X-line).

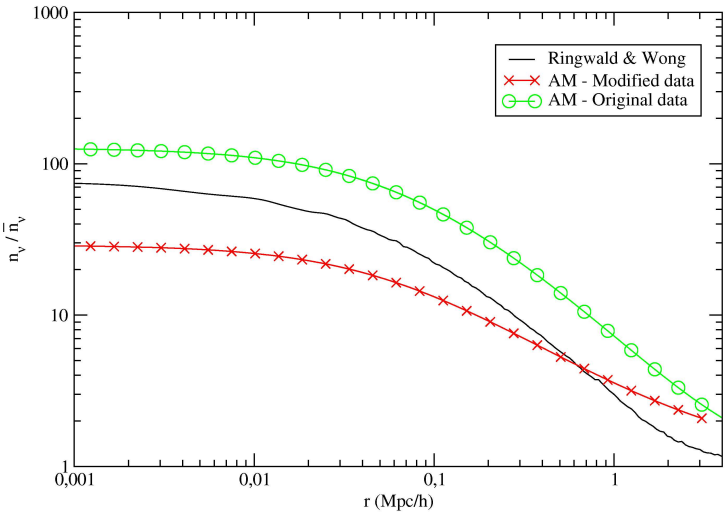

Figure A.36: Number densities n_ν normalized to present average $\bar{n}_\nu$ for the $m_\nu = 0.6\,\text{eV}$ neutrino in a $M_{\text{vir}} = 10^{13}\,M_\odot$ NFW halo. Included in the plot are the data from RW (solid line), original NFW data (O-line) and the phase-space modified data (X-line).

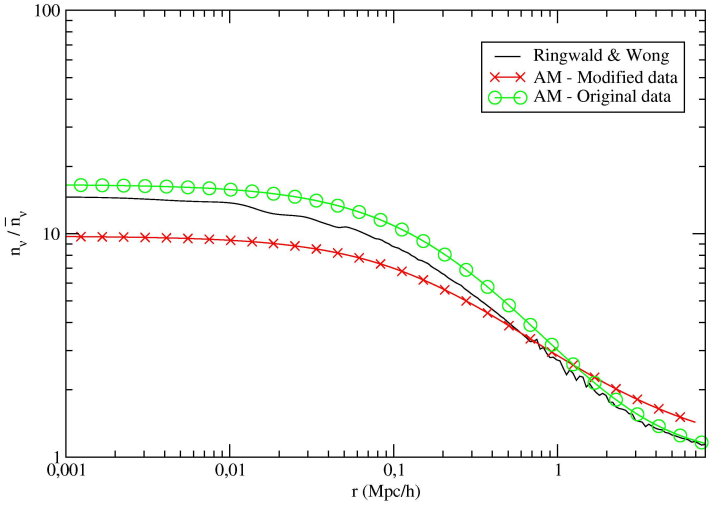

Figure A.37: Number densities n_ν normalized to present average $\bar{n}_\nu$ for the $m_\nu = 0.15\,\text{eV}$ neutrino in a $M_{\text{vir}} = 10^{14}\,M_\odot$ NFW halo. Included in the plot are the data from RW (solid line), original NFW data (O-line) and the phase-space modified data (X-line).

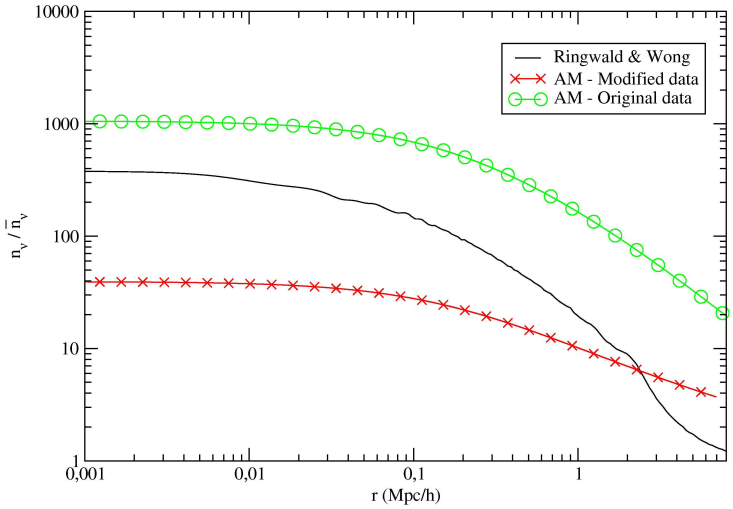

Figure A.38: Number densities n_ν normalized to present average $\overline{n}_\nu$ for the $m_\nu = 0.6\,\mathrm{eV}$ neutrino in a $M_{\mathrm{vir}} = 10^{14}\,M_\odot$ NFW halo.Included in the plot are the data from RW (solid line), original NFW data (O-line) and the phase-space modified data (X-line).

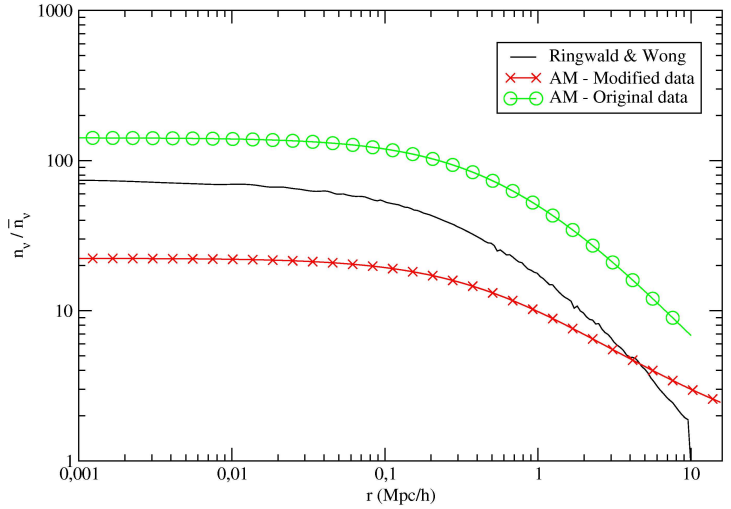

Figure A.39: Number densities n_ν normalized to present average $\overline{n}_\nu$ for the $m_\nu = 0.15\,\mathrm{eV}$ neutrino in a $M_{\mathrm{vir}} = 10^{15}\,M_\odot$ NFW halo. Included in the plot are the data from RW (solid line), original NFW data (O-line) and the phase-space modified data (X-line).

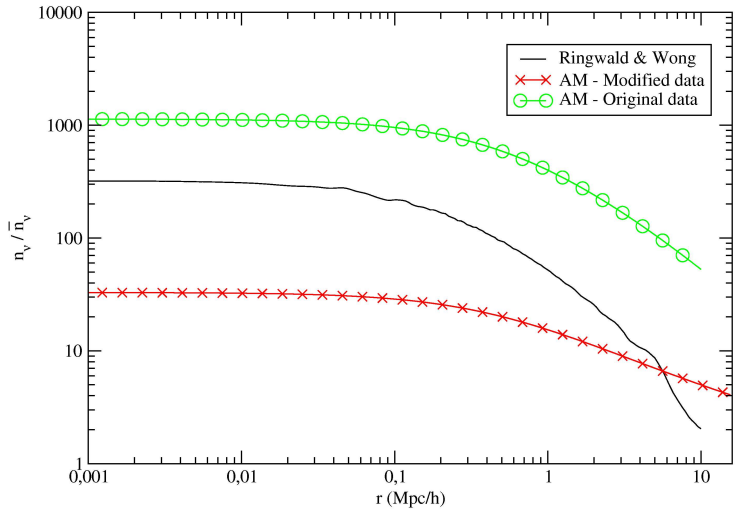

Figure A.40: Number densities n_ν normalized to present average $\bar{n}_\nu$ for the $m_\nu = 0.3\,\mathrm{eV}$ neutrino in a $M_{\mathrm{vir}} = 10^{15}\,M_\odot$ NFW halo. Included in the plot are the data from RW (solid line), original NFW data (O-line) and the phase-space modified data (X-line).

A.3.2 Mass

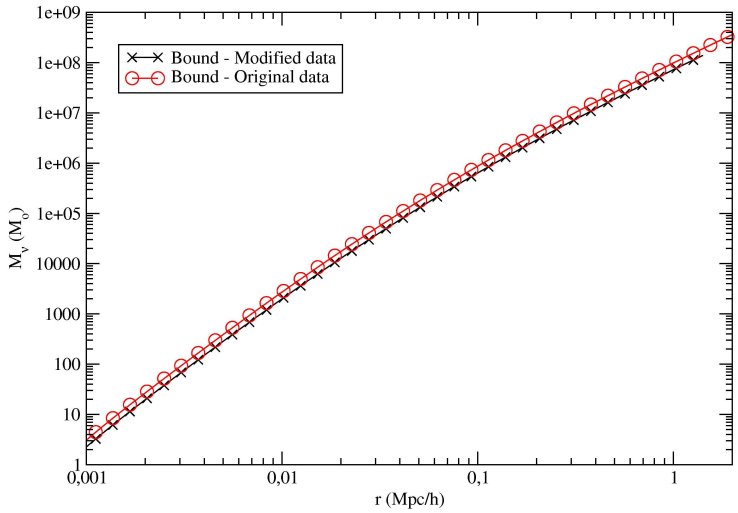

Figure A.41: Bound masses used in a $M_{\mathrm{vir}} = 10^{12}\,M_\odot$ NFW halo. Neutrino mass is $m_\nu = 0.3\,\mathrm{eV}$. The plot compares original NFW data (O-line) with the phase-space modified data (X-line).

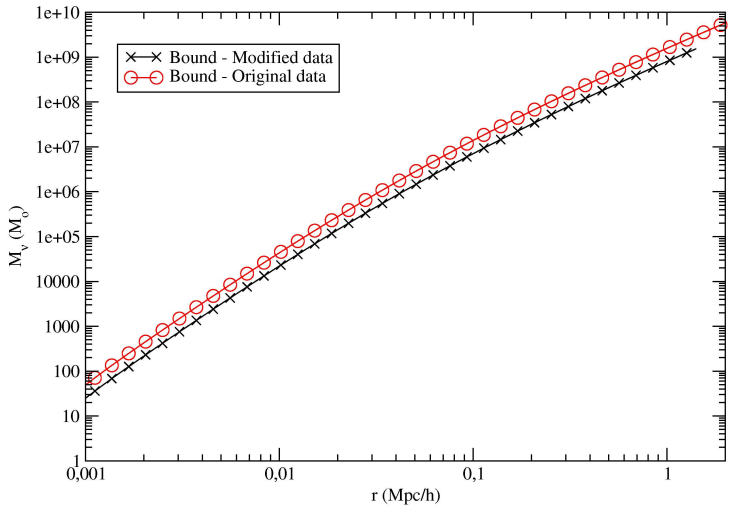

Figure A.42: Bound masses used in a $M_{\rm vir} = 10^{12}\,M_{\odot}$ NFW halo. Neutrino mass is $m_{\nu} = 0.6\,\mathrm{eV}$. The plot compares original NFW data (O-line) with the phase-space modified data (X-line).

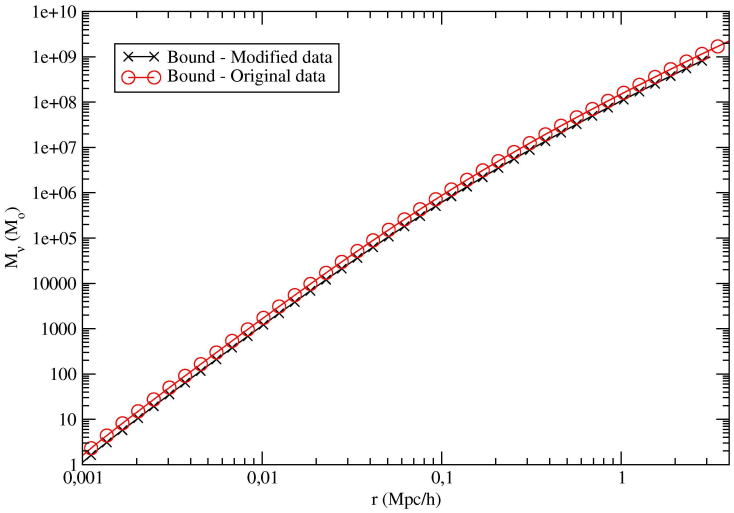

Figure A.43: Bound masses used in a $M_{\rm vir} = 10^{13}\,M_{\odot}$ NFW halo. Neutrino mass is $m_{\nu} = 0.15\,\mathrm{eV}$. The plot compares original NFW data (O-line) with the phase-space modified data (X-line).

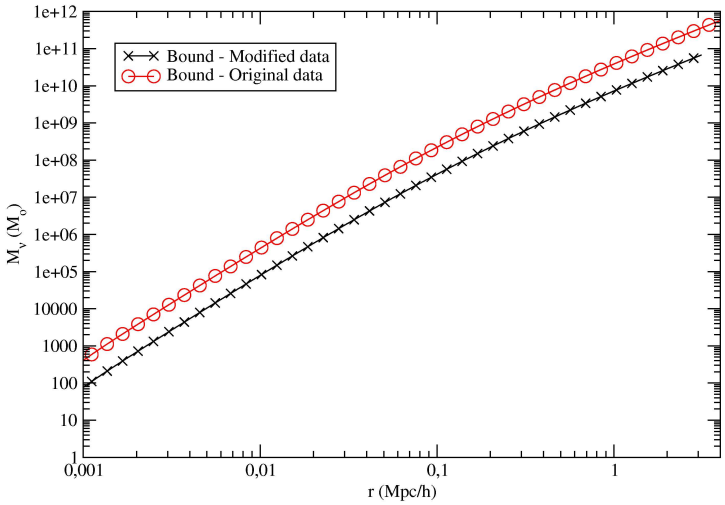

Figure A.44: Bound masses used in a $M_{\rm vir} = 10^{13}\,M_{\odot}$ NFW halo. Neutrino mass is $m_{\nu} = 0.6\,\mathrm{eV}$. The plot compares original NFW data (O-line) with the phase-space modified data (X-line).

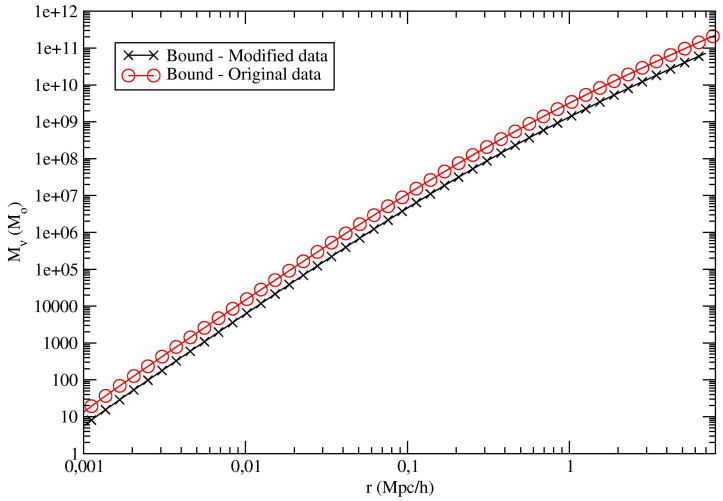

Figure A.45: Bound masses used in a $M_{\rm vir} = 10^{14}\,M_{\odot}$ NFW halo. Neutrino mass is $m_{\nu} = 0.14\,\mathrm{eV}$. The plot compares original NFW data (O-line) with the phase-space modified data (X-line).

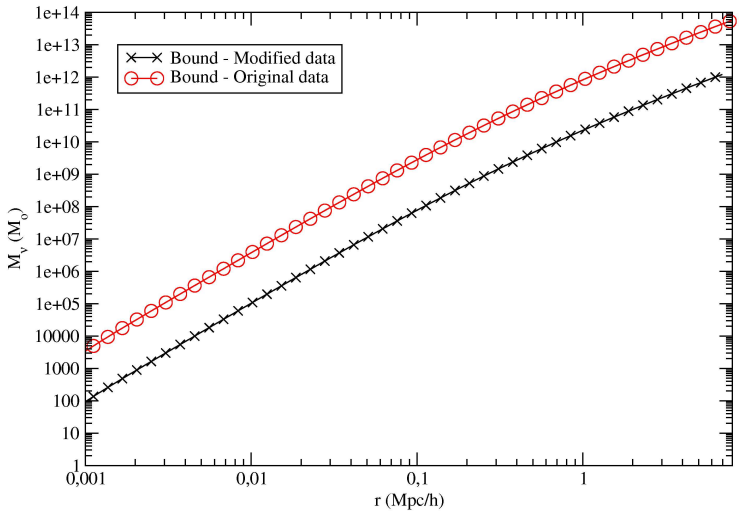

Figure A.46: Bound masses used in a $M_{\text{vir}} = 10^{14}\, M_{\odot}$ NFW halo. Neutrino mass is $m_{\nu} = 0.6\,\text{eV}$. The plot compares original NFW data (O-line) with the phase-space modified data (X-line).

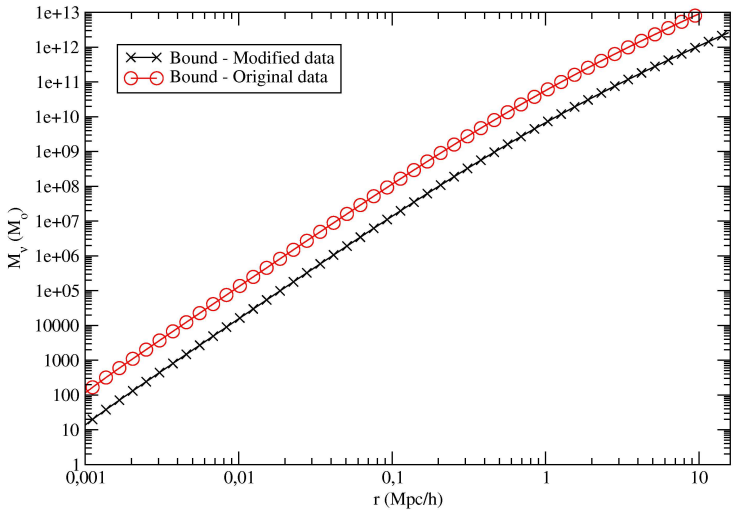

Figure A.47: Bound masses used in a $M_{\text{vir}} = 10^{15}\, M_{\odot}$ NFW halo. Neutrino mass is $m_{\nu} = 0.15\,\text{eV}$. The plot compares original NFW data (O-line) with the phase-space modified data (X-line).

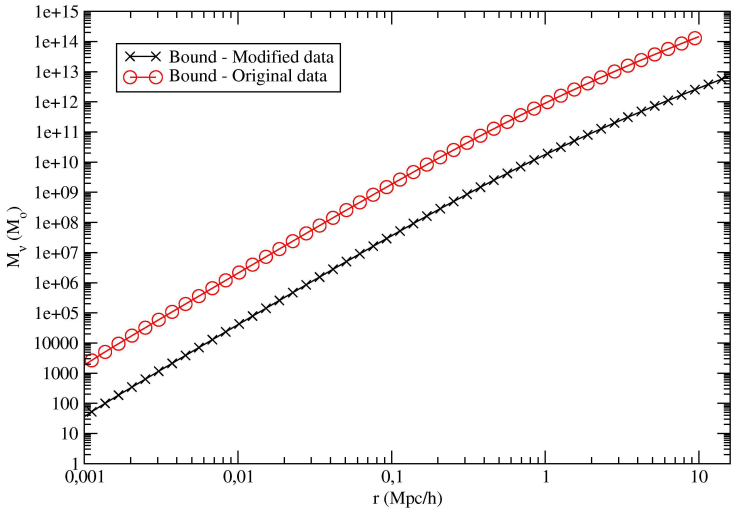

Figure A.48: Bound masses used in a $M_{\rm vir} = 10^{15}\,M_\odot$ NFW halo. Neutrino mass is $m_\nu = 0.3\,\mathrm{eV}$. The plot compares original NFW data (O-line) with the phase-space modified data (X-line).

A.4 NFW + Black Hole

Below are all the remaining plots from chapter 6

A.4.1 Number density

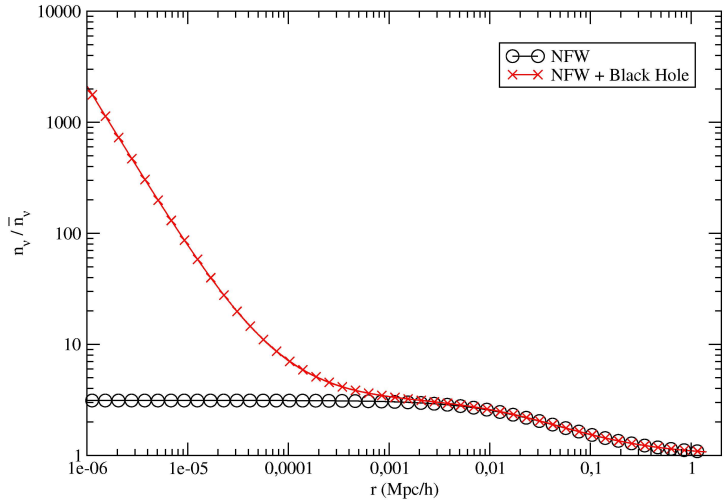

Figure A.49: Normalized number density in a $M_{\text{vir}} = 10^{12}\,M_\odot$ NFW halo with a central $3.7 \cdot 10^9\,M_\odot$ black hole. Neutrino mass is $m_\nu = 0.3\,\text{eV}$. The plot compares the clean phase-space modified NFW (O-line) with the phase-space modified NFW + Black Hole (X-line).

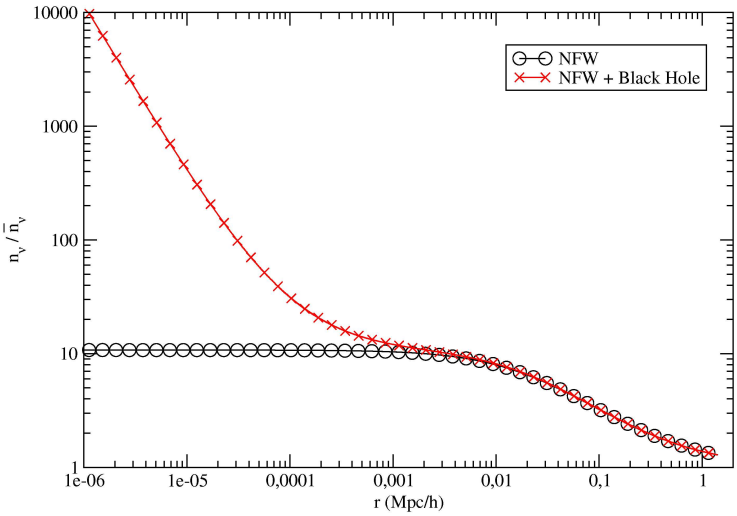

Figure A.50: Normalized number density in a $M_{\rm vir} = 10^{12}\,M_\odot$ NFW halo with a central $3.7 \cdot 10^9\,M_\odot$ black hole. Neutrino mass is $m_\nu = 0.6\,\text{eV}$. The plot compares the clean phase-space modified NFW (O-line) with the phase-space modified NFW + Black Hole (X-line).

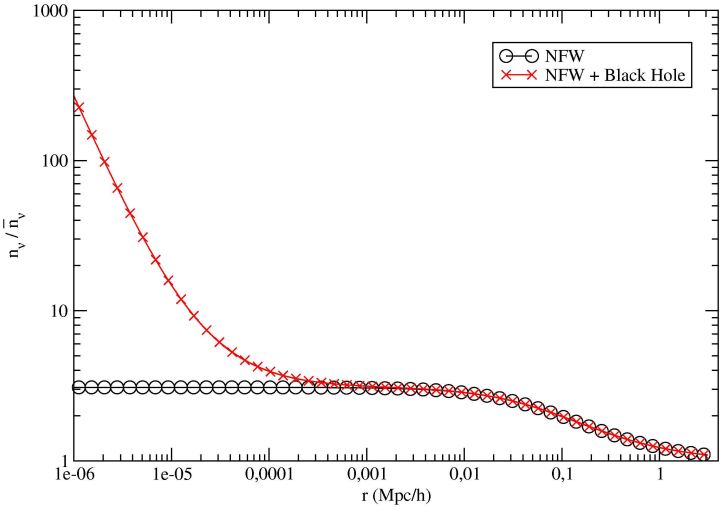

Figure A.51: Normalized number density in a $M_{\rm vir} = 10^{13}\,M_\odot$ NFW halo with a central $3.7 \cdot 10^9\,M_\odot$ black hole. Neutrino mass is $m_\nu = 0.15\,\text{eV}$. The plot compares the clean phase-space modified NFW (O-line) with the phase-space modified NFW + Black Hole (X-line).

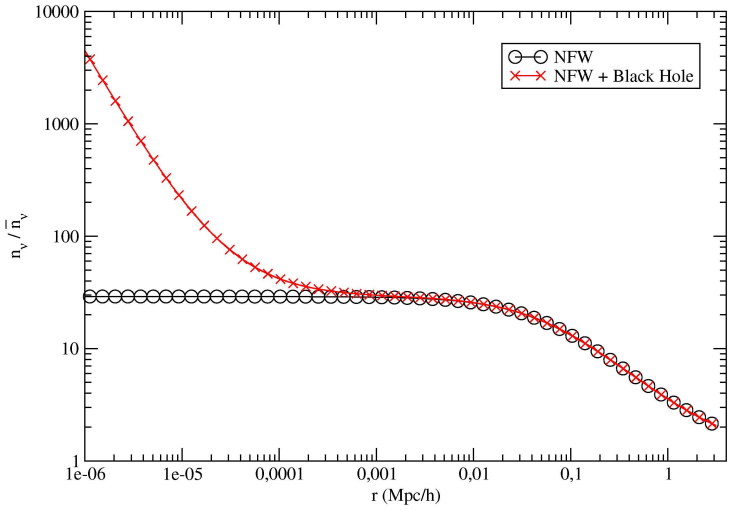

Figure A.52: Normalized number density in a $M_{\rm vir} = 10^{13}\,M_\odot$ NFW halo with a central $3.7 \cdot 10^9\,M_\odot$ black hole. Neutrino mass is $m_\nu = 0.6\,\text{eV}$. The plot compares the clean phase-space modified NFW (O-line) with the phase-space modified NFW + Black Hole (X-line).

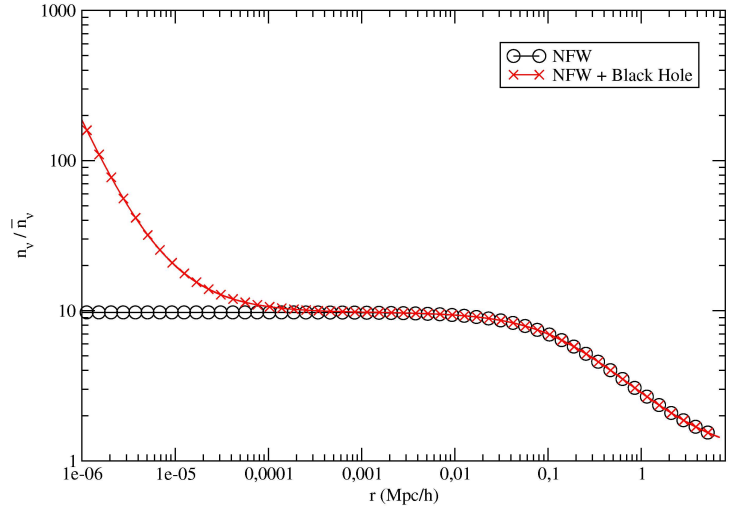

Figure A.53: Normalized number density in a $M_{\rm vir} = 10^{14}\,M_\odot$ NFW halo with a central $3.7 \cdot 10^9\,M_\odot$ black hole. Neutrino mass is $m_\nu = 0.15\,\text{eV}$. The plot compares the clean phase-space modified NFW (O-line) with the phase-space modified NFW + Black Hole (X-line).

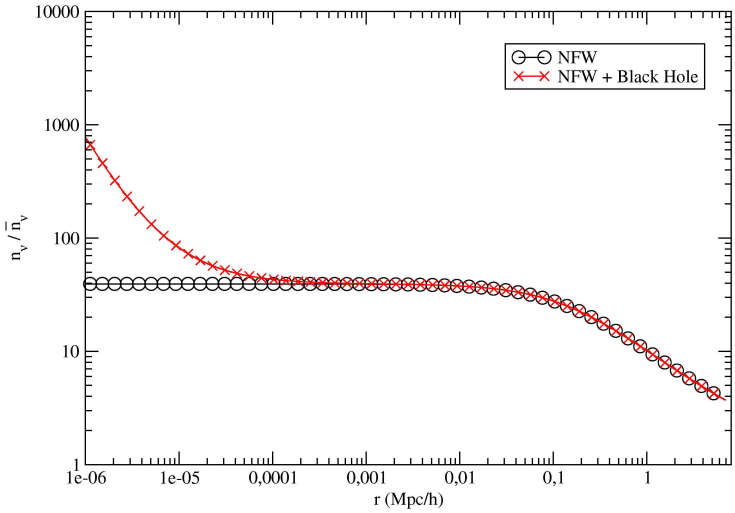

Figure A.54: Normalized number density in a $M_{\rm vir} = 10^{14}\,M_\odot$ NFW halo with a central $3.7 \cdot 10^9\,M_\odot$ black hole. Neutrino mass is $m_\nu = 0.6\,\text{eV}$. The plot compares the clean phase-space modified NFW (O-line) with the phase-space modified NFW + Black Hole (X-line).

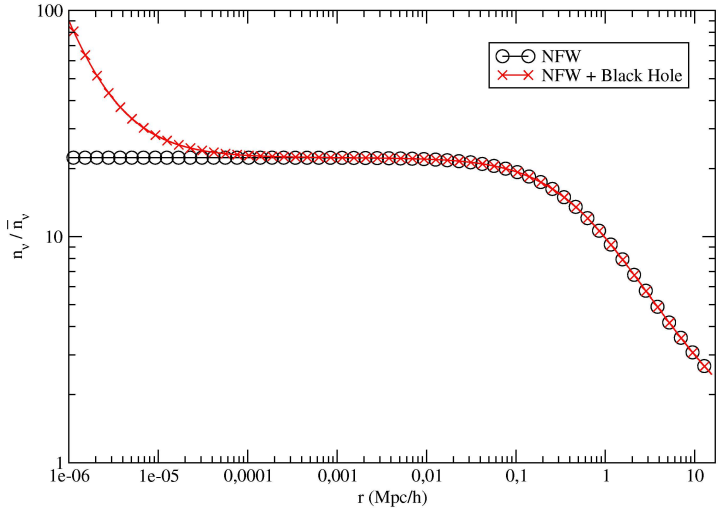

Figure A.55: Normalized number density in a $M_{\rm vir} = 10^{15}\,M_\odot$ NFW halo with a central $3.7 \cdot 10^9\,M_\odot$ black hole. Neutrino mass is $m_\nu = 0.15\,\text{eV}$. The plot compares the clean phase-space modified NFW (O-line) with the phase-space modified NFW + Black Hole (X-line).

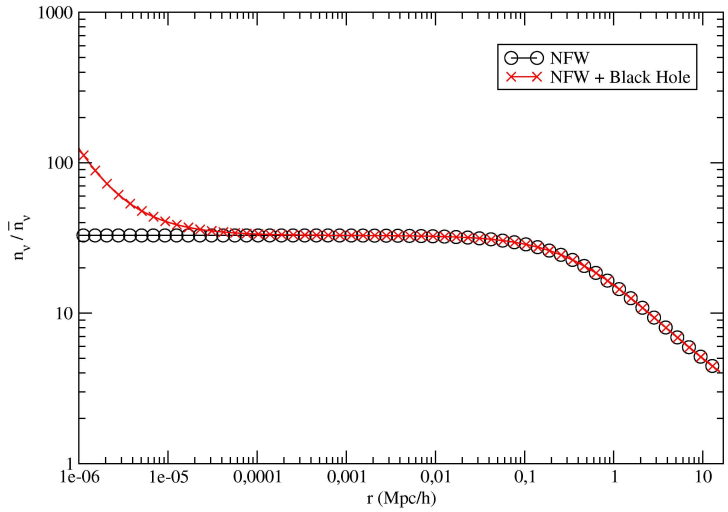

Figure A.56: Normalized number density in a $M_{\rm vir} = 10^{15}\,M_\odot$ NFW halo with a central $3.7 \cdot 10^9\,M_\odot$ black hole. Neutrino mass is $m_\nu = 0.3\,\text{eV}$. The plot compares the clean phase-space modified NFW (O-line) with the phase-space modified NFW + Black Hole (X-line).

A.4.2 Mass

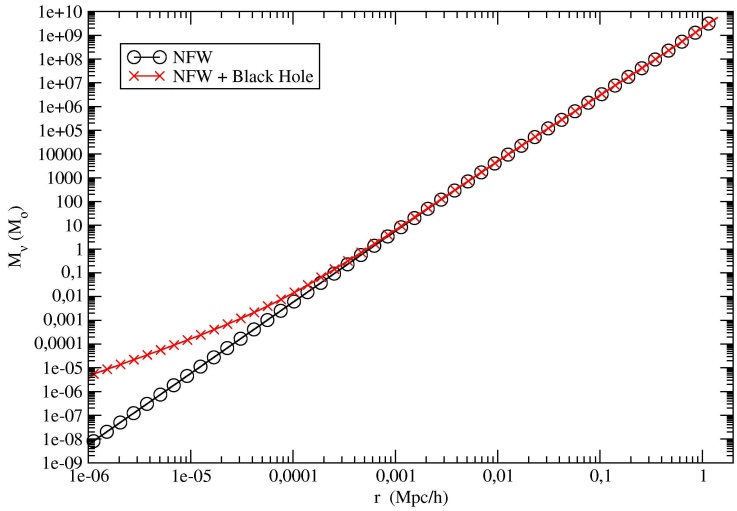

Figure A.57: Total masses used in a $M_{\rm vir} = 10^{12}\,M_\odot$ NFW halo with a central $3.7 \cdot 10^9\,M_\odot$ black hole. Neutrino mass is $m_\nu = 0.3\,\text{eV}$. The plot compares the clean phase-space modified NFW (O-line) with the phase-space modified NFW + Black Hole (X-line).

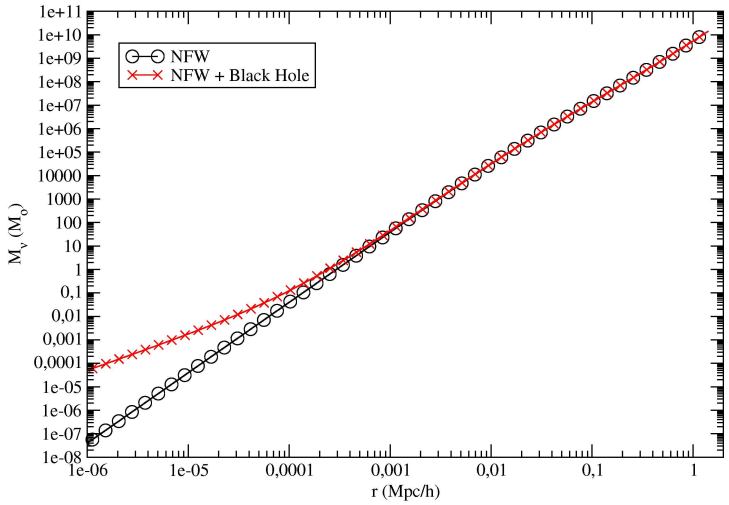

Figure A.58: Total masses used in a $M_{\text{vir}} = 10^{12}\, M_{\odot}$ NFW halo with a central $3.7 \cdot 10^{9}\, M_{\odot}$ black hole. Neutrino mass is $m_{\nu} = 0.6\,\text{eV}$. The plot compares the clean phase-space modified NFW (O-line) with the phase-space modified NFW + Black Hole (X-line).

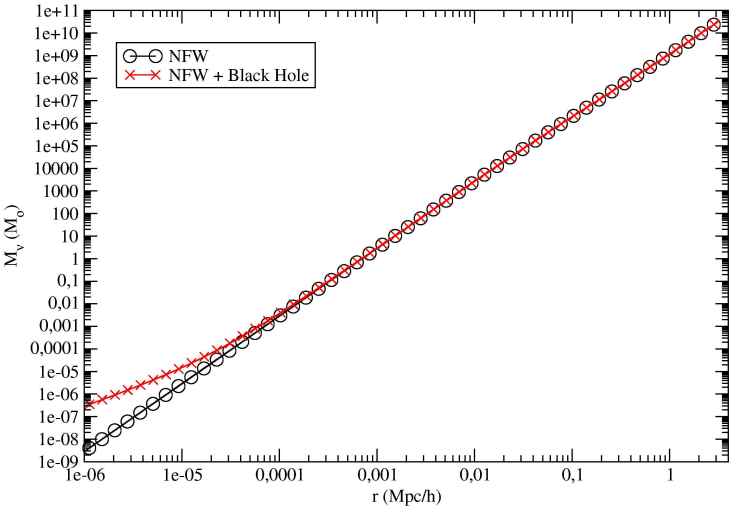

Figure A.59: Total masses used in a $M_{\text{vir}} = 10^{13}\, M_{\odot}$ NFW halo with a central $3.7 \cdot 10^{9}\, M_{\odot}$ black hole. Neutrino mass is $m_{\nu} = 0.15\,\text{eV}$. The plot compares the clean phase-space modified NFW (O-line) with the phase-space modified NFW + Black Hole (X-line).

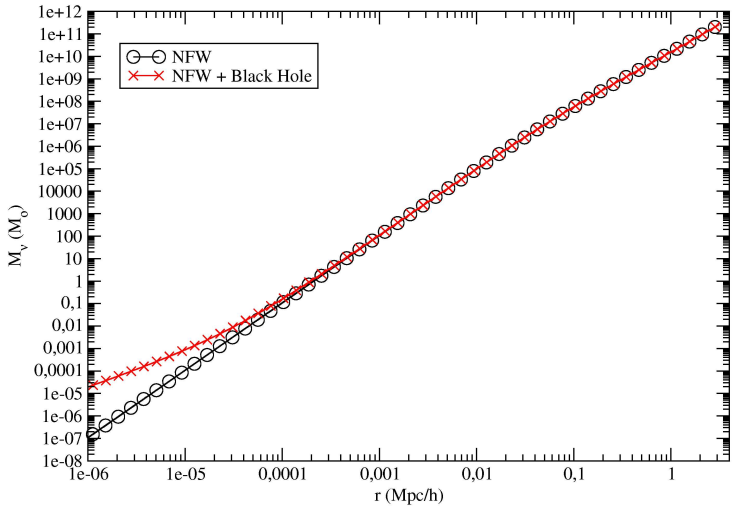

Figure A.60: Total masses used in a $M_{\text{vir}} = 10^{13}\, M_{\odot}$ NFW halo with a central $3.7 \cdot 10^{9}\, M_{\odot}$ black hole. Neutrino mass is $m_{\nu} = 0.6\,\text{eV}$. The plot compares the clean phase-space modified NFW (O-line) with the phase-space modified NFW + Black Hole (X-line).

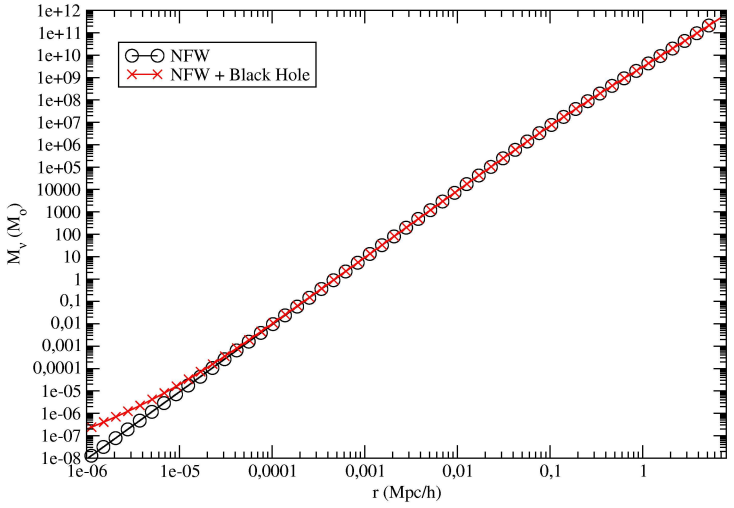

Figure A.61: Total masses used in a $M_{\text{vir}} = 10^{14}\, M_{\odot}$ NFW halo with a central $3.7 \cdot 10^{9}\, M_{\odot}$ black hole. Neutrino mass is $m_{\nu} = 0.15\,\text{eV}$. The plot compares the clean phase-space modified NFW (O-line) with the phase-space modified NFW + Black Hole (X-line).

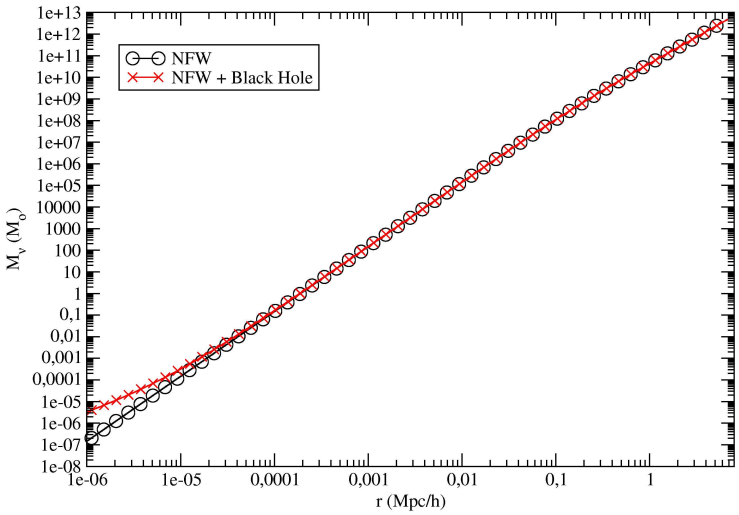

Figure A.62: Total masses used in a $M_{\text{vir}} = 10^{14}\, M_{\odot}$ NFW halo with a central $3.7 \cdot 10^{9}\, M_{\odot}$ black hole. Neutrino mass is $m_{\nu} = 0.6\,\text{eV}$. The plot compares the clean phase-space modified NFW (O-line) with the phase-space modified NFW + Black Hole (X-line).

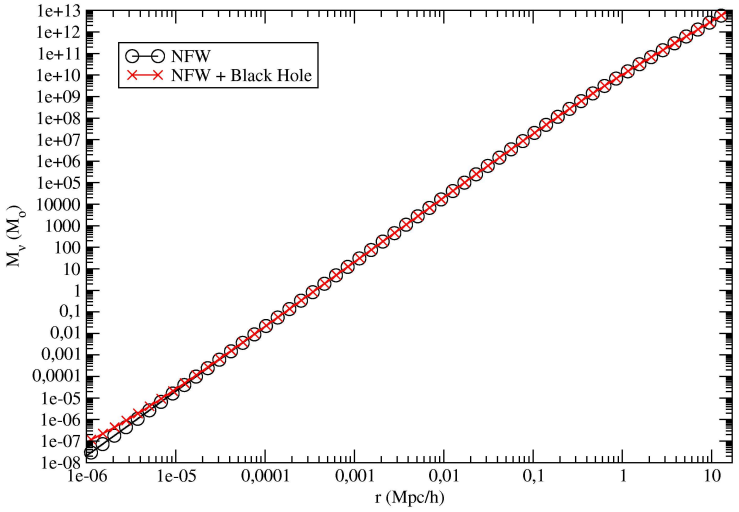

Figure A.63: Total masses used in a $M_{\text{vir}} = 10^{15}\, M_{\odot}$ NFW halo with a central $3.7 \cdot 10^{9}\, M_{\odot}$ black hole. Neutrino mass is $m_{\nu} = 0.15\,\text{eV}$. The plot compares the clean phase-space modified NFW (O-line) with the phase-space modified NFW + Black Hole (X-line).

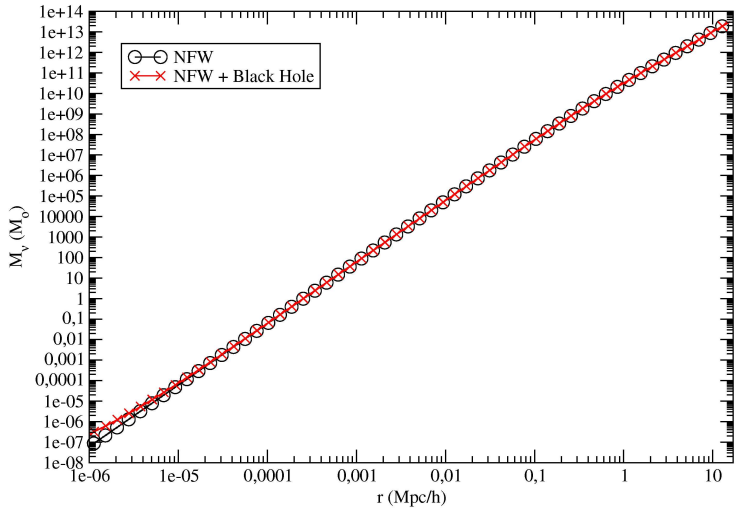

Figure A.64: Total masses used in a $M_{\mathrm{vir}} = 10^{15}\,M_{\odot}$ NFW halo with a central $3.7 \cdot 10^{9}\,M_{\odot}$ black hole. Neutrino mass is $m_{\nu} = 0.3\,\mathrm{eV}$. The plot compares the clean phase-space modified NFW (O-line) with the phase-space modified NFW + Black Hole (X-line).

BIBLIOGRAPHY

Binney, J. and Tremaine, S. (1987). *Galactic Dynamics*. Princeton University Press.

Bullock, J. S., Kolatt, T. S., Sigad, Y., Somerville, R. S., Kravtsov, A. V., Klypin, A. A., Primack, J. R., and Dekel, A. (2001). Profiles of dark haloes: evolution, scatter and environment. *MNRAS*, **321**, 559–575.

Carrol, B. W. and Ostlie, D. A. (1996). *An Introduction to Modern Astrophysics*. Addison-Wesley Publishing Company, Inc.

d'Inverno, R. A. (1992). *Introducing Einstein's Relativity*. Oxford University Press.

Dolgov, A. D., Hansen, S. H., Pastor, S., Petcov, S. T., Raffelt, G. G., and Semikoz, D. V. (2002). Cosmological bounds on neutrino degeneracy improved by flavor oscillations. *Nucl. Phys. B*, **632**, 363–382.

Duda, G., Gelmini, G., and Nussinov, S. (2001). Expected signals in relic neutrino detectors. *Phys. Rev. D*, **64**(12), 122001–+.

Fargion, D., Mele, B., and Salis, A. (1999). Ultra-High-Energy Neutrino Scattering onto Relic Light Neutrinos in the Galactic Halo as a Possible Source of the Highest Energy Extragalactic Cosmic Rays. *ApJ*, **517**, 725–733.

Fodor, Z., Katz, S. D., and Ringwald, A. (2002). Determination of Absolute Neutrino Masses from Bursts of Z Bosons in Cosmic Rays. *Phys. Rev. Lett.*, **88**(17), 171101–+.

Fukuda, Y., Hayakawa, T., Ichihara, E., and 117 coauthors (1998). Evidence for Oscillation of Atmospheric Neutrinos. *Phys. Rev. Lett.*, **81**, 1562–1567.

Ghez, A. M., Salim, S., Hornstein, S. D., Tanner, A., Lu, J. R., Morris, M., Becklin, E. E., and Duchêne, G. (2005). Stellar Orbits around the Galactic Center Black Hole. *ApJ*, **620**, 744–757.

Greisen, K. (1966). End to the Cosmic-Ray Spectrum? *Phys. Rev. Lett.*, **16**, 748–750.

Herrnstein, J. R., Moran, J. M., Greenhill, L. J., Diamond, P. J., Inoue, M., Nakai, N., Miyoshi, M., Henkel, C., and Riess, A. (1999). A geometric distance to the galaxy NGC 4258 from orbital motions in a nuclear gas disk. *Nature*, **400**, 539–541.

Kolb, E. W. and Turner, M. S. (1994). *The Early Universe*. Addison-Wesley Publishing Company.

Kull, A., Treumann, R. A., and Boehringer, H. (1996). Violent relaxation of indistinguishable objects and neutrino hot dark matter in clusters of galaxies. *ApJ*, **466**, L1+.

Macchetto, F., Marconi, A., Axon, D. J., Capetti, A., Sparks, W., and Crane, P. (1997). The Supermassive Black Hole of M87 and the Kinematics of Its Associated Gaseous Disk. *ApJ*, **489**, 579–+.

Madsen, J. (1985). *Astrophysical bounds on dark matter properties*. Ph.D. thesis, Institute of Physics and Astronomy - University of Aarhus.

Madsen, J. and Epstein, R. I. (1984). Firm bounds on the neutrino mass from the distribution of dark matter in galaxies. *ApJ*, **282**, 11–18.

Magorrian, J., Tremaine, S., Richstone, D., Bender, R., Bower, G., Dressler, A., Faber, S. M., Gebhardt, K., Green, R., Grillmair, C., Kormendy, J., and Lauer, T. (1998). The Demography of Massive Dark Objects in Galaxy Centers. *AJ*, **115**, 2285–2305.

Melissinos, A. C. (1999). In *Probing Luminous and Dark Matter*, pages 262–285, Rochester, USA.

Müller, M. (1987). In *10th Workshop on Particles and Nuclei: Neutrino Physics*, pages 269–278, Heidelberg, Germany.

Navarro, J. F., Frenk, C. S., and White, S. D. M. (1996). The structure of cold dark matter halos. *ApJ*, **462**, 563–+.

Particle Data Group, Eidelman, S., Hayes, K. G., Olive, K. A., and 153 coauthors (2004). Review of Particle Physics. *Physics Letters B*, **592**, 1–4.

Ringwald, A. and Wong, Y. Y. Y. (2004). Gravitational clustering of relic neutrinos and implications for their detection. *Journal of Cosmology and Astro-Particle Physics*, **12**, 5–+, [hep–ph/0408241].

Shapiro, S. L. and Teukolsky, S. A. (1983). *Black Holes, White Dwarfs, and Neutron Stars*. John Wiley & Sons, Inc.

Singh, S. and Ma, C. (2003). Neutrino clustering in cold dark matter halos: Implications for ultrahigh energy cosmic rays. *Phys. Rev. D*, **67**(2), 023506–+.

Tegmark, M., Strauss, M. A., Blanton, M. R., and 64 coauthors (2004). Cosmological parameters from SDSS and WMAP. *Phys. Rev. D*, **69**(10), 103501–+.

Tremaine, S. and Gunn, J. E. (1979). Dynamical role of light neutral leptons in cosmology. *Phys. Rev. Lett.*, **42**, 407–410.

Tremaine, S., Henon, M., and Lynden-Bell, D. (1986). H-functions and mixing in violent relaxation. *MNRAS*, **219**, 285–297.

Weiler, T. (1982). Resonant Absorption of Cosmic-Ray Neutrinos by the Relic-Neutrino Background. *Phys. Rev. Lett.*, **49**, 234–237.

Weiler, T. J. (2001). In *Neutrino Telescopes*, pages 613–636, Venice, Italy.

Zatsepin, G. T. and Kuzmin, V. A. (1966). Upper limit of the spectrum of cosmic rays. *JETP Lett.*, **4**, 78–80.